CANADIAN THESES ON MICROFICHE

I.S.B.N.

THESES CANADIENNES SUR MICROFICHE

National Library of Canada
Collections Development Branch

Canadian Theses on
Microfiche Service

Ottawa, Canada
K1A 0N4

Bibliothèque nationale du Canada
Direction du développement des collections

Service des thèses canadiennes
sur microfiche

NOTICE

The quality of this microfiche is heavily dependent upon the quality of the original thesis submitted for microfilming. Every effort has been made to ensure the highest quality of reproduction possible.

If pages are missing, contact the university which granted the degree.

Some pages may have indistinct print especially if the original pages were typed with a poor typewriter ribbon or if the university sent us a poor photocopy.

Previously copyrighted materials (journal articles, published tests, etc.) are not filmed.

Reproduction in full or in part of this film is governed by the Canadian Copyright Act, R.S.C. 1970, c. C-30. Please read the authorization forms which accompany this thesis.

THIS DISSERTATION
HAS BEEN MICROFILMED
EXACTLY AS RECEIVED

AVIS

La qualité de cette microfiche dépend grandement de la qualité de la thèse soumise au microfilmage. Nous avons tout fait pour assurer une qualité supérieure de reproduction.

S'il manque des pages, veuillez communiquer avec l'université qui a conféré le grade.

La qualité d'impression de certaines pages peut laisser à désirer, surtout si les pages originales ont été dactylographiées à l'aide d'un ruban usé ou si l'université nous a fait parvenir une photocopie de mauvaise qualité.

Les documents qui font déjà l'objet d'un droit d'auteur (articles de revue, examens publiés, etc.) ne sont pas microfilmés.

La reproduction, même partielle, de ce microfilm est soumise à la Loi canadienne sur le droit d'auteur, SRC 1970, c. C-30. Veuillez prendre connaissance des formules d'autorisation qui accompagnent cette thèse.

LA THÈSE A ÉTÉ
MICROFILMÉE TELLE QUE
NOUS L'AVONS REÇUE

NL-339 (r. 82/08)

Canada

0-315-05980-X

National Library of Canada | Bibliothèque nationale du Canada

Canadian Theses Division | Division des thèses canadiennes

Ottawa, Canada
K1A 0N4

53900

PERMISSION TO MICROFILM — AUTORISATION DE MICROFILMER

• Please print or type — Écrire en lettres moulées ou dactylographier

Full Name of Author — Nom complet de l'auteur

SYLVAIN DUFOUR

Date of Birth — Date de naissance

8 JANUARY 1956

Country of Birth — Lieu de naissance

CANADA

Permanent Address — Résidence fixe

26-7200 HUNTERCREST Rd N.W.
CALGARY ALTA
T2K 5S4

Title of Thesis — Titre de la thèse

VIBRATORY PILE DRIVING IN FROZEN SAND

University — Université

UNIVERSITY OF ALBERTA

Degree for which thesis was presented — Grade pour lequel cette thèse fut présentée

MASTER OF SCIENCE

Year this degree conferred — Année d'obtention de ce grade

1981

Name of Supervisor — Nom du directeur de thèse

N.R. MORGENSTERN

Permission is hereby granted to the NATIONAL LIBRARY OF CANADA to microfilm this thesis and to lend or sell copies of the film.

The author reserves other publication rights, and neither the thesis nor extensive extracts from it may be printed or otherwise reproduced without the author's written permission.

L'autorisation est, par la présente, accordée à la BIBLIOTHÈQUE NATIONALE DU CANADA de microfilmer cette thèse et de prêter ou de vendre des exemplaires du film.

L'auteur se réserve les autres droits de publication; ni la thèse ni de longs extraits de celle-ci ne doivent être imprimés ou autrement reproduits sans l'autorisation écrite de l'auteur.

Date

OCTOBER 19TH 1981

Signature

Sylvain Dufour

NL-91 (4/77)

THE UNIVERSITY OF ALBERTA

VIBRATORY PILE DRIVING IN FROZEN SAND

by

© SYLVAIN DUFOUR

A THESIS

SUBMITTED TO THE FACULTY OF GRADUATE STUDIES AND RESEARCH

IN PARTIAL FULFILMENT OF THE REQUIREMENTS FOR THE DEGREE

OF MASTER OF SCIENCE

DEPARTMENT OF CIVIL ENGINEERING

EDMONTON, ALBERTA

FALL, 1981

THE UNIVERSITY OF ALBERTA

RELEASE FORM

NAME OF AUTHOR SYLVAIN DUFOUR

TITLE OF THESIS VIBRATORY PILE DRIVING IN FROZEN SAND

DEGREE FOR WHICH THESIS WAS PRESENTED MASTER OF SCIENCE

YEAR THIS DEGREE GRANTED FALL, 1981

Permission is hereby granted to THE UNIVERSITY OF ALBERTA LIBRARY to reproduce single copies of this thesis and to lend or sell such copies for private, scholarly or scientific research purposes only.

The author reserves other publication rights, and neither the thesis nor extensive extracts from it may be printed or otherwise reproduced without the author's written permission.

(SIGNED) Sylvain Dufour

PERMANENT ADDRESS:

26, 7200 Huntercrest rd, N.W.

Calgary, Alberta

T2K 5S4

DATED June 19th, 1981

THE UNIVERSITY OF ALBERTA

FACULTY OF GRADUATE STUDIES AND RESEARCH

The undersigned certify that they have read, and recommend to the Faculty of Graduate Studies and Research, for acceptance, a thesis entitled VIBRATORY PILE DRIVING IN FROZEN SAND submitted by SYLVAIN DUFOUR in partial fulfilment of the requirements for the degree of MASTER OF SCIENCE.

.....

Supervisor

.....

.....

.....

Date: JUNE 19th, 1981

ABSTRACT

The literature on pile driving in both unfrozen and frozen soils is reviewed. An experimental program was developed to drive model piles in artificially prepared frozen soil. The goal of the research was to find which factors influenced the penetration of piles in frozen sand. Although several technical problems were associated with the experiments, factors influencing the penetration of piles in frozen sand were identified. These factors are temperature of the soil, density of the soil matrix and driver characteristics.

The energy consumed by the soil was calculated to determine the mode of penetration of piles in frozen sand. It was found that an elasto-plastic deformation of the soil took place at the pile tip. Melting does not cause penetration, it is caused by penetration.

RESUME

La littérature du fonçage des pieux par vibrations dans les sols non-gelés et dans les sols gelés est passée au peigne fin. Un programme expérimental fut créé afin d'évaluer l'influence de différents paramètres sur la pénétration des pieux dans les sols gelés. Même s'il y a plusieurs problèmes d'ordre technique inhérents à l'appareil d'essai, les paramètres qui influencent la pénétration des pieux dans les sables gelés ont été identifiés. Ces paramètres sont la température du sol, la densité du sol et les caractéristiques du vibrateur.

L'énergie consommée par le sol lors du foncage a été calculée afin de déterminer le méchanisme de pénétration des pieux dans le sable gelé. Il fut déterminé que la pénétration de pieux est due à une déformation élasto-plastique du sol à la pointe du pieu. La fonte du pergélisol n'est pas la cause de la pénétration mais plutôt en découle.

ACKNOWLEDGEMENTS - REMERCIEMENTS

Il serait de mise de remercier tout d'abord M. Marcel Dufour, M.Eng, ing., pour avoir suggérer de faire mes études supérieures à l'université de l'Alberta. Mes parents, Lise et Julien, ont aussi aidé par leur compréhension et encouragements.

Dr. Morgenstern should be thanked most sincerely for proposing this research topic and keeping a continuous and critical interest to the end. Dr. Sego should also be most kindly thanked for the several pertinent discussions that kept the testing program going in the right direction. His assistance during some part of the testing was greatly appreciated.

All the support staff of the university who contributed to the design and construction of the experimental apparatus. In particular, Mr. Roy Gitzel of the civil engineering electronics shop and Mr. Al Muir of the civil engineering machine shop.

The Department of National Defence is acknowledged for funding this research and supporting the author throughout the research.

LIST OF SYMBOLS

a =acceleration of vibratory motion

A =cross-sectional area of a pile

b =dimensionless displacement coefficient

B =width of footing

c $=\sqrt{E/\rho}$, velocity of compressional wave in pile material

d =pile displacement due to vibratory motion

d_o =displacement amplitude

dp =permanent plastic soil deformation for one motion cycle

dr =required pile tip displacement for penetration

Da =dimensionless amplitude

Df =dimensionless frequency

DF =dimensionless force

Dp =dimensionless power

Dr =dimensionless damping

Dx =dimensionless coordinate

e =soil elasticity coefficient

E =Young's modulus

E_1 =energy to penetrate pile 1 cm

f =frequency

fr =resonance frequency

F =force in pile

Fe =oscillator force at a given time

F_o =peak oscillator force

g =acceleration due to gravity (9.806 m/s^2)

h =depth

hm =maximum penetration depth

H =1/K, flexibility

J =point resistance force of pile

K =rigidity (spring constant)

L =pile length

Le =equivalent pile length

mb =sprung bias mass

mp =pile mass

M =moment of the eccentric masses of the vibrator

N =number of blows per 30 cm in the Standard Penetration Test

p =perimeter of pile section

P =power

Ps =total instantaneous soil reaction

qu =unconfined compressive strength

r =uniform damping constant (damping constant per unit length)

rp =penetration rate

R =mass of pile/mass of driver

S =side resisting force on pile

t =time

th =time required to drive a pile to a given depth

T =periodic motion period

v =velocity of vibratory motion

vr =required tip velocity for penetration

Wb =mb×g, sprung bias weight

W_p =$m_p \times g$, weight of pile

W_s =work done on soil

W_t =$W_p + W_b$, total weight of the pile-driver system

x =pile coordinate measured downward from the top

z =depth from the surface

Z_o =$\sqrt{m_p \times K}$, characteristic impedance of a pile

α =oscillation amplification factor

Δr_p=change in penetration rate during one motion period

Δz =irreversible pile penetration

ι =Blekhman's dimensionless parameter

θ =temperature

λ =wave length

λ' =Blekhman's dimensionless parameter

π =3.1415 926 535

ρ =mass density

σ_r =required pile pressure on soil for penetration

σ_w =soil resistance stress on pile wall

ϕ =Blekhman function for penetration rate

ψ =Blekhman function for penetration time

ω =$2\pi f$, angular frequency

ω_r =angular resonance frequency

Table of Contents

Chapter — Page

CHAPTER 1
INTRODUCTION 1

CHAPTER 2
HIGH FREQUENCY DRIVING IN UNFROZEN GROUNDS 4

2.1 Description of Vibratory Drivers 5

2.2 Resonant Frequencies of Piles 9

2.3 The Oscillatory Motion 15

2.4 Penetration 23

2.4.1 The Soviet Theory of Vibro-driving 23

2.4.1.1 Basic Assumptions 26

2.4.1.2 Basic Equations 28

2.4.1.3 Driving Equations 31

2.4.1.4 Conditions for Driving 38

2.4.1.5 Practical Use of Driving Equations 41

2.4.2 Soil Reactions and Penetration 42

2.5 Bearing Capacity 50

2.5.1 In Granular Soils 50

2.5.2 In Cohesive Soils 51

2.5.3 Point Bearing Piles 52

2.5.4 Conclusion 52

2.6 Summary of Actual Understanding 52

CHAPTER 3
HIGH FREQUENCY DRIVING IN PERMAFROST 55

3.1 Resonance Frequency 56

3.2 Penetration 56

3.3 Temperature at Pile Tip 62

3.4 Soviet Experience 62

3.5 Conclusion 64

CHAPTER 4
EXPERIMENTAL PROGRAM 66

4.1 General Concepts of Model Pile Behavior 66

4.2 Independent Variables and Measurable Quantities ..69

4.2.1 Sample Temperature 71

4.2.2 Bias Surcharge 72

4.2.3 Driving Frequency 73

4.2.4 Ice Content 73

4.2.5 Soil Density 74

4.2.6 Pile Oscillatory Displacement 75

4.2.7 Penetration Rate 75

4.2.8 Energy Transferred to Soil as Heat 75

4.2.9 Energy Transmitted to the Soil as Body Waves 76

4.3 Testing Program 77

CHAPTER 5
TEST RESULTS AND ANALYSIS 82

5.1 Observations and Results 82

5.1.1 Sample Properties 82

5.1.2 Pile 83

5.1.3 Thawed Film 83

5.1.4 Pile Acceleration and Soil Response Load ..87

5.1.5 Penetration Rate 90

5.1.6 Influence of the Independent Variables 97

5.1.6.1 Bias Surcharge 98

5.1.6.2 Soil Temperature 100

5.1.6.3 Driving Frequency 100

5.1.6.4 Soil Type 103

5.2 Analysis of Results 105

5.2.1 Introduction 105

5.2.2 Soil Deformation at Pile Tip 106

5.2.3 Soil Dynamic Response 112

5.2.4 Distribution of Energy 114

5.2.4.1 Energy Required to Create a Permanent Deformation 114

5.2.4.2 Energy Required to Create Thawed Film 120

5.2.4.3 Energy Dispersed throughout Sample as Body Waves 124

5.2.5 Conclusion of Analysis 128

5.3 Recent Field Tests 129

5.3.1 Field Observations 130

5.3.2 Low Frequency Driving 130

5.3.3 Resonant Driving 132

5.3.4 Conclusion 133

5.4 Summary 134

CHAPTER 6
CLOSURE 136

6.1 Recommendations for Future Laboratory Tests 136

6.2 Recommendations for Future Field Tests 137

6.3 Recommendations for Analytical and General Background Research 138

6.4 Conclusion 139

BIBLIOGRAPHY 141

APPENDIX A
DRIVING APPARATUS AND LABORATORY FACILITIES 145

A.1 Cold Room 145
A.2 Driver Support and Guiding System 147
A.3 Pile Attachment 153
A.4 Sample Container 155
A.5 Freezing Stand 156
A.6 Driver and Controls 158
A.7 Accelerometers 161
A.8 Load Cell 162
A.9 FM Recorder 163
A.10 Temperature Measurements 163
A.11 Displacement Transducers 164
A.12 Sample Preparation 164
A.13 Oscilloscope 165

APPENDIX B
TESTING PROCEDURE 166
B.1 Loose Samples 166
B.2 Dense Samples 167
B.3 Test Procedure 168

APPENDIX C
PENETRATION VERSUS TIME CURVES 171

APPENDIX D
INTEGRATION OF IDEALIZED ACCELERATION SIGNAL 198
D.1 Double Integration of Idealized Damped Vibration Wave Form 198
D.2 Double Integration of Idealized Normal Acceleration Wave Form 199

APPENDIX E
TEST DATA AND ANALYSIS RESULTS 208

List of Tables

Table		Page
2.1	Vibratory pile driver characteristics.	6
2.2	Influence of frequency and damping ratio on the peak force in the pile, tip displacement and total power; after Smart (1969).	18
2.3	Displacement amplitude and force as functions of damping and position along pile, for Df=$\pi/2$; after Smart (1969).	18
2.4	Displacement amplitude and force as functions of damping and position along pile, for Df=$5\pi/6$; after Smart (1969).	19
2.5	Displacement amplitude and force as functions of damping and position along pile, for Df=π(resonance); after Smart (1969).	19
2.6	Penetration performance of the resonant driver, for steel H-piles and open end steel pipe piles.	24
2.7	Side resisting stress for various pile and soil types, after Catoire (1963).	36
2.8	Necessary oscillatory displacement of pile tips, after Catoire (1963).	40
2.9	Performance of the resonant driver in granular materials (gravels, sands and silts) for small base area piles, after Smart (1969).	44
2.10	Performance of the resonant driver in cohesive soils (clays) for small base area piles, after Smart (1969)	45
3.1	Bodine Resonant Driver-100 performance in permafrost, after Huck and Hull (1971).	57
4.1	Experimental program carried out for the research	78
5.1	Influence of soil type on penetration rate.	104
5.2	Comparison of total pile tip displacement and permanent soil deformation per motion	

Table Page

cycle. 109

5.3 Thermal properties of loose and dense sand, after Andersland and Anderson (1978). 122

5.4 Energy (in Joules) required to thaw a soil volume equal to the thawed film area plus the pile area on a length of 1 cm. 123

5.5 Measured acceleration of dispersed waves 126

E.1 Test results 209

List of Figures

Figure		Page
2.1	Schematic representation of a vibratory pile driver, after Smart (1969).	7
2.2	Components of force acting on pile during driving.	8
2.3	First resonance frequency versus pile length, typical curve. Field data after Kovacs and Michitti (1970).	13
2.4	Soviet theoretical pile models, after Catoire (1963)	27
2.5	Soil resistance behavior for pile models	30
2.6	Blekhman function ϕ for penetration, after Catoire (1963).	34
2.7	Blekhman function Ψ for driving time, after Catoire (1963)	37
3.1	Basic soil profiles at Alaskan field test sites, after Huck and Hull (1971).	60
4.1	Grain size curve for Ottawa sand used as the experimental material	70
5.1	Grain size of sand in the thawed film	86
5.2	Effect of bias surcharge on penetration rate.	99
5.3	Effect of soil temperature on penetration rate.	101
5.4	Effect of driving frequency on penetration rate.	102
5.5	Permanent plastic deformation for one motion cycle	107
5.6	Acceleration wave models.	111
5.7	Free body diagram of the pile at a given time.	113
5.8	Deformation behavior of experimental material	115
5.9	Plastic work done on soil to achieve 1 cm	

Figure Page

of penetration 118

A.1 Side view of the testing apparatus 148

A.2 Front view of the testing apparatus 149

A.3 Top view of the testing apparatus 150

A.4 Pile attachment to the driver 154

A.5 Freezing stand for samples 157

A.6 Controls of the small exciter, 4808PM. 159

A.7 Controls of the large exciter, 4812. 160

C.1 Penetration versus time curve, test DS1-1. 172

C.2 Penetration versus time curve, test DS1-2. 173

C.3 Penetration versus time curve, test DS1-3. 174

C.4 Penetration versus time curve, test DS1-4. 175

C.5 Penetration versus time curve, test DS1-5. 176

C.6 Penetration versus time curve, test DS2-1. 177

C.7 Penetration versus time curve, test DS2-2. 178

C.8 Penetration versus time curve, test DS2-4. 179

C.9 Penetration versus time curve, test DS2-5. 180

C.10 Penetration versus time curve, test DS2-6. 181

C.11 Penetration versus time curve, test DS2-7. 182

C.12 Penetration versus time curve, test DS3-3. 183

Figure Page

C.13 Penetration versus time curve, test DS3-5. 184

C.14 Penetration versus time curve, test DS3-6. 185

C.15 Penetration versus time curve, test LS2-1. 186

C.16 Penetration versus time curve, test LS2-2. 187

C.17 Penetration versus time curve, test LS2-3. 188

C.18 Penetration versus time curve, test LS2-4. 189

C.19 Penetration versus time curve, test LS2-5. 190

C.20 Penetration versus time curve, test LS2-6. 191

C.21 Penetration versus time curve, test LS3-1. 192

C.22 Penetration versus time curve, test LS3-2. 193

C.23 Penetration versus time curve, test LS3-4. 194

C.24 Penetration versus time curve, test LS3-5. 195

C.25 Penetration versus time curve, test LS3-6. 196

C.26 Penetration versus time curve, test LS3-7. 197

List of Plates

Plate		Page
5.1	Thawed film around pile	85
5.2	Typical recorded data	88
5.3	Typical signals when driver is overloaded.	91
A.1	General view of test facilities	151
A.2	Detailed view of test facilities	152

CHAPTER 1

INTRODUCTION

In this era of depleting conventional energy and mineral resources the boundaries of exploration, and development in resource industry, have been pushed northward especially within the last twenty years. Today, they are beyond the discontinuous permafrost meridional limit, well into the continuous permafrost zone.

The presence of man in these environmentally fragile areas is not without problems; customary construction practice has to adapt to the climate and buildings have to be insulated from the underlying frozen ground to avoid the catastrophic consequences of its melting.

Standard practice in insulating a structure from permafrost is to erect it on a thick gravel pad. When it is impractical to have a gravel pad, piles are used so that enough air can circulate under the building to dissipate the heat radiating from the floor.

Traditionally, in the cold regions of Canada, piles have been placed in frozen ground by one of the following methods:

1. inserted into an oversized hole advanced by steam or hot water jetting or by dry augering, and then frozen back within a slurry;
2. driven in an undersized hole advanced as above;

3. driven directly with an impact hammer, in warm permafrost zones.

Now, the concept of vibratory driving, in use for many years in the Soviet Union, has been extended and applied in North America. It has been proven that the penetration is astonishingly rapid when the pile is excited at its first resonance frequency with a net downward force of a fraction of its bearing capacity.

Today, new horizons are opening to vibratory driving techniques in permafrost. Drilling for oil through permafrost disturbs the natural ground thermal regime. Thermal degradation can be such that downdrag of thawed soil causes rupture of the well. Vibratory driving of casing and multiple casing of wells can effectively minimize thermal disturbance of permafrost.

Discovery of offshore oil in the Arctic, especially in the Beaufort Sea, may eventually lead to the construction of offshore exploitation platforms. Presence of sea bottom permafrost makes impact driving a difficult task. Conventional permafrost piling techniques, as discussed earlier, can not be used in submerged conditions for obvious reasons. Vibratory driving of platform piles (which are large in diameter) is an appealing solution.

At this point in time, vibratory pile driving in permafrost is not well understood. Experience in North America is limited to a few driving tests carried out by private industry for feasibility studies of pile placement

methods on large projects. It transpires from the field tests carried out that pile resonance is associated with the best penetration rates. Penetration is also associated to melting of permafrost at the pile tip.

Because of the limited experience of resonant pile driving in permafrost, resonant driving (or high frequency driving) in unfrozen soils is reviewed in Chapter 2. The review is intended to shed light upon prediction of the frequency of resonance and upon the mechanics of pile penetration in unfrozen soils. This Chapter shall be treated as pertinent background but not as being closely and directly related to the aims of the present investigation. Chapter 3 presents a review of all published experience in vibratory driving in frozen ground. From that experience, the experimental program is discussed in Chapter 4. Details of facilities and experimental procedure are described in Appendix A and B respectively. Experimental results are presented and analysed in Chapter 5. Distribution of energy and mechanics of penetration are discussed. Results of recent private field tests are compared to experimental findings of this research. Finally, Chapter 6 concludes the experimental program and gives recommendations for future research.

CHAPTER 2

HIGH FREQUENCY DRIVING IN UNFROZEN GROUNDS

This Chapter contains a review of all high frequency vibratory driving experience in unfrozen ground. The information contained herein contitutes a pertinent background to the general understanding of what vibratory driving at resonance is all about.

The objective in high frequency driving is to excite the pile at its first resonance frequency, ordinarily lying in the range from 85 to 135 Hz. When the pile is vibrated at resonance, the displacement amplitudes and the induced forces at the two extremities of the pile are at a maximum. This facilitates the input of energy at the top and maximizes the transfer of energy to the soil at the tip of the pile.

High-power vibratory drivers will first be described. Then, the techniques for predicting resonance frequencies of piles will be discussed. To assist the reader in understanding the mechanics of penetration, the very nature of the oscillatory motion will be examined. Following these studies, the earlier work in vibratory driving techniques will be briefly reviewed. This will lead the reader to the mechanism of penetration as it is understood today. Prediction methods are reviewed before attention is finally given to the loading capacity of vibration-driven piles with

respect to that of impact-driven piles.

2.1 Description of Vibratory Drivers

Many vibratory drivers can be found on the market but most operate only in the low frequency range. Driver frequencies are classified basically in two ranges: low range when operating frequencies are around the first natural frequency of the soil, i.e. 10 to 35 Hz; and high frequency range when operating frequencies are above the natural frequency of the soil and into the natural frequency range of piles, i.e. 40 to 135 Hz. The only high frequency driver widely found in North America is the Bodine Resonant Driver whose characteristics are shown in Table 2.1.

A vibratory driver can best be visualized in three parts as illustrated in Figure 2.1: a sprung bias weight, an oscillator and a device to transmit the vibrations to the pile.

The sprung bias weight is a dead weight added to the system to produce a net downward force and ensure that the tip of the pile is well in contact with the soil during the oscillatory motion. The weight is isolated from the oscillator by a soft spring or an air cushion in order not to take part in the dynamic motion. The dynamic force developed by the oscillator is shown in Figure 2.2.

The oscillator consists of two counter-rotating eccentric masses synchronized in such a way that the

Table 2.1 Vibratory pile driver characteristics.

MODEL	FREQUENCY Hz	POWER kW	MASS tonnes	FORCE AMPLITUDE kN
BRD-1000	40-135	745	10	1200 @ 135 Hz* 500 @ 70 Hz
RDU-400**	60-130	298	8.2	1200

* Allows for a 35% increase at resonance.
**Smaller version of the BRD-1000, made in Canada.

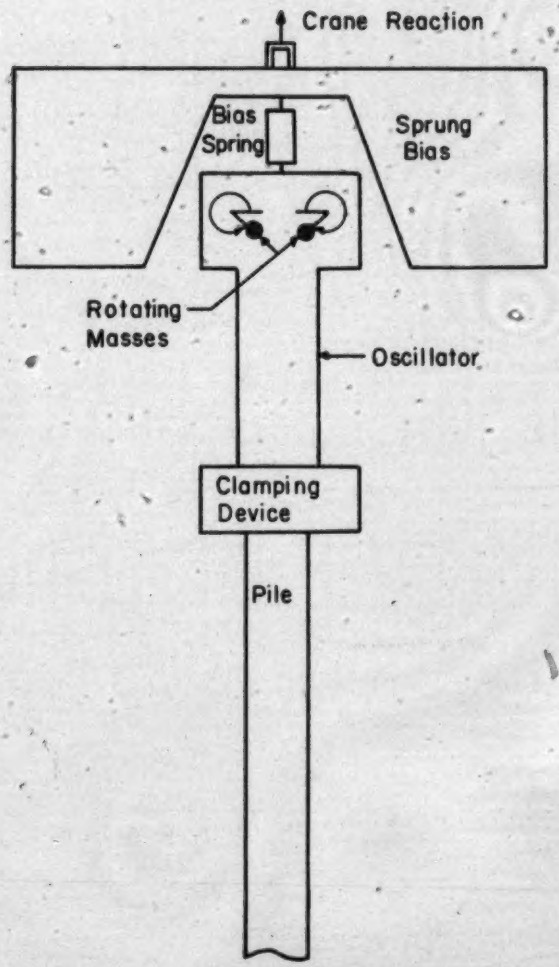

Figure 2.1 Schematic representation of a vibratory pile driver, after Smart (1969).

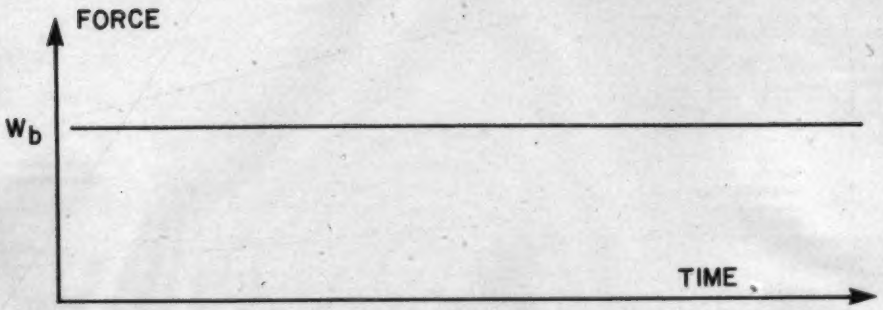

a) force on the pile when the oscillator is at rest; W_b is the bias weight.

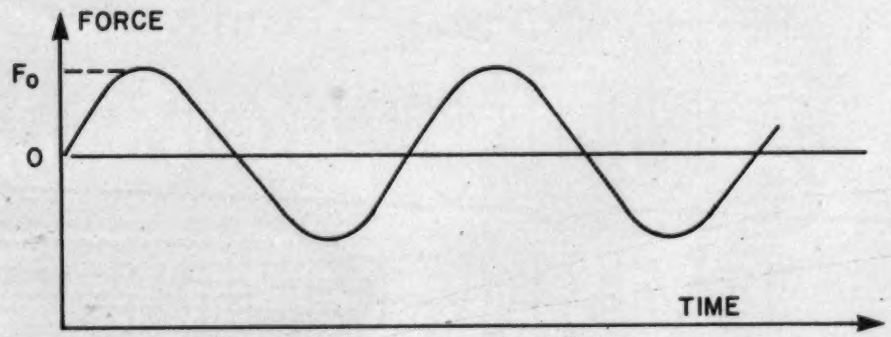

b) dynamic force developed by the oscillator;

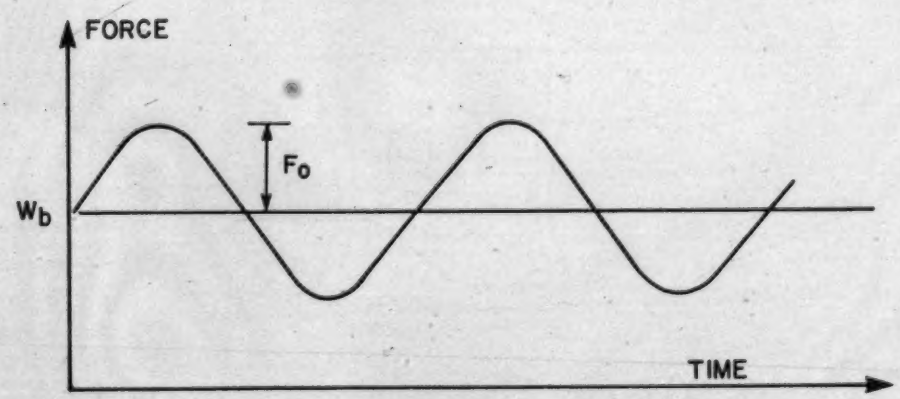

c) total force input at the top of the pile when the oscillator is in motion.

Figure 2.2 Components of force acting on pile during driving.

horizontal components of their centrifugal forces cancel and a vertical sinusoidally varying force is produced. The eccentric masses can be changed to produce the desired peak force. Their rotational velocity can also be varied to produce the desired peak force.

Finally, a clamp strongly secures the top of the pile to the oscillator to ensure the force and motion of the oscillator are transfered to the pile.

2.2 Resonant Frequencies of Piles

The main objective in resonant vibro-driving is to excite the pile at resonance to maximize the energy transfer from the top to the bottom of the pile. Hence, it is very important to be able to predict the first resonance frequency for a given pile.

According to elastic theory, the wave length at the first resonance mode will be twice the length of the pile when both ends of the pile are free. A pile with one end fixed and one free will have a wave length of four times its length. Since the frequency (f), the wave length (λ) and the elastic wave velocity (c) are related by:

$$f \times \lambda = c' \qquad (2.1)$$

---

[1] This equation is derived from fundamental physical considerations and is contained in any elementary physics or dynamics book. See Halliday and Resnik (1967).

a free ended rod with a wave length of twice the pile length (L) gives the resonance frequency (fr) as:

$$fr=c/(2\times L) \qquad (2.2)$$

A rod with one end fixed and one end free will have a resonance frequency of:

$$fr=c/(4\times L) \qquad (2.3)$$

In reality, piles do not have both their ends free nor their tip fixed and top free. Piles carry at the top a significant mass: the sprung bias and the driver. Davisson (1965) suggested that the analogy of a vibrating pile-driver system to a vibrating free ended rod with a mass sitting on top could be made to approximate the first resonance frequency of pile-driver systems:

$$R=(\omega rL/c)\times\cot an(\omega rL/c) \qquad (2.4)$$

where R is the ratio of the mass of the pile to the mass of the driver and ωr the angular resonance frequency.

Since the preceding theoretical relations are not satisfactory to predict the resonance frequencies, Kovacs (1966) modified empirically an equation first presented by Rayleigh (1926) to take into account the mass of material brought into play as a result of the pile motion. He

concluded that

$$f=(c/2\pi)\sqrt{5.25/(Le\times L)} \quad [2] \qquad (2.5)$$

where Le is the equivalent pile length, equal to the actual pile length plus the length of the clamp and driver attached to the pile, and 5.25 is an empirical constant. The equivalent length is approximately 1.8 meters for the Bodine Resonant Driver.

In a continued effort to find an universal expression for the resonance frequency, Bernhard (1967a) determined experimentally using model piles that the wave length at the first resonance mode was three times the length of the pile. Therefore, the resonance frequency of a pile from experimental results is given by:

$$fr=c/(3\times L) \qquad (2.6)$$

Kovacs and Michitti (1970) compared resonance frequencies computed from various formulae to observed frequencies from field studies. A plot of resonance frequency versus pile length, for all the equations

---

[2] This formula was first described in an unpublished report on file at U.S.A. C.R.R.E.L., Hanover, N. H.. Its first and only publication, as far as the author knows, was in a C.R.R.E.L. report by Kovacs and Michitti (1970). The formula in the report is incorrect. The error was never reported in any publication or note from the authors. Dr. Kovacs was contacted personally to acknowledge the error and obtain the correct expression.

previously presented and using Kovacs and Michitti's (op. cit.) data, is shown in Figure 2.3. It can be seen that the theoretical free tip and fixed tip[3] frequencies provide an upper and lower bound estimate while Kovacs' and Bernhard's equations are the best fits for the observed frequencies. Davisson's equation undoubtedly misrepresents the behavior and should not be used to predict the data.

Kovacs and Michitti (op. cit.) studied other cases as well and came to the forementioned conclusion that Kovacs' and Bernhard's equations were the best approximations of field resonance frequencies.

It is very interesting to note that formulae 2.1 to 2.6, except that of Davisson (2.4) which can be disregarded, have only the pile's compressional wave velocity ($c=\sqrt{E/\rho}$) and the length of the pile as parameters. In other words, they only take into account the physical properties of the pile. Kovacs' equation however contains an empirical constant to consider the mass of the soil brought into play along with the pile.

This observation causes one to wonder what the influence of embedment really is. Even before the entry on the market of high frequency drivers, Eastwood (1955) concluded, after a series of tests, that the resonance frequency of a pile-soil system could be considered constant throughout the penetration of the pile into the soil.

---

[3] The top of a pile is always assumed to be free. Therefore, free tip designates a free-free end condition and fixed tip a fixed-free end condition.

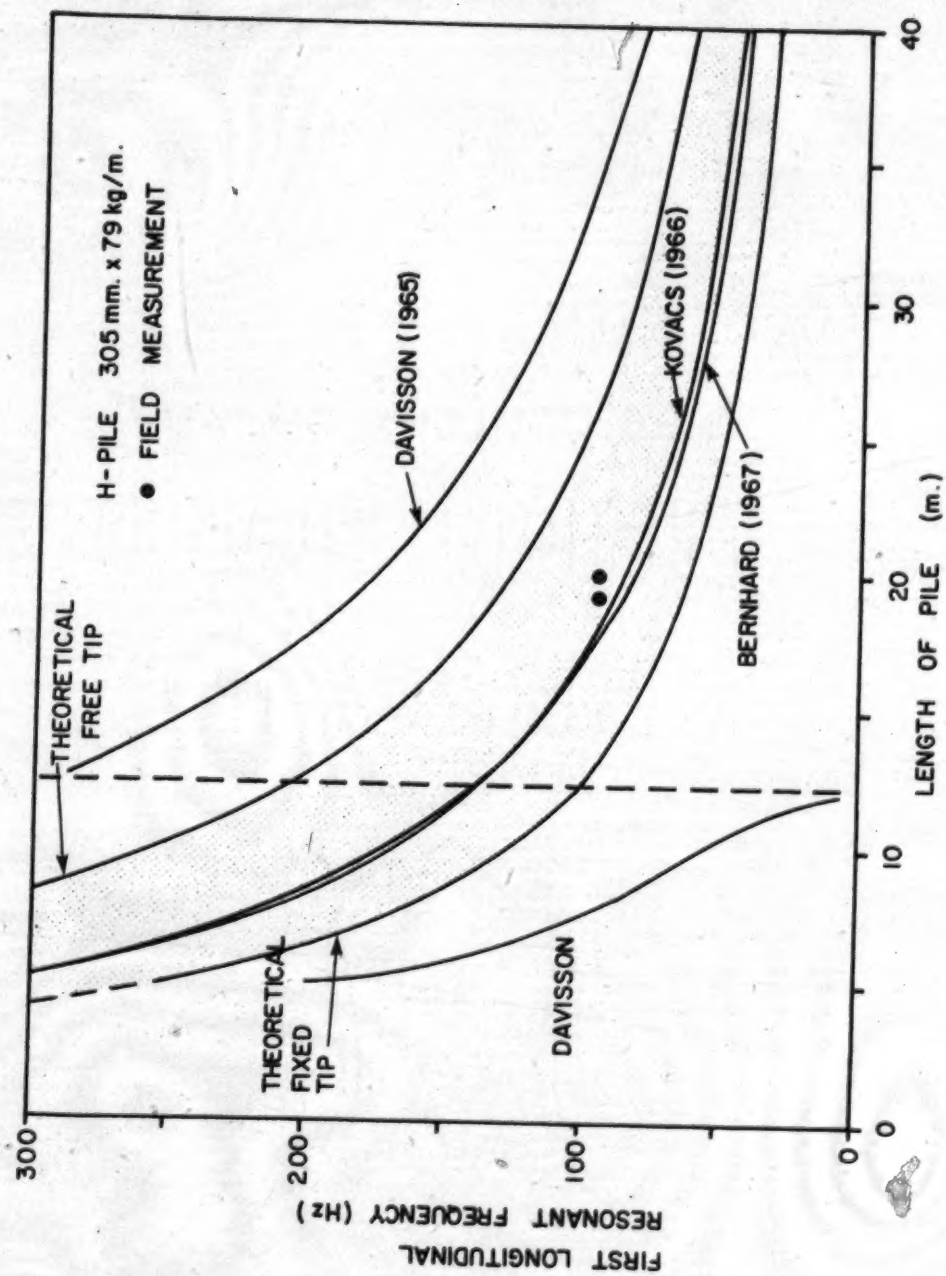

Figure 2.3 First resonance frequency versus pile length, typical curve. Field data after Kovacs and Michitti (1970).

Ghahramani (1967) computed resonance frequencies for embedded and unembedded piles and found insignificant differences. Meanwhile, Griggs (1967) demonstrated with his idealized models that the side resisting forces due to embedment reduce the displacement magnitude but have no effect whatsoever on the resonance frequency of the system.

For completeness, it should be added that Schmid (1969) concluded after a series of model tests conducted at Princeton University that there exists two types of resonance:

> ". . . the first is a rigid body-system type of resonance which has a rather flat peak, and the resonance frequency depends on the masses of vibrator and pile and the properties of the soil. For this rigid body-type system driving at the resonance frequency is not essential. The second, and all higher resonance frequencies, are those of the elastic rod resonance. They depend only on the velocity of sound[4] in the pile material and the pile length L."

While one can satisfactorily predict the resonance frequency of piles, it is important to remember that the resonance of a pile-driver-soil system depends solely upon the physical characteristics of the pile. Therefore, use of equations 2.5 and 2.6 is recommended to predict the resonance frequency of piles.

---

[4] Compressional wave velocity (c).

2.3 The Oscillatory Motion

The knowledge of the nature and shape of the oscillatory motion is important not only in predicting the resonance frequencies as seen in the previous section, but also in estimating the magnitude of the displacement at the pile tip. The magnitude of the motion at the tip is used to calculate the amount of energy transmitted to the soil and, to some extent, the penetration of the pile.

Bernhard (op. cit.) shed some light upon the shape of the vibratory motion when he reported that the wave length was equal to three pile lengths, but probably the most comprehensive study was carried out by Smart (1969). He performed a dimensionless parametric study on a uniform section, weightless pile with uniform viscous damping along its wall and no point resistance. His parameters were defined as follow:

1. the dimensionless frequency:

$$Df=\omega \times L/c \qquad (2.7)$$

note that the first theoretical resonance is at $Df=\pi$ and the second at 2π;

2. the dimensionless amplitude:

$$Da=\omega \times d \times Z_o/F_o \qquad (2.8)$$

where Z_o is the characteristic impedance of the pile,

defined as the square root of mass times rigidity, F_o is the peak oscillator force, and d the current displacement;

3. the dimensionless force:

$$DF=F/F_o \qquad (2.9)$$

where F is the current force;

4. the dimensionless power:

$$Dp=P\times Z_o/F_o \qquad (2.10)$$

where P is the current power;

5. the dimensionless damping:

$$Dr=r\times L/Z_o \qquad (2.11)$$

where r is the uniform viscous damping constant[5];

6. and finally, the dimensionless coordinate:

$$Dx=x/L \qquad (2.12)$$

where x is the distance measured from the top of the pile.

---

[5] Damping or "dashpot" constant per unit length.

In his analysis Smart (op. cit.) took the pile as fully embedded in soil. The input force, frequency, total damping and the characteristic impedance of the pile were assumed to be independent variables. The displacements, internal forces and power consumption were on the other hand, considered as dependent variables. Great care should be taken in interpreting the results of the analysis. In most cases, parameters were held constant to find out what the effect on the others would be. In real cases, they might not be constant. A change in section or characteristic impedance for example, has an effect on the dimensionless damping ratio. The results of the analysis are presented in Tables 2.2 to 2.5. Before they are discussed, general conclusions from inspection of the dimensionless expressions will be drawn.

From equation 2.8, it can be said, if all else is held constant, that the displacement magnitude is inversely proportional to the frequency. The velocity (v) and acceleration (a) are respectively the first and second time derivative of the displacement. Hence, from the harmonic motion equation

$$d=d_o \times \sin(\omega \times t) \qquad (2.13)$$

where d_o is the displacement amplitude, it can be shown that

$$v/d=\omega \qquad (2.14)$$

Table 2.2 Influence of frequency and damping ratio on the peak force in the pile, tip displacement and total power; after Smart (1969).

Df	Dr	DF (peak)	Da (tip)	DP (total)
$\pi/3$	0.1 1.5	1.0 1.0	1.2 0.63	0.05 0.24
$\pi/2$	0.1 1.5	1.0 1.0	1.0 0.70	0.024 0.23
$2\pi/3$	0.1 1.5	1.1 1.0	1.2 0.81	0.03 0.30
π	0.1 1.5	20 1.3	20 1.2	9.0 0.79

Table 2.3 Displacement amplitude and force as functions of damping and position along pile, for Df=$\pi/2$; after Smart (1969).

Dx	Dr	Da	DF
0	0.1 1.5	0.053 0.53	1.0 1.0
0.50	0.1 1.5	0.70 0.52	0.70 0.71
0.93	0.1 1.5	- -	0.12 0.10
1.00	0.1 1.5	1.00 0.68	0.0 0.0

Table 2.4 Displacement amplitude and force as functions of damping and position along pile, for Df=5π/6; after Smart (1969).

Dx	Dr	Da	DF
0	0.1 1.5	1.7 1.3	1.0 1.0
0.50	0.1 1.5	0.50 0.48	1.9 1.2
0.975	0.1 1.5	- -	0.13 0.10
1.00	0.1 1.5	2.0 1.1	0.0 0.0

Table 2.5 Displacement amplitude and force as functions of damping and position along pile, for Df= π (resonance); after Smart (1969).

Dx	Dr	Da	DF
0	0.1 1.5	20.0 1.3	1.0 1.0
0.5	0.1 1.5	0.55 0.48	20.0 1.30
0.975	0.1 1.5	- -	1.3 0.10
1.0	0.1 1.5	20.0 1.2	0.0 0.0

and

$$a/d=-\omega^2 \tag{2.15}$$

Therefore, the acceleration is directly proportional to the frequency.

The power consumption is the input oscillator force times the velocity of the top of the pile, averaged over one time period. In terms of velocity, equation 2.8 becomes

$$Da=v\times Z_o/F_o \tag{2.16}$$

Hence we can say that the power is proportional to the square of the oscillator force. Similarly, from equations 2.8 and 2.10, if all else is maintained constant, it appears that the displacement and the power are inversely proportional to the characteristic impedance of the pile.

From Table 2.2, as the frequency is increased from zero, the tip displacement and power delivered to the pile decrease to a minimum at one half the resonance frequency and reach a peak at resonance. This is true for any amount of damping, the lower value of Dr representing less damping. Two values of dimensionless damping are presented to illustrate the effect of increased damping on the motion shape and nature. The peak force is amplified at resonance. The increase in peak force is noticeable from about two thirds of resonance ($Df=2\pi/3$). The amplification of the peak force is maximum at resonance and decreases again past

resonance in the same manner as it increased with frequency before resonance. The force is unchanged between the resonance peaks.

It is interesting to note on Tables 2.3 to 2.5 that the forces near the tip of the pile are around 10% of the oscillator force except for the undamped pile at resonance. In fact, in the last 3 to 5% of the length of the pile, the forces drop drastically from 10% to 0% of the oscillator force. This is because the tip must have zero force to satisfy the assumed boundary condition. In the case of the undamped pile, the drop is steeper because the amplification in the center of the pile is much larger.

The dimensionless damping ratio has very little influence on the magnitude of the forces at any point along the pile. At resonance, however, the forces in the pile are highly dependent on damping, see Table 2.5. Damping lessens resonance of the forces at all points along the pile. As in the preceding cases, forces quickly drop to zero in the last portion of the pile length. The displacements at resonance are affected by damping in a similar fashion as the forces. The displacement can be a large amplification of the rigid body displacement depending upon the amount of damping.

If a resistance was offered to the tip of a pile, it can be conceived that the shape of the force distribution along the pile and hence the displacement distribution would be altered in such a way to make the wave length shorter than the free tip wave length. This model then clarifies

why the free tip resonance frequency is an upper bound value, refer to section 2.2.

Smart (op. cit.) observed on the lower frequencies response curves, which are not reported here, that at less than one quarter of the resonance frequency, the pile essentially behaves like a rigid body. This theoretical finding confirms the experimental observations of Schmid (op. cit.).

From Smart' study, it is important to keep in mind that at resonance

1. the tip displacement can be a large multiple of the rigid body displacement;
2. the magnitude of the forces and displacements in the pile are highly dependent upon the amount of damping;
3. the consumed power is proportional to the square of the oscillator force if all other parameters are held constant;
4. the characteristic impedance of the pile has a definite effect on the displacements and the amount of power used to drive the pile.

Thus with this better understanding of the pile motion, the soil reactions along the side and at the tip will be better visualized. Hence, the problem of penetration can now be probed.

2.4 Penetration

A limited amount of data on pile penetration is available in the literature. A thorough literature review for piles of small cross-sectional area is presented in Table 2.6. It should be noted that all non-scientific papers with incomplete information, such as Rayner (1974) or Reseigh (1961), have been disregarded. The amount of data on large displacement piles, like closed end piles, is comparable to the amount presented in Table 2.6. The data presented in Table 2.6 demonstrates very convincingly the ability of the resonant drivers to economically place piles in any type of soil.

Catoire (1963) reviewed the Soviet theory of vibratory driving. It is not intended here to give the Russians more credit than they deserve but, since Catoire's (op. cit.) paper reports on the early work in vibro-driving, is the only available reference on Soviet work and has not been published in the english-speaking literature, it will be the object of a special section. Following that section on the Soviet theory of vibro-driving, the major landmarks in the mechanics of penetration and understanding of soil reactions will be reviewed.

2.4.1 The Soviet Theory of Vibro-driving

The following lines constitute a detailed presentation of Catoire (op. cit.). As previously said, this only constitutes a review of the early work. Hence, the relative

Table 2.6 Penetration performance of the resonant driver, for steel H-piles and open end steel pipe piles.

SITE AND PILE NO.	PILE SIZE TYPE	TIP AREA cm^2	DRIVING DEPTH	DESCRIPTION OF TRAVERSED STRATA	PEN RATE MEAN m/min	PEN RATE FINAL m/min	Cu/ϕ kPa/° N(blows/30 cm)	REFERENCE
#62-USA	H-Pile 356 mm 174 kg/m	222	25.60 33.10	Sand, silt, clay Medium sand	3.34 0.75	- 1.53	<30 ~40 42 80	Fawcett (1973)
#2 -UK	H-Pile 305 mm 117 kg/m	150	16.46 17.68 19.81	Very silty organic clay Stiff sandy Keuper marl Hard sandy Keuper marl	13.87 7.18 0.34	- - 0.23	24/0° 24/0° 87/18° 87/18° <150 >150	Fawcett (1973)
#9-Holland	Pipe pile 406 mm	157	6.00 17.00 21.00 24.50	Sand fill Dense sand, silt layers Layers of sand, silt and clay Layers of sand, silt and clay	10.9 3.46 		10-30 55 25-50 28	Fawcett (1973)
#12-UK	Hollow box Larssen 38	158	6.10 14.02 17.07 22.57 23.17	Fill and sand with gravel Medium sand Medium sand Medium sand Very soft sandstone	4.52 2.56 0.62 0.78 -	 1.68 0.38 0.61 0.019	 26 32 45 45 35 35 90 90	Fawcett (1973)
#13-USA	H-Pile 356 mm 132 kg/m	169	23.16 24.38	Interbedded silt and sand Dense sandy till	 1.52		3-43 >80	Smart (1969)
#16A-USA (3 piles)	H-Pile 203 mm 54 kg/m	68	4.77 9.14 10.06	Fill Sand & gravel Clayey silt Bedrock (shale)	1)0.30 2)0.15 3)0.15		7-34	Smart (1969)
#20-10 USA	Pipe pile ~~0 mm	99	7.62 9.45 16.15	Gravelly or silty sand Clay Gravelly or silty sand	 3.04 		27-63	Smart (1969)
#20-9 USA	H-Pile 356 mm 109 kg/m	139	10.67 11.28 16.15	Gravelly or silty sand Clay Gravelly or silty sand	 6.08 		27-63	Smart (1969)
#27 (7 piles)	H-Pile 356 mm 109 kg/m	139	18.29 ~22.10	Medium Density sand Dense sand	1)0.41 2)0.91 3)1.68 4)1.14 5)0.61 6)0.30 7)7.62		20-30 >40	Smart (1969)
#46 (2 piles)	H-Pile 254 mm 62 kg/m	80	~ 9.14 ~30.50	Soft silt and clay Alternating stiff clay dense sand and gravel	1)6.10 2)6.71		17-55	Smart (1969)
#63-USA (3 piles)	H-Pile 254 mm 85 kg/m	108	18.29 to 24.38	Dense sand and gravel	1)4.57 2)5.49 3)1.83		>100	Smart (1969)
#87-USA	H-Pile 305 mm 79 kg/m	101	4.88 6.10 9.14 18.59	Loose dredge sand fill Loose alluvium sand Silty clay to clayey silt Loose alluvium	 4.36 		 2-18 2-18	Smart (1969)
#92-USA	H-Pile 356 mm 132 kg/m	169	33.53 35.66	Dense sand & gravel Shale bedrock	0.26		18-172 (N=90)	Smart (1969)

size of this section is not representative of the relative importance of the presented work with respect to the actual state of the art.

The work on vibratory driving in the Soviet Union has followed two main schools of thought. The first was led by the famous Dr. Barkan and advocated the vibroviscosity of the soil. The second, led by Newmark and in parallel by Blekhman, Koushoul and Shliakhtin, preached that there is no need to worry about the vibroviscosity of the soil. They arrived at a theory using usual concepts of bearing capacity and soil resistance, assuming that dry friction took place along the skin of the pile. They also assumed that there existed a relationship between the force exerted by the tip of the pile and the penetration of the pile.

Barkan's theory takes into account the change in physico-mechanical properties of the soil but fails to explain some important and fundamental field behaviors such as the absence of penetration at small tip displacements and refusal at depth.

Newmark's work fails to recognize the change in physico-mechanical properties of the soil but successfully accounts for refusal and absence of penetration at small tip displacements. In certain materials like saturated sands, such a theory is erroneous because of pore pressure build-up. Newmark's theory will be examined in detail because it models satisfactorily the field behavior, and because it has similar assumptions to those of his school's

followers.

2.4.1.1 Basic Assumptions

Several models were adopted to develop the theory of vibro-driving. They are illustrated in Figure 2.4. It is assumed for the first model that

1. the pile is a perfectly rigid body;
2. the soil around the pile remains still at all times;
3. the soil friction on the wall of the pile is dry friction, i.e. it does not depend upon the velocity of the motion but upon the normal force;
4. the point resistance does not depend upon the penetration rate;
5. the relationship between the point resistance and the penetration of the pile is constant. The same point resistance holds for any penetration of pile;
6. the exciter produces a sinusoidally varying vertical force independent of the pile motion.

The first model consists of a rod sinking in a straight shaft and held back by a weightless plug near its tip. Newmark assumes that the soil resistance at the point and the resisting soil friction can be obtained experimentally.

The second model is different from the first in that the soil elasticity is taken into account. There are springs that bind a weightless soil cylinder to the pile. The side friction and the spring at the tip of the pile keep the weightless plug at the tip away from direct impacts by

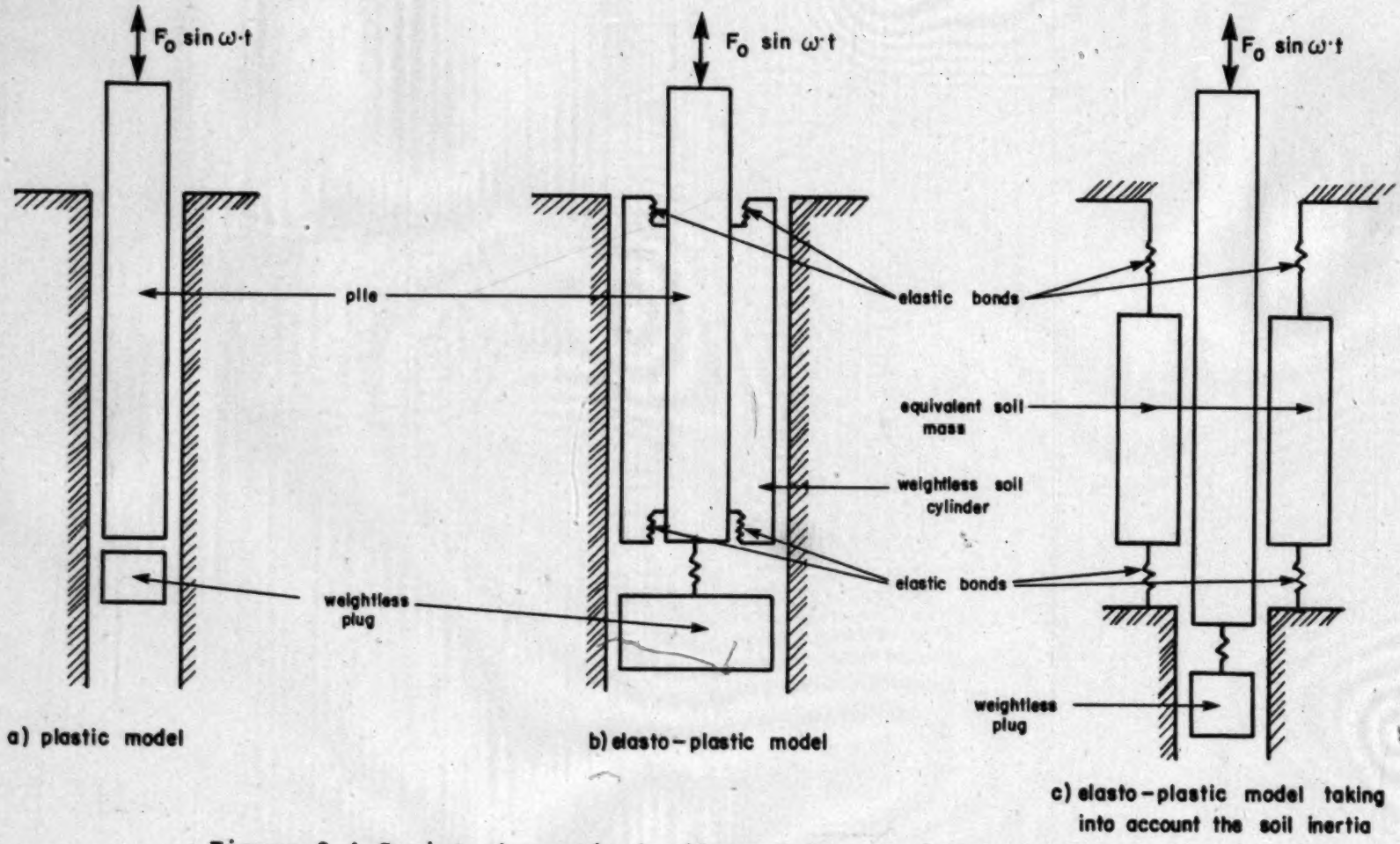

Figure 2.4 Soviet theoretical pile models, after Catoire (1963)

the pile. When the pile is excited, the soil cylinder stays still until the forces in the binding springs equal the side resisting forces. At the tip of the pile, the spring first compresses until its force reaches the magnitude of the point resistance force. Then, the plug starts to move down.

As can be seen, the models do not consider the inertia of the soil surrounding the pile. The influence of the inertia of the soil is far from being negligible. This is why a more appropriate model such as the one shown in Figure 2.4c should be used. The soil around the pile is replaced by an equivalent mass resting on springs. This equivalent mass has the same frictional properties as the real soil. This model was first imagined by Newmark but never used in any analysis.

2.4.1.2 Basic Equations

The penetration condition for the first model is at all times:

$$F_o > S \tag{2.17}$$

where S is the total side resisting force.

For the second model, the condition becomes

$$K \times d > S \tag{2.18}$$

where K is the spring constant of the soil-pile elastic

bonds.

The soil models for the point resistance are shown in Figure 2.5. The resistance for the first pile model is purely plastic. The point resistance is always the same regardless of the pile penetration. The resistance for the second model is elasto-plastic. The elastic portion of the relationship corresponds to the compression of the binding soil-pile springs.

Newmark stated that the irreversible penetration (Δz) of a pile of mass (mp) hitting the soil at a velocity (v), is for the elasto-plastic model:

$$\Delta z=((mp\times v^2/J)-d)/2 \qquad (2.19)$$

where J is the point resistance force.

In practice, the point resistance is often larger than the weight of the pile. It is therefore obvious that penetration can only be achieved if the displacement at the tip of the pile is larger than the elastic settlement under the pile weight. The point resistance can then be overcome by the shock effect of the loading in dry soils or by taking advantage of the effective stress reduction in saturated soils. Hence the additional condition:

$$Wp/F_o<\alpha \qquad (2.20)$$

where Wp is the weight of the pile and α the oscillation

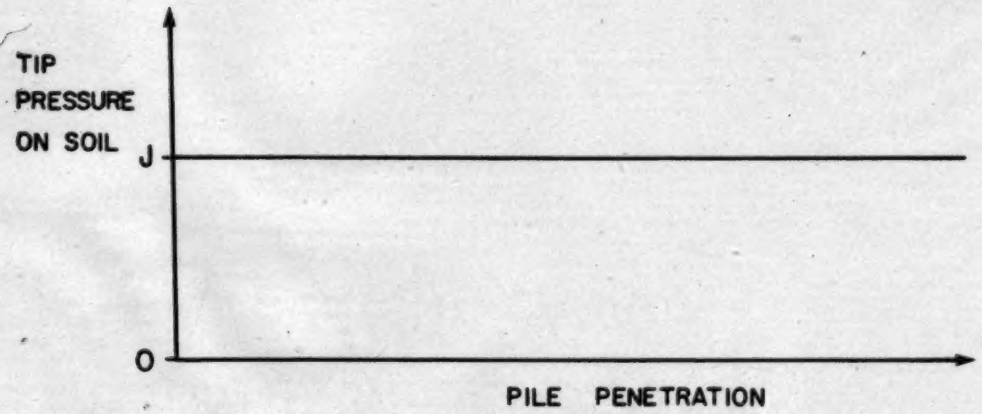

a) PLASTIC MODEL FOR 1st PILE MODEL

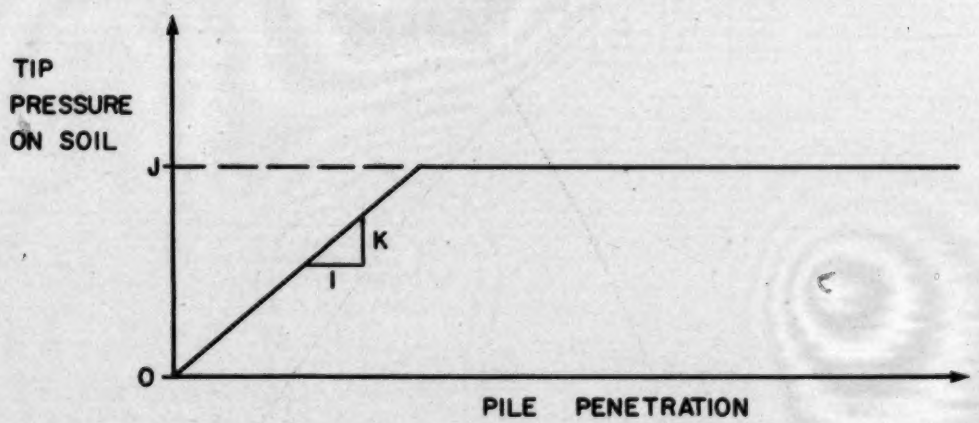

b) ELASTO-PLASTIC MODEL FOR 2nd & 3rd PILE MODEL

Figure 2.5 Soil resistance behavior for pile models

amplification factor. The parameter α is highest at resonance and about 1.0 at low frequencies. From that equation, the ratio Wp/F. has to be less than 1.0 at low frequencies but can be higher than 1.0 at resonance as long as it remains less than α.

2.4.1.3 Driving Equations

As previously stated, a pile driving solution that takes into account both the elasticity and inertia of the soil does not yet exist. The second model, Figure 2.4b, was analyzed by Newmark using the harmonic equilibrium method. Koushoul and Shliakhtin used the initial parameter method to solve the same problem[‘]. Their solutions are very complex in spite of the sweeping assumptions made to simplify the problem. The solutions are interesting to the extent that they allow a qualitative estimate of the influence of the soil elasticity during driving.

As far as the first model, Figure 2.4a, is concerned, Newmark and Blekhman obtained simple equations giving the maximum depth of penetration, the average rate of penetration and the time required for driving the pile. These relations are sufficient and satisfactory in cases where oscillatory displacements and penetration rates are large. Newmark states that these two conditions are fulfilled when

---

[‘] The author, Boris Catoire, does not give any further information on these two methods of analysis.

$$S<<K\times d \tag{2.21}$$

and

$$d<<rp/(2\times f) \tag{2.22}$$

where rp is the penetration rate of the pile in the soil.

Only the final results of Newmark's and Blekhman's work are presented in the following lines. The method of solution for this model, the first, is not given. To calculate the magnitude of the pile oscillatory displacement, Newmark proposed:

$$d=(M/Wp)\sqrt{(1-(4S/(\pi F_o))^2)} \tag{2.23}$$

where M is the moment of the eccentric masses of the vibrator. M is related to F_o in the following manner:

$$F_o=M\times\omega^2/g \tag{2.24}$$

When the side resisting force S is much less than the vibrator force F_o, the magnitude of the oscillatory displacements becomes equal to M/Wp or exactly what it would be without any soil surrounding the pile.

If $(S+J)>Wt>(S+J-F_o)$, Blekhman proposed an expression to calculate the penetration rate:

$$rp=(M\times\omega/(\pi\times Wt))\times\phi(\lambda',\iota)\times sgn\iota \tag{2.25}$$

where Wt is the total weight of the system (Wp+Wb), λ' and ι are dimensionless parameters given by the following expressions:

$$\lambda' = (S+J/2)/F_e \tag{2.26}$$

$$\iota = (Wt-J/2)/F_e \tag{2.27}$$

$\phi(\lambda', \iota)$ is a function of the dimensionless parameters λ' and ι, and is given in Figure 2.6. sgnι is equal to +1 when ι is greater than 0 and to -1 when ι is less than 0. sgnι's only purpose is to give the formula the ability to represent either sinking or extraction of piles. Extraction rates are of course negative.

Formula 2.25 is valid when there is no point resistance. In most cases where the point resistance is small compared to other forces in the system, the equation would apply. The existence of a significant point resistance reduces the penetration rate.

For small λ and ι, an approximation of equation 2.25 can be used:

$$rp = (\pi \times M \times \omega \times (Wt-J/2))/(2Wt \times (S+J/2)) \tag{2.28}$$

Blekhman also proposed an expression and a graph to determine the time required to drive a pile to a given depth:

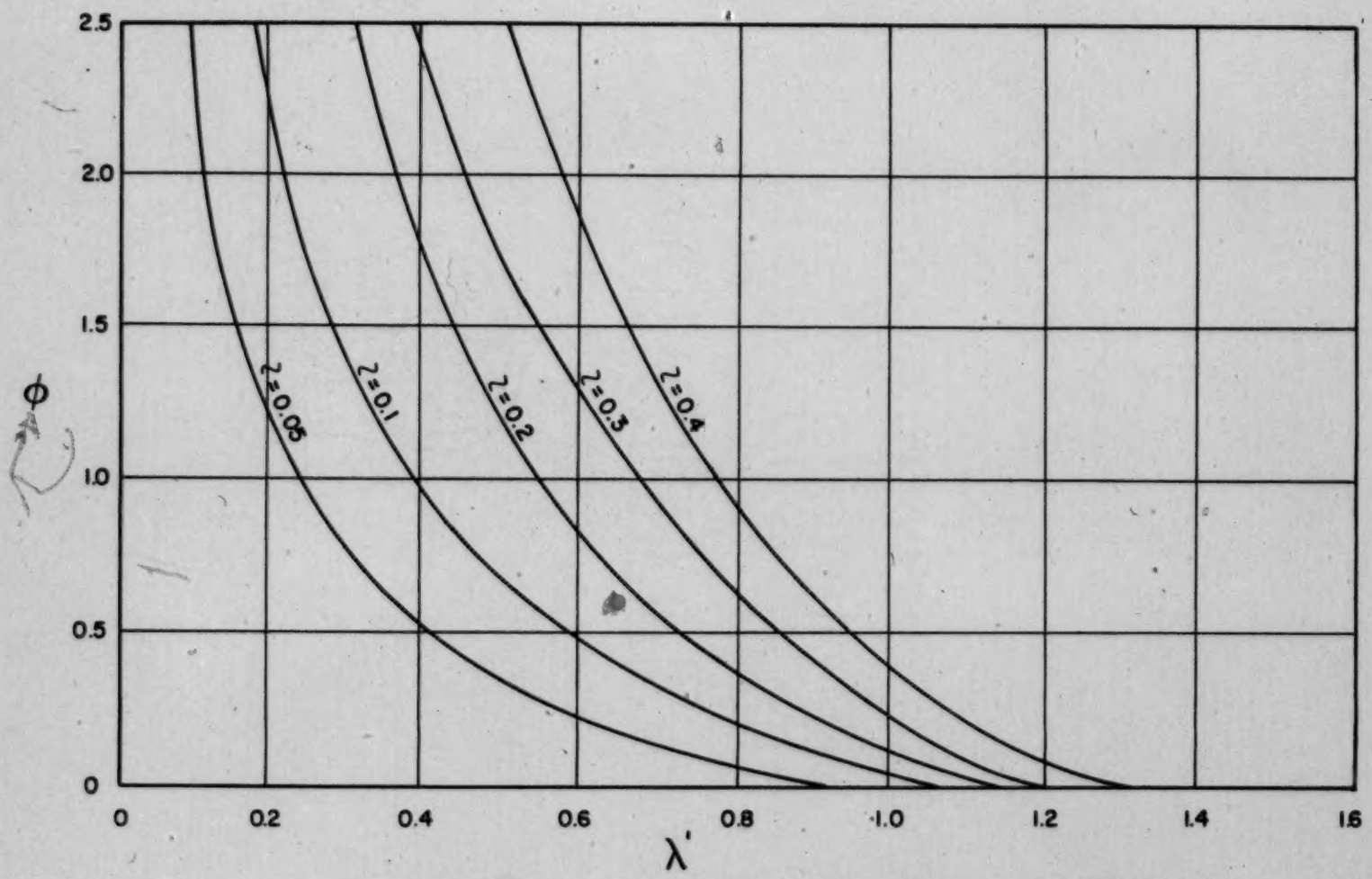

Figure 2.6 Blekhman function ϕ for penetration, after Catoire (1963).

$$th=\pi\times Wt\times h\times\omega\times\psi(\lambda',\iota)/(g\times S) \qquad (2.29)$$

where $\psi(\lambda',\iota)$ is a function of the previously defined dimensionless parameters λ' and ι, th is the required time to drive a pile to depth h. The function ψ is shown in Figure 2.7. To get that equation, equation 2.25 was integrated. The point resistance was assumed constant with depth whereas the side resistance was assumed to vary linearly with depth (z):

$$S=\delta w\times p\times z \qquad (2.30)$$

where δw is the side resisting stress given in Table 2.7 for various pile and soil conditions and p is the perimeter of the pile section. Where there is more than one stratum, a summation of the side resistance in each stratum has to be carried out. In such a case, z becomes the thickness of the considered stratum.

The maximum depth of penetration, hm, is given by:

$$hm=(F_o+Wt-J)/(p\times\delta w) \qquad (2.31)$$

During driving, energy is spent to overcome the side wall friction and the point resistance. To drive a pile, a driver must at least supply the consumed energy:

Table 2.7

Side resisting stress for various pile and soil types,

after Catoire(1963).

Soil Type	Soil resistance stress on pile wall				
	Piles (t/m²)			Sheet piles (t/m)	
	wooden piles, metal tubes	reinforced concrete piles	open RC and tubular pre-drilled caissons	light	heavy
Saturated sandy soils, soft to firm plastic clays	0.6	0.7	0.5	1.2	1.4
Same as above but interbedded with stiff clay or dense gravel	0.8	1.0	0.7	1.7	2.0
Low plasticity clayey soils	1.5	1.8	1.0	2.0	2.5
Very stiff to hard clayey soils	2.5	3.0	2.0	4.0	5.0

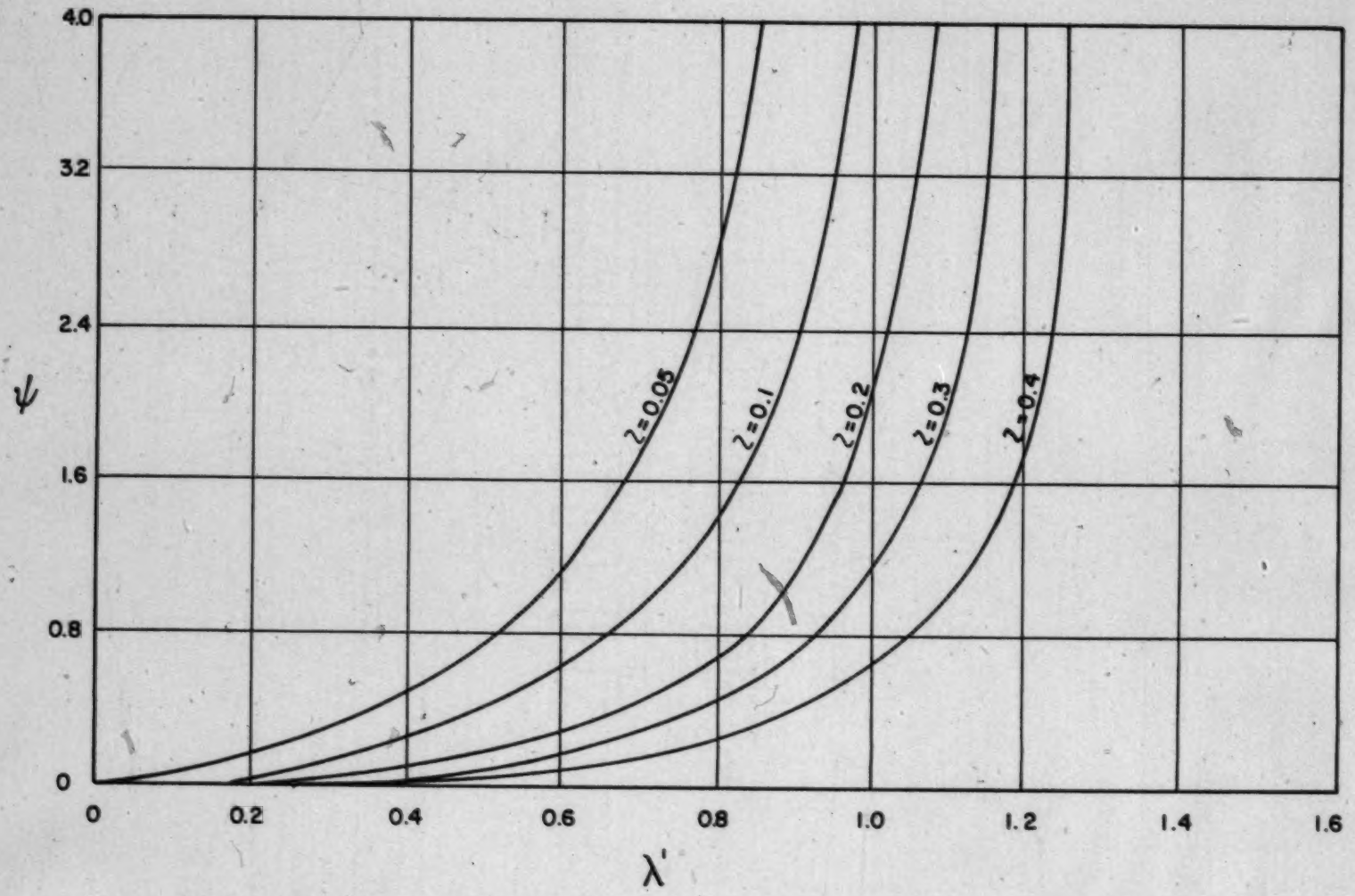

Figure 2.7 Blekhman function ψ for driving time, after Catoire (1963)

$$P=((2\times S\times M\times\omega/(\pi\times Wt))\times\sqrt{(1-4\times S/(\pi\times F_o))})+J\times rp \qquad (2.32)$$

All the simplified theoretical relationships that were reported in this sub-section are useful to make a comparative study of the various types of vibrators, according to Catoire (op. cit.).

2.4.1.4 Conditions for Driving

The conditions for successful driving of piles in soil, as briefly seen in the previous section, are that

1. the vibratory force be larger than the soil resistance for the considered depth. Introducing a coefficient e to take into account the elasticity of the soil, equation 2.17 becomes

$$F_o=M\times\omega^2/g\geq e\times S \qquad (2.33)$$

where $0.6\leq e\leq 0.8$ for low frequency vibrators, $e=1.0$ for high frequency vibrators and $0.4\leq e\leq 0.5$ for variable frequency vibrators operating in the very low frequency range, 5 to 10 Hz. S is calculated as per equation 2.30.

2. the oscillatory displacements must be amplified enough to overcome the soil elastic displacements. When the displacement is close enough to the undamped value M/Wp, the condition can mathematically be expressed as:

$$b \times M/Wp \geq dr \qquad (2.34)$$

where dr is the required tip displacement and b a dimensionless pile displacement coefficient. The coefficient b is taken as 0.8 for reinforced concrete piles and 1.0 for any other type of piles. Values of dr are given in Table 2.8 for different types of soils and piles.

If b is neglected, equations 2.14 and 2.24 substituted for d and F_e, and equation 2.34 blended with equation 2.33, the second condition expressed in equation 2.33 is obtained in terms of frequency:

$$\omega \geq e \times g \times S/(Wp \times vr) \qquad (2.35)$$

where vr is the required oscillation velocity which can be taken as 0.5 to 0.8 m/s for a first estimate.

3. the resultant of all external forces applied to the pile guarantees penetration:

$$Wt \geq \sigma r \times A \qquad (2.36)$$

and

$$n_1 < F_e/Wt < n_2 \qquad (2.37)$$

where σr is the required average tip pressure on the soil, n_1 and n_2 are coefficients that depend upon the nature of the pile. n_1 and n_2 take the following values:

Table 2.8

Necessary oscillatory displacement of pile tips,

after Catoire(1963).

Pile Type	dr (mm)					
Soil Type→	Sandy Soils			Clayey Soils		
Frequency→(Hz)	5-11.7	13.3-16.7	20-25	6.7-11.7	13.3-16.7	20-25
Metal piles; open-end tubular piles and piles of section less than 100 to 150 cm²		8-10	4-6		10-12	6-8
Wooden piles and closed-end tubular metal piles of section less than 800 cm²		10-12	6-8		12-15	8-10
Reinforced concrete piles, square or polygonal, of section less than 2000 cm²	12-15			15-20		
Large diameter tubular reinforced concrete caissons driven in pre-drilled holes	6-10	4-6		8-12	6-10	

a. for metal piles, $n_1=0.15$ and $n_2=0.50$;

b. for light piles, $n_1=0.30$ and $n_2=0.60$;

c. for heavy piles, like concrete piles, and tubular caissons, $n_1=0.40$ and $n_2=1.0$.

The recommended values for σr are

a. for small diameter metal piles ($A \leq 150$ cm^2):
$1.5 \leq \sigma r \leq 3.0$ kg/cm^2;

b. for wooden and closed end metal pipe piles ($A \leq 800$ cm^2):
$4.0 \leq \sigma r \leq 5.0$ kg/cm^2;

c. for reinforced concrete piles of rectangular or square cross-sectional area less than 2000 cm^2:
$6.0 \leq \sigma r \leq 8.0$ kg/cm^2.

2.4.1.5 Practical Use of Driving Equations

To properly use the equations of section 2.4.1.3, the following steps must be taken:

1. find S for the desired driving depth as per equation 2.30, parting the soil into strata if necessary;
2. knowing the weight of the pile and its type, determine M from condition 2.34. After, find ω from equation 2.33. If it is not known in which frequency range ω will be, equation 2.35 has to be used to find ω.
3. Using equation 2.36 to find the minimum weight required for penetration, the bias weight can now be deduced. Equation 2.37 also has to be satisfied. If the ratio F_o/Wt is too low, the vibrator force has to be increased

and if the ratio is too high, the bias weight has to be increased.

4. The final values of eccentric moment, angular frequency and total weight are picked and verified following the method of section 2.4.1.4.
5. The power can be calculated from equation 2.32 or from Sinelnikov's formula (in kilowatts):

$$P \approx 3 \times 10^{-8} \times M^2 \times \omega^3 / Wp \qquad (2.38)$$

Where M and Wp are respectively in Newton-meters and in Newtons. The formula includes a 20% allowance for the energy spent to excite the surrounding soil.

2.4.2 Soil Reactions and Penetration

After the work of the Soviets, no engineering theory was derived to predict the penetration rate and depth of piles driven by vibrations. Probably because of the limited access to Soviet theory, the predictions in the western world, at least in North America, have always been based chiefly on experience. It is true though that several attempts were made to fit equations to penetration versus time curves. Undoubtedly the most noteworthy of such attempts is that carried out by Littlejohn and Rodger (1980).

Some explanations of penetration like the vibroviscosity of the surrounding soil are appealing,

academically speaking, but have shortcomings when time comes to explain some field behaviors as was discussed in the previous section. In order to provide a good understanding of the mechanics of penetration, the efforts of Smart (op. cit.) are first examined. The discussion then goes on with the findings of the Princeton group of researchers who shed light upon the soil reactions at the tip of a pile. This prepares the reader for the classification of vibratory driving proposed by Littlejohn and Rodger (op. cit.). Finally, to conclude the section, a brief discussion on the latest elasto-plastic penetration theory is presented.

Because the predictions are based primarily on experience, Smart (op. cit.) tried to provide a theoretical framework for an intelligent use of the acquired field experience, which is summarized in Tables 2.9 and 2.10. For that, he looked at the impulse and momentum relation of the driver-pile-soil system:

$$(-1/T)\int_{t}^{t+T} Ps \times dt = mb \times (g - \Delta rp/T) \qquad (2.39)$$

where Δrp is the change in penetration rate over one motion period, Ps the total instantaneous soil reaction and mb, the mass of the system, considered to be the bias mass for all practical purposes. The crane reaction is assumed to be zero and the term $\Delta rp/T$ represents the acceleration of the translatory motion. By inspection it can be seen that the weight of the system, represented by the right hand side of

Table 2.9

Performance of the resonant driver in granular materials

(sands, silts, gravels) for small area piles, after Smart (1969)

STEEL PILE TYPE	LOOSE N<10*	MEDIUM 10<N<30	DENSE 30<N<50	VERY DENSE N>50	MISCELLANEOUS MATERIALS
H-Pile 356 mm 174 kg/m 132 kg/m 109 kg/m	Satisfactory	Satisfactory	Satisfactory	Satisfactory	Rip-rap: satisfactory Cemented sands: poor V. dense silty fine sand fill: poor
H-Pile 305 mm 79 kg/m H-Pile 254 mm 85 kg/m	Satisfactory	Satisfactory	Satisfactory	Satisfactory	
H-Pile 254 mm 62 kg/m H-Pile 203 mm 54 kg/m	No Experience	Satisfactory	Satisfactory	Satisfactory	Brick & Rockfill: Satisfactory
Pipe 1829 mm 13 mm wall	No Experience	Satisfactory	No Experience	No Experience	
Pipe 406 mm 10 mm wall	No Experience	Satisfactory	Satisfactory	No Experience	

Notes:

*Standard penetration test in blows/30 cm
.Satisfactory means penetration time of the order of 15 minutes and design depth reached
Poor means slow penetration and/or refusal above desired depth

Table 2.10

Performance of the resonant driver in cohesive soils

(clayey materials) for small area piles, after Smart (1969)

STEEL PILE TYPE	SOFT qu<24*	MEDIUM 48<qu<96	STIFF 96<qu<192	VERY STIFF 192<qu<384	HARD qu>384
H-Pile 356 mm 109 kg/m	Satisfactory	Satisfactory	No Experience	No Experience	No Experience
H-Pile 305 mm 79 kg/m H-Pile 254 mm 63 kg/m	No Experience	No Experience	Satisfactory	Satisfactory	Satisfactory
Pipe 406 mm 10 mm wall	No Experience	No Experience	No Experience	Satisfactory	Satisfactory

Notes:

*Unconfined compressive strength in kPa.
Satisfactory means penetration time of the order of 15 minutes and design depth reached

the equation, is equal in magnitude but opposite in direction to the total instantaneous soil reaction averaged over one motion time period. If the penetration rate increases, the average soil reaction decreases and vice-versa.

To explain penetration with equation 2.39, Smart (op. cit.) discussed qualitatively the average reactions from the pile walls and from the pile tip. Elasto-plastic soil behavior was found to be the most satisfactory model for explaining penetration. It was also found that elastic soil reactions along the walls and, or, at the tip explained refusal. Hence the need of large enough displacements to ensure penetration.

Smart's (op. cit.) conclusions were that:

1. viscous soil behavior to explain pile penetration has no basis;
2. the soil needs to be strained to a point of plastic deformation for penetration to occur;
3. the correlation of soil conditions and vibratory driver performance is probably the best approach if it is properly guided by a theory of oscillation and translation;
4. minimum tip double amplitudes of about 3.8 mm are required for penetration in granular materials;
5. incomplete data and experience in cohesive soils inhibits definite conclusions about the necessary tip displacements.

Littlejohn and Rodger (op. cit.) went further in their review of vibratory driving. After formulation of an elasto-plastic penetrative motion for vibration-driven piles, they claim that it is not necessary to exactly explain the mechanics of penetration. Penetration will occur as long as the total dynamic and surcharge forces are larger than the soil resistance. The elasto-plastic reaction mechanism, first pointed out by Smart (op. cit.), was substantiated by Schmid (op. cit.) after the work of Ghahramani (op. cit.). They identified three domains of dynamic soil response:

1. The Sinusoidal Resistance Domain in which the elastic soil resistance is larger than the dynamic driving force. No plastic motion is allowed and hence no penetration occurs. The dynamic soil response varies sinusoidally in phase with the dynamic loading force.
2. The Impact Domain in which the dynamic driving force has exceeded the elastic resistance threshold but still remains below an impact threshold. The notion of impact threshold will clarify itself as the reader moves on. The dynamic response of the soil, at the pile tip, is a distorted sine wave gradually becoming impact peaks of short duration separated by longer periods of loss of contact with the soil.
3. The Instability Domain in which the maximum tip resistance is reached. The dynamic driving force has exceeded the total dynamic soil resistance or impact

threshold. The wave form is short impact peaks separated by longer periods of loss of contact with the soil. A phase difference occurs between the tip resistance and the driving force. Further increase of the dynamic force beyond the impact threshold only increases the kinetic energy of the pile, hence increasing its acceleration.

The impact threshold sinusoidal force was found to vary with frequency and surcharge, Ghahramani (op. cit.). The higher the frequency, the lower the threshold is and the higher the surcharge, the higher the threshold. He also found that the impact time duration did not vary significantly with force, surcharge or frequency for a given soil. Hence, it can be considered as a soil property.

Littlejohn and Rodger (op. cit.) confirmed the above findings in their experiments. From there, they classify vibratory driving as fast and slow. Fast driving is when the penetrative motion is due to the progressive compactive collapse of the voids in the soil, assuming that any resistance is attributable to reduction in shear strength of the soil. Fast driving is characteristic of loose granular soils. Slow driving, on the other hand, occurs when an elasto-plastic impact situation arises. The end resistance is elasto-plastic whereas the side resistance is viscous. Slow driving is typical of dense granular soils.

Under the assumption of fast and slow driving, Littlejohn and Rodger (op. cit.) arrive at two most

interesting mathematical models, one for each type of driving. For fast vibratory driving, they treat the vibratory and penetrative motion separately. They assumed that the sole purpose of the vibratory motion is to reduce resistance to penetration. The shear resistance per unit length of pile is assumed independent of depth and end resistance is assumed proportional to depth. The authors arrive at two differential equations of motion: one for the penetrative motion and one for the vibratory motion. Because fast vibratory driving is rarely encountered, the equations are not solved. The motion considered in the elasto-plastic model of slow vibratory driving is more complex. It consists of periods of penetration during which resistance is plastic, separated by phases of reversal of motion and recovery against elastic soil resistance. The reversal motion may be large enough to cause a loss of contact between the pile and the soil. If loss of contact occurs, there is no end resistance during part of the reversal phase. The model for slow driving consists of one differential equation which satisfies static equilibrium of the penetrative motion curve at all times. This equation is complex in form since it involves a time dependent side resistance and a displacement and time dependent end reaction.

To solve the complex differential equation, the authors resorted to numerical methods. Their approach to the solution of the problem was to develop an interactive

computer simulation of the theoretical equations and then perform a parametric study. The theoretical simulation was fitted to the results of the parametric study. Hence, the solution is semi-empirical in nature.

Littlejohn and Rodger (op. cit.) undertook an experimental pile driving program to verify the theory. Soil resistance parameters were varied to fit the computer model to the test results. The simulation proved successful and showed that soil resistance increases exponentially with depth. Lack of knowledge about the initial soil parameters and their exact relationship with depth, acceleration and displacement amplitudes is the limitation of the model as of now.

2.5 Bearing Capacity

To find out wether there are any disadvantages to place a pile by resonant driving, Smart (op. cit.) conducted a review and carried out a study of comparative bearing capacity tests between impact-driven and vibration-driven piles from which the following conclusions were drawn.

2.5.1 In Granular Soils

The ultimate total capacity in granular soils are about the same regardless of the driving method. When broken down

into its two components, the skin friction[7] and the point bearing, vibration-driven piles get a larger portion of their ultimate capacity from skin friction compared to impact-driven piles. This was also substantiated by Hunter and Davisson (1968).

It is believed that while particles jar loose beneath piles during vibratory driving, they rearrange to a denser state around them. Conversely, soil beneath impact-driven piles densifies. The combined action of these two effects is, as previously stated, to increase the relative contribution of skin friction to the total bearing capacity for vibration driven piles, or to increase the point bearing in the total bearing capacity for impact-driven piles with respect to vibration-driven piles.

2.5.2 In Cohesive Soils

In cohesive soils, less data is available than for granular soils. However, pipe piles driven in clays by vibrations were observed to have a higher bearing capacity than their impact-driven counterparts in the same material. The high frequency vibrations of resonance are thought to improve the adhesion of the soil to the pile wall, hence the increased bearing capacity.

---

[7] Resistance or part of bearing capacity due to the friction at the pile-soil interface.There is no soil adherence to the pile in granular materials.

2.5.3 Point Bearing Piles

Point bearing piles, particularly on weathered bedrock, have not performed as well when driven by vibration as when driven by impact. This is attributed to the fact that piles sunk by vibration can not as effectively displace large chunks of weathered or broken rock to sit securely on a firm base as impact-driven piles. It should be recalled that particles beneath an impact-driven pile densify, hence the better performance than the vibration-driven piles.

2.5.4 Conclusion

From the above observations, it has been shown that the bearing capacity of vibration-driven piles is better than that of impact-driven piles in cohesive soils, equivalent to that of impact-driven piles in cohesionless materials and inferior to that of impact-driven piles under point bearing.

2.6 Summary of Actual Understanding

The present status of theoretical understanding of high frequency or resonant vibratory driving in unfrozen ground is summarized in the following lines.

The resonance frequency of a real pile driven in any type of soil lies between the theoretical free tip and fixed tip resonance frequencies. The actual resonance frequency can be predicted with fair accuracy using equations 2.5 or 2.6.

A pile-soil-driver system has a flat peak resonance associated with rigid-body motion of the pile and resonance frequency of the soil. During rigid-body motion the pile does not deform, or in other words, the tip displacement is unchanged from the top. Most of the low frequency driving takes place in the range of frequencies associated with rigid-body motion. Rigid-body motion of piles occurs when the excitation frequency is lower than about one quarter the resonance frequency. At resonance, tip displacements can be up to twenty times larger than input displacements.

Vibratory driving can be classified into fast and slow driving. The first is associated with the progressive compactive collapse of soil voids beneath the pile and the second with elasto-plastic tip reactions. Fast vibratory driving is a condition for which resistance to penetration is attributable to a reduction in shear strength of the material in which the pile is driven. Slow vibratory driving occurs when an elasto-plastic reaction occurs at the pile tip. Then, side reactions are viscous and small when compared to tip reactions. The elasto-plastic reaction at pile tips can be classified in three ranges depending upon the magnitude of the driving force:

1. the Sinusoidal Resistance Domain,
2. the Impact Domain,
3. the Instability Domain.

These three Domains were described in detail in Section 2.4.2.

Finally, the total bearing capacity of vibration-driven friction piles is the same or larger than the total bearing capacity of impact-driven friction piles. This, however, can not be said of point bearing piles because of the inability of vibratory drivers to displace large chunks of rock to sit firmly on unweathered bedrock.

CHAPTER 3

HIGH FREQUENCY DRIVING IN PERMAFROST

The need for driving large numbers of piles in permafrost being fairly recent, resonant driving was first tried in the late 60's-early 70's by Raymond International Inc. for the Alyeska Pipeline Co.. The method proved to be the most time effective in placing piles directly in permafrost following a series of field tests conducted at various sites in Alaska. However, there were a few drawbacks: the high rate of breakdown of the driver and the unreliability of driving in cold coarse grained materials (Huck and Hull (1971) and Hull (1977)).

The technique of driving at resonance is also applied to the retrieval of statigraphically intact but structurally disturbed permafrost cores in the Arctic (Huck and Hull (op. cit.), Hayley (1979)). Since the pipe sizes involved are much smaller (less than 200 mm) and the powers much lower (less than 75 kW), coring of soil samples will not be dealt with in this discussion.

The Soviets do not use resonant driving to place their piles in permafrost. Their technique is a blend of impact and low frequency driving associated with pre-drilled holes. A section of this chapter will outline the technique used in the Soviet Union. Before this is done, conclusions from field observations on the resonance frequency, the

penetration and the temperatures at the tip of piles driven in permafrost will be reported under separate headings.

3.1 Resonance Frequency

A study of longitudinal resonance frequencies by Kovacs and Michitti (op. cit.) reported field data of piles driven in permafrost. The data reported from frozen and unfrozen soils were very similar. Therefore, this allows a similar conclusion as was drawn in chapter 2 to be applied to piles driven in frozen soils. It is that the resonance frequency depends solely upon the physical properties of the pile.

3.2 Penetration

Huck and Hull (op. cit.) reported on the resonant driving tests performed at various sites in Alaska. The basic soil profiles at the sites are shown in Figure 3.1 and the test data are presented in Table 3.1. The result show that resonant pile driving is feasible in each type of soil tested. The rate of penetration in coarser materials is lower than in the finer materials. Cobbles and boulders can inhibit pile penetration. Massive ice bodies do not offer a major obstacle as a rate of 9.2 m/min was reported when driving through such a layer at the Alaskan Field Station.

During penetration, it was observed that a slurry was expelled along the sides of the piles as the pile advanced. Hence, it is believed that penetration is associated with

Table 3.1

Bodine resonant driver - 100

performance in permafrost, after Huck & Hull(1971)

(For piles larger than 200 mm)

SITE	TEST #	PILE TYPE & SIZE	PILE AREA (cm^2)	DRIVEN DEPTH (m)	PENETRATION AVERAGE (m/min)	PENETRATION ULTIMATE (m/min)	REMARKS
Alaska Field Station	1	Pipe 273 mm	30	5.49	1.70	0.80	Distorted tip
	4	Pipe 219 mm	42	5.79	6.09	3.05	
	5	H - 150 mm 37 kg/m	47	9.83	1.50	0.68	
	6	H - 150 mm 23 kg/m	29	8.23	4.81	3.66	
	7	Pipe 273 mm	40	4.57	1.54	1.66	Distorted tip
	9	Pipe 219 mm	29	5.61	2.94	1.52	
	20	Pipe 273 mm	30	5.11	0.60	1.41	Distorted tip
	36	Pipe 219 mm	42	5.69	4.15	1.52	Distorted tip
	37	H - 150 mm 37 kg/m	47	5.18	6.31	2.03	
	38	Pipe 273 mm	40	5.05	3.97	1.83	Distorted tip
	42	Pipe 273 mm	30	4.42	2.51	2.03	Distorted tip
	43	Pipe 219 mm	29	4.39	7.96	1.83	Distorted tip
	45	H - 150 mm 37 kg/m	47	5.64	8.71	4.57	
	47	H - 150 mm 23 kg/m	29	5.64	8.32	2.62	
Goldstream Creek	12	H - 150 mm 23 kg/m	29	8.23	3.51	1.02	

Table 3.1 (Cont'd)

Bodine resonant driver - 100

performance in permafrost, after Huck & Hull(1971)

(For piles larger than 200 mm)

SITE	TEST #	PILE TYPE & SIZE	PILE AREA (cm^2)	DRIVEN DEPTH (m)	PENETRATION AVERAGE (m/min)	PENETRATION ULTIMATE (m/min)	REMARKS
Goldstream Creek	14	Pipe 219 mm	42	5.49	0.59	0.16	Core of active zone soil removed before final drive
	15	Pipe 219 mm	42	7.87	1.02	0.48	Core of active zone soil removed before final drive refusal with full core
	16	Pipe 219 mm	29	8.23	0.80	0.35	Core of active zone soil removed before final drive refusal with full core
	17	Pipe 273 mm	30	5.46	0.91	0.20	Core of active zone soil removed before final drive
Chatanika	24	Pipe 219 mm	29	5.13	2.85	0.97	Distorted tip

Table 3.1 (Cont'd)

Bodine resonant driver - 100

performance in permafrost, after Huck & Hull(1971)

(For piles larger than 200 mm)

SITE	TEST #	PILE TYPE & SIZE	PILE AREA (cm²)	DRIVEN DEPTH (m)	PENETRATION AVERAGE (m/min)	PENETRATION ULTIMATE (m/min)	REMARKS
Chatanika	25	Pipe 219 mm	42	4.57	0.93	0.27	Core of active zone soil removed before final drive
	26	H - 150 mm 37 kg/m	47	4.11	1.02	0.22	
Eielson Air Force Base	28	H - 150 mm 37 kg/m	47	3.56	0.42	0.31	
	29	H - 150 mm 23 kg/m	29	3.07	0.77	0.16	
	31	Pipe 273 mm	30	2.74	0.79	0.24	Distorted tip
	32	Pipe 273 mm	40	2.82	0.82	1.02	Distorted tip
	33	Pipe 219 mm	29	3.15	0.82	0.15	Distorted tip
	34	Pipe 219 mm	42	2.92	1.30	0.55	

a) ALASKA FIELD STATION

0.0	Surface Active zone: organic silt
3.05	Silt (vs) occasional bands of organic material
11.58	Massive ice
14.63	Sand and gravel to 50 mm size (Nb)
17.58	End of hole

b) GOLDSTREAM CREEK BRIDGE

0.0	Surface Active zone: organic silt
2.74	Organic silt (Vr)
4.57	Organic sandy silt (Nb)
7.62	Silty fine to medium sand (Nb)
10.67	Medium sand (Nb)
12.80	End of hole

Figure 3.1 Basic soil profiles at Alaskan test sites, after Huck and Hull (1970).

c) CHATANIKA VILLAGE

0.0	Surface Active zone: sand & gravel
1.83	..... Gravel and cobbles to 150 mm cemented with fine sand & silt (Nb)
7.92	..... End of hole

d) EIELSON AIR FORCE BASE

0.0	Surface Sand and gravel
1.52	..... Sand & gravel to 50 mm (Nb)
4.11	..... Sand & gravel with cobbles to 125 mm
4.57	..... End of hole

Note: Temperatures were estimated between -2.8°C and -0.6°C; depths to permafrost varied from 0.6 to 3.35 m.

Figure 3.1(Cont'd) Basic soil profiles at Alaskan test sites, after Huck and Hull (1970).

melting at the tip of the pile. Mechanical energy changes to thermal energy at the tip of the pile. The extent of thaw on retrieved inner cores was measured to be 3 mm thick on average with occasional depths of 10 mm.

3.3 Temperature at Pile Tip

Tip temperatures during resonant driving in permafrost have not been measured. The only indication of their order of magnitude comes from the Soviet experience in driving piles with low frequency vibrators. They instrumented, with thermocouples, piles that were driven at frequencies ranging from 8 to 17 Hz with input double amplitudes of 20 to 30 mm. The next section gives more details on the method they currently use. It is just necessary to point out that the piles were driven by vibration in an undersized hole whose core had previously been extricated by a vibrating leader. Vyalov and Targulyan (1968) and Vyalov et al. (1969) report temperatures of up to 40°C near the tip of the leader and varying between 10° and 30°C on the skin of the pile and leader.

3.4 Soviet Experience

Vyalov et al. (op. cit.) and Vyalov and Targulyan (op. cit.) report on the vibratory driving method used in the permafrost areas of the Soviet Union. It is to be noted that most of the permafrost in which the work reported was

carried out was warm ($\theta > -1°C$). The vibratory method has one variant: a cutting point leader is added to the tip of the pile. This variant is termed the impact-vibration method because of its penetration mechanism as it will be seen later.

A low frequency vibrator, 8 to 17 Hz, intensely transmits energy to the pile and further to the soil. The input oscillation amplitude range from 20 to 30 mm. The energy is expended to raise the temperature of the surrounding soil by heat transfer at the tip and by friction along the sides. The friction along the sides creates a film of liquified thawed permafrost. Hence, the friction opposing the pile motion along the side of the pile is reduced to a very low level, just expending enough energy to maintain the slurry. The method is most successful with open end pipe piles because of their small point resistance, a direct result of their small cross-sectional area.

The variant is, as briefly mentionned before, to add a cutting point leader to the tip of the hollow pile. Then, the major portion of the energy is spent to push the cutting point into the frozen soil. The cutting point partly loosens the soil which thaws near the point. A slurry is formed near the point and pushed to the surface through the thawed film along the sides of the pile as the pile advances. Hence the impact-vibration name. Because of the high frequency of the impacts with respect to conventional impact driving, the energy can not be all diffused through

the thawed film and therefore concentrates near the skin of the pile. The effect is to increase the temperature of the skin of the pile.

To drive piles, a hollow pipe with a cutting point is introduced in the soil. The core of the pipe is extricated as the assembly is pulled out of the hole. A pile of a slightly larger diameter than the hole is then vibrated into place. The piles need not be round in section nor hollow since they are driven in a hole. In fact, square reinforced concrete piles are often used in the Soviet Union.

3.5 Conclusion

Both the Soviet experience with low frequency driving and the North American experience with resonant vibratory driving led reporters to conclude that mechanical energy is changed into thermal energy at the tip of the pile to allow penetration by melting in frozen soil. Although this mechanism is unclear and undefined, there is a conscensus about it in the literature.

If the melting explanation is accepted, it can be reasonned that low frequency driving is not as effective in permafrost cooler than in the Soviet reports because it can not deliver enough energy to thaw the soil and hence permit the pile to advance. This is exactely what the Alyeska field tests concluded.

To say that thawing only governs penetration of piles in permafrost is to oversimplify the problem. Thawing is likely to be an important consumer of energy because of the existence of the thawed film, but energy spent to displace the material has to be considered, especially as penetration increases. All aspects to be considered to clarify the penetration mechanism of piles driven by vibrations in permafrost will be discussed in the next Chapter.

CHAPTER 4

EXPERIMENTAL PROGRAM

Following the discussion of Chapter 3, the global energy balance of a pile-soil-driver system has to be carefully examined. Before this is done and that an experimental program is drafted, it is good to meditate on the energy which can effectively be delivered to the soil in both cases of model piles and full size or real piles. This will allow general concepts of pile-soil behavior to be brought forward. At that point, a testing material will be selected and thought will be directed to the parameters which should be measured or evaluated in order to provide weight to the ideas brought forward. The testing program will be outlined in the last part of this Chapter.

The reader interested in a description of the testing apparatus and facilities of the Department of Civil Engineering is referred to Appendix A. Similarly, those interested in the experimental procedure, beginning with the sample preparation, can refer to Appendix B.

4.1 General Concepts of Model Pile Behavior

In a first reflection, let us look at the resonance frequencies and the energy produced by that particular pile motion. A real pile, 10 to 30 m long, will have its

resonance frequency lying in the range from 50 to 170 Hz, according to the discussion of section 2.2. The power delivered to the pile and, as a result, the energy consumed in resonance can be one order of magnitude larger than the energy consumed by the rigid-body motion. This is because the force is magnified, the underlying material sustains large displacements and there is some geometric body wave dispersion of the said energy.

In a model pile, 30 to 50 cm long, the resonance frequency will be in excess of 3000 Hz. The displacements are inversely proportional to the frequency as was discussed in section 2.3. They are also inversely proportional to the square of the frequency if the acceleration is held constant. Rigid-body displacements occur when the frequency is less than about one quarter of the resonance frequency (refer to section 2.3). Rigid-body displacements develop when the displacements at the top of the pile are transmitted almost completely to the tip of the pile. Verification of the laboratory driver (B&K 4812 exciter) specifications shows that amplitudes of 1 to 5 mm occur at low frequencies while at 3000 Hz or more (resonance of model piles) 4 to 5 orders of magnitude lower displacement is achieved. Since the exciter delivers an approximately constant force, the energy delivered at resonance (force times displacement) is several orders of magnitude less than that delivered at low frequencies (less than 200 Hz).

Preliminary driving tests showed that penetration indeed could not be achieved at resonance of the model pile. The pile penetrated best at frequencies of 60 to 80 Hz. Schmid (op. cit.) observed that there existed a rigid-body type of resonance which has a rather flat peak (e.g. a low amplification compared to the pile resonance), in other words a low magnification (refer to section 2.2). The excitation frequency at that rigid-body type of resonance was very low with respect to the pile resonance frequency: 80 Hz versus more than 3000 Hz. Considering that frozen soil is stiffer than unfrozen soil, such a resonance may well occur in the experiments. All the studies to date on the dynamic response of frozen soils have been carried out for very low (≤10 Hz) or very high frequencies (≥1000 Hz), Anderson and Andersland (1978). Therefore, the dynamic response of frozen soils in the frequencies of interest (50-100 Hz) is left open to speculation.

The important conclusion to draw from the above discussion is that the problem of pile driving by vibrations in frozen ground should be approached in terms of energy consumption. In other words, in a real case the optimum amount of energy transmitted to the tip of the pile occurs at resonance while in a model pile it occurs at a resonance associated with a rigid-body type of motion. The following section will focus on the various components of the energy balance.

Since a global picture of the problem has been drawn, a specific testing material should be selected before experiments can be detailed further. An inexpensive and well known material, geotechnically speaking, is desired. To examine the promising avenue of the energy approach, a clean, thermodynamically simple and chemically inert material is extremely desirable. For the above reasons, Ottawa sand was selected. It is a uniform, rounded to subrounded, white, medium-grained sand. A typical grain size curve is shown in Figure 4.1. This material can be used in a loose or dense state by simply changing the water content and the placement method.

4.2 Independent Variables and Measurable Quantities

The main components of the energy balance for vibratory pile driving are:

1. Energy transferred to soil as heat (at the tip and along the sides);
2. Energy lost to soil as body waves;
3. Energy expended to displace soil to make room for pile.

These energy components can not be measured directly but can be evaluated either qualitatively or quantitively from measurements taken during tests. The third component of energy listed above is complex to evaluate. The method used for its analysis will be explained in details in Section 5.2 of the next Chapter. Hence, no more will be

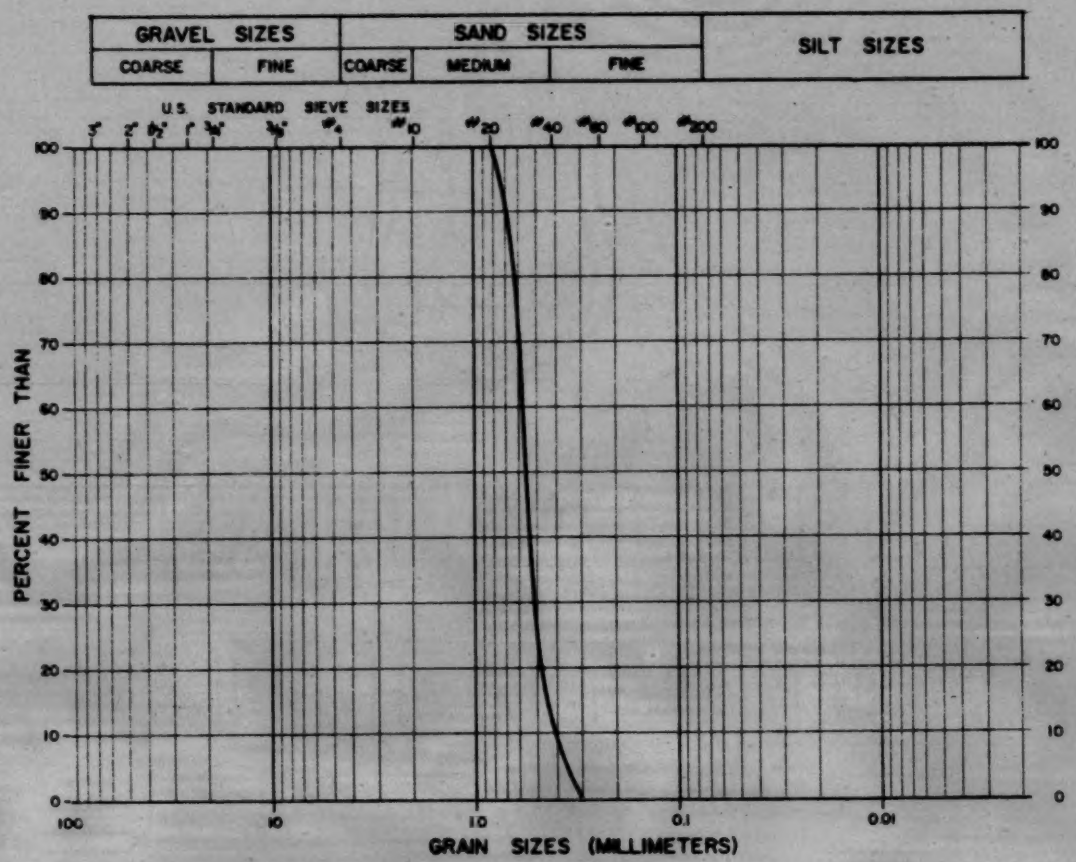

Figure 4.1 Grain size curve for Ottawa sand used as the experimental material

said about it in this Chapter.

The first two global energy components are treated for the remainder of this Chapter as dependent variables. Pile oscillatory displacement and penetration rate are also dependent variables. In the driving problem, the independent variables could be identified as:

- sample temperature (θ);
- bias surcharge (mb or Wb);
- driving frequency (f);
- ice content;
- soil density (ρd).

After all the variables have been identified, one way or another has to be found to evaluate them. The variables will now be discussed one by one in the following sections along with the method used to measure them. Independent variables will be discussed before dependent variables.

4.2.1 Sample Temperature

The temperature has a definite influence on the strength of the frozen soil used as a sample. It influences the amount of unfrozen water in fine grained soils and the strength of the ice in any frozen soil. A lengthy discussion is unnecessary since the interested reader can refer to Anderson and Andersland (op. cit.) for details on the influence of temperature on frozen soil behavior. Let it just be known for our purposes that, generally speaking, the cooler the temperature, the stronger the soil is.

Thermocouples within the sample were used to measure its temperature in the first series of tests. Time to freeze as well as time to reach a new equilibrium when the room temperature is changed was evaluated. Two days were found to be adequate for the sample to freeze. Twelve hours were found to be sufficient for a sample to reach a new room temperature. Thermocouples were not used in all samples because they are cumbersome and favor differential water flow along them during freezing. This is because of the volume expansion of water freezing from the bottom of the sample toward the top during the sample preparation (Appendix B.1 and B.2).

4.2.2 Bias Surcharge

The bias surcharge, as was discussed in section 2.4, has a definite influence on the magnitude and type of soil response. It has to be large enough to ensure penetration. That is, in our case, to make the soil response spikes described in section 2.4.2 larger than the soil elastic resistance if the penetration mechanism is similar to that of unfrozen soils, or to displace the molten soil if penetration is due to melting at pile tip.

In the experimental system used, the total load carried by the pile at rest is known. That is the effective load transferred to the top of the pile plus any losses that may occur in the transfer system (see Appendix A.2 for discussion). A load cell is placed between the pile and the

oscillator to measure the dynamic soil resistance during the experiment.

4.2.3 Driving Frequency

The driving frequency will determine the displacement and force passed to the pile and hence the amount of work done by the pile on the soil. The frequency of driving will preferably be at the rigid body resonance of the pile-soil system. This frequency ultimately depends upon the soil and pile characteristics. Therefore, it is not a thoroughly independent variable.

The driving frequency will be regulated from the exciter control digital read-out and can be checked from the accelerometer records of an experiment.

4.2.4 Ice Content

Ice gives frozen soil a great deal of its strength. Since ice weakens when warmed, the amount of ice will determine how much energy should be fed in the soil to thaw it enough for penetration of the pile to take place. Penetration occurs because resistance to driving in warmed frozen soil is less.

The material used in the experimental program was a uniform frozen sand. It should be pointed out that soil saturation and soil density are related. The same soil water content can theoretically exist for several densities at different saturation. But because of the uniform

character of our sand, it was impossible to ensure an homogeneous water distribution for conditions other than full saturation. Hence, only fully saturated samples were produced. Given the nature of the material, it is safe to assume that all the water present in the sand upon freezing has effectively changed phase. Therefore, the moisture content of a frozen sample is the same as its ice content. Samples for moisture content were taken from retrieved cores in good condition and also directly from the soil mass upon thawing. The dense samples were found to have an ice content of around 11% and the loose samples around 19%.

4.2.5 Soil Density

The denser a soil is, the more difficult it is to displace individual grains within the mass. It also is stronger. Two states of density were created: the loosest and the densest possible states. The actual procedure to achieve these two density states is outlined in Appendix B. The actual density of the soil sample was obtained by carefully recording the weight of all the saturated material after thawing. The volume of soil in the mould is of course known. The dry density was obtained by dividing the total density measured as above by one plus the ice content. Loose dry densities were consistently around 1.67 tonnes/m^3 and dense around 1.80 tonnes/m^3.

4.2.6 Pile Oscillatory Displacement

The displacements are critical in the evaluation of the work done by the pile as was previously emphasized. The accelerations were measured with the help of an accelerometer placed at the top of the pile. It is assumed, because of the rigid-body type of motion, that it represents exactly the behavior at the tip of the tube. The pile displacements were found from these accelerations by double integration.

4.2.7 Penetration Rate

Ultimately, one would like to predict the penetration rate of a pile. The rate likely depends on all the other variables enumerated in this section.

It was measured electronically using a Data Acquisition System to record the output voltage of a LVDT (linear voltage displacement transducer). Details are given in Appendix A.11.

4.2.8 Energy Transferred to Soil as Heat

This is a very difficult if not an impossible quantity to measure. It determines whether the soil is thawing enough to allow penetration by displacement of melted soil or by failure of weakened soil. Or, it could simply tell how much energy is expended in melting. The amount of soil melted by the pile can be evaluated by visually inspecting the surroundings of the pile after a driving test. Visual

inspection was rendered possible by the diffusion into the thawed film of a grey steel powder produced by the abrasive action of sand on the pile. It effectively dyed the thawed film. The thawed film was found to be quite constant in thickness for all soil temperatures. It was approximately 1.5 to 2.5 mm in thickness both on the inside and outside of the tubular model pile.

Successful attempts were made to fix RTD'S (F2105, series F1, Omega Engineering Ltd.) near the pile tip along the sides of the pile wall. Details on RTD's are given in Appendix A.10. A surface temperature was measured and an amount of energy obtained from heat analysis.

4.2.9 Energy Transmitted to the Soil as Body Waves

Some energy is lost under the form of body waves dispersing throughout the sample. A triaxial accelerometer measured the vibration level right in the center of a dense sample. Lack of availability of equipment has inhibited measurements in every sample. It is felt that extrapolation can be made from the few measurements without considerable error. The mass and physical size of the sample have to be taken into consideration when the measurements are analysed. The possible reflection of body waves from container sides must also be considered and evaluated.

4.3 Testing Program

Several aspects are involved in the evaluation and measurement of the various parameters affecting the penetration of piles in frozen grounds. One goal of the undertaken research is to define the influence of various parameters on the penetration rate of piles driven by vibration into frozen sand. Another objective is to find out whether there is any relationship between the energy consumed at the tip of piles during driving and the penetration rate of the said piles (e.g. to find the penetration mechanism). The latter objective is answered in the analytical part of the research. Analysis of test results will be the object of the next chapter. In order to meet our first objective, the four parameters which can easily be set (i.e. density, temperature, bias surcharge and frequency) have to be changed in every test in order to cover all possibilities. The experimental program has to be flexible enough to be modified as new findings are made.

Rather than reviewing the intended experimental program, the accomplished program is presented in this section. The tests conducted in this research are summarized in Table 4.1. It should be pointed out that five tests can easily be conducted in one sample without interference. One test is carried out at the center of the mould and four more in a cross pattern at mid-distance between the center and the edge of the mould. A total of six samples were made for the experimental program. Thirty

Table 4.1 Experimental program carried out for the research

SAMPLE No	TEST No	FREQUENCY Hz	SURCHARGE kg	TEMPERATURE °C
LS1	1	80	24.62	-10
	2	80	24.62	-10
DS1	1	80	24.62	-10
	2	70	24.62	-10
	3	70	19.98	-8
	4	70	12.50	-8
	5	70	17.14	-8
LS2	1	80	24.62	-2
	2	80	19.98	-2
	3	70	19.98	-2
	4	70	17.14	-2
	5	70	19.98	-7.2
	6	70	17.14	-7.2
DS2	1	70	17.14	-2
	2	70	12.50	-2
	3	80	12.50	-2
	4	80	17.14	-2
	5	70	17.14	-5
	6	70	17.69	-7.2
	7	80	17.69	-7.2
LS3	1	70	17.14	-5
	2	70	19.98	-5
	3	80	19.98	-2
	4	60	19.98	-2
	5	70	17.14	-2
	6	70	12.50	-2
	7	75	19.98	-2

Table 4.1 (foll'd) Experimental program carried out for the research

SAMPLE No	TEST No	FREQUENCY Hz	SURCHARGE kg	TEMPERATURE °C
DS3	1	70	12.50	-5
	2	80	17.14	-5
	3	70	19.98	-2
	4	60	12.50	-2
	5	60	17.14	-2
	6	60	17.69	-7

two tests were carried out. In order to easily relate a test to the sample in which it was carried out, a standard numbering system was devised. A typical test number would be DS2-4 where the first two letters identify the sample type (LS for loose, DS for dense), the digit attached to the two letters represents the sample number and the last digit the test number. When the last digit is larger than 5, it simply means extra tests were conducted where previous test did not achieve a significant penetration.

The first loose sample (LS1) was not prepared in the same manner as LS2 and LS3. The method used for LS1 was found to leave several relatively large air pockets within the sample. For that reason the current method outlined in Appendix B was created. The tests of LS1 were rejected because of the unreliability of the material. Tests LS2-2 and LS2-4 had to be done again because of the short duration of the data.

After tests were conducted following the procedure presented in Appendix B, penetration versus time curves were plotted. Locations of steady penetration rate were identified on the penetration versus time curves and tape recorder. Then, representative pile acceleration and soil response signals were photographed from an oscilloscope (see Appendix A for details about equipment). The photographs were identified with a coded number based on the test numbering system. A letter representing the time (on the penetration versus time curve) at which the photograph was

taken is appended to the test number. A code for the type of signal photographed and the number of the photograph is separated from the rest by a dash. The code is A for pile acceleration, L for soil response load, X for soil acceleration in the x direction, Y for the soil acceleration in the y direction and Z for the soil acceleration in the z direction. Hence, a typical number would be LS3-1B-L2. It means the second photograph of soil response load at time B on the penetration versus time curve of test LS3-1. The last digit (photograph number) was only used when there was more than one photograph taken at a given location.

CHAPTER 5

TEST RESULTS AND ANALYSIS

This chapter presents observations and results of the experiments conducted throughout this research. After inspection of the results, the data will be analysed. Potential relationships between consumed power and penetration rate will be investigated. Discussion will be made as the analysis is unfolded. Finally, results of recent private field tests will be compared to laboratory findings.

5.1 Observations and Results

5.1.1 Sample Properties

Loose samples LS2 and LS3 had dry densities respectively of 1.67 and 1.66 tonnes/m³. The ice content of the former two samples were respectively 19.3% and 20.1%. Dense samples DS1, DS2 and DS3 had dry densities of 1.79, 1.80 and 1.80 tonnes/m³. The ice contents of the dense samples were, in the same order, 12.0%, 11.1% and 11.9%. The total mass density of all samples was very close to 2.00 tonnes/m³.

5.1.2 Pile

The pile used in the experiments was 30 cm long at the start of the experimental program. The pile was tubular and made of steel. It had a wall thickness of 1.3 mm and an outside diameter of 25.4 mm. The tip of the tube was trimmed flat. It was not reinforced nor tapered. After driving, it was noticed that the outside wall of the pile at the tip was worn and formed a sharp edge. There was no evidence of excessive wear on the inside of the pile. It is estimated that the pile shortened by about 2 to 3 mm during approximately 25 tests. This figure does not include filing to reshape the pile during the testing program.

In addition to the above "standard" pile, two model piles with the same physical characteristics were fitted with two RTD's each (see Appendix A.10). The first pile had one RTD located at 53 mm from the tip and the other at 33 mm from its tip. They were at an angle of 90° to each other. The second model pile had one RTD at 14 mm and the other at 8 mm from its tip. One of these two instrumented piles was used in each one of the following tests: DS1-2, DS1-4, DS1-5, LS2-1, LS2-2 and DS3-4. Measurements are discussed in the next section.

5.1.3 Thawed Film

In all tests, a thawed zone formed around both the outside and the inside of the tubular model pile. This film was contaminated by steel dust produced by the abrasive

action of sand on the oscillating model pile. The dust gave the thawed zone a grey color that allowed easy measurement of the extent of melting. This is illustrated in Plate 5.1. The photograph is a cross-section of an unearthed pile hole after driving. The melted zone varied in thickness from about 1.5 to 2.5 mm. The instrumented piles showed that the maximum temperature reached at the film-pile interface during driving was +4°C. The average temperature was around +2°C. No temperature gradient was found to exist between the two measuring locations on the pile.

It was noted that in addition to very fine steel dust in the thawed film, there was a considerable amount of crushed sand particles. Grain size analysis were performed on representative samples of sand contained in the thawed film. The results of the grain size analysis are presented in Figure 5.1. It can be seen that about 12% of the material was crushed.

In rare instances and only in loose samples, a slurry flowed to the surface of the sample along the pile wall. This extensive melting seems to be associated with fast penetration rates, over 2.50 cm/min. However, it did not occur frequently enough nor consistently enough to allow any other comment than a statement about its occurrence.

It is also very interesting to note that there was no thawed soil bulb ahead of the pile tip. This observation together with grain crushing is casting doubt about melting governing penetration.

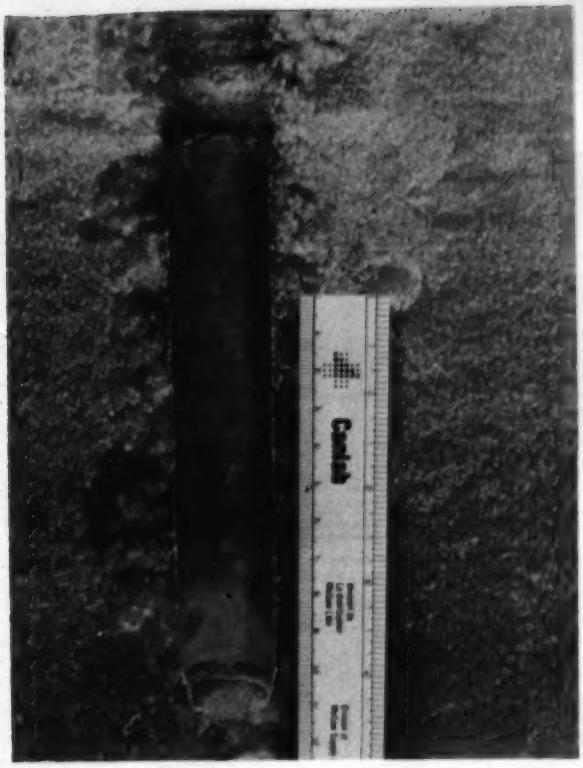

Plate 5.1 Thawed film after driving.

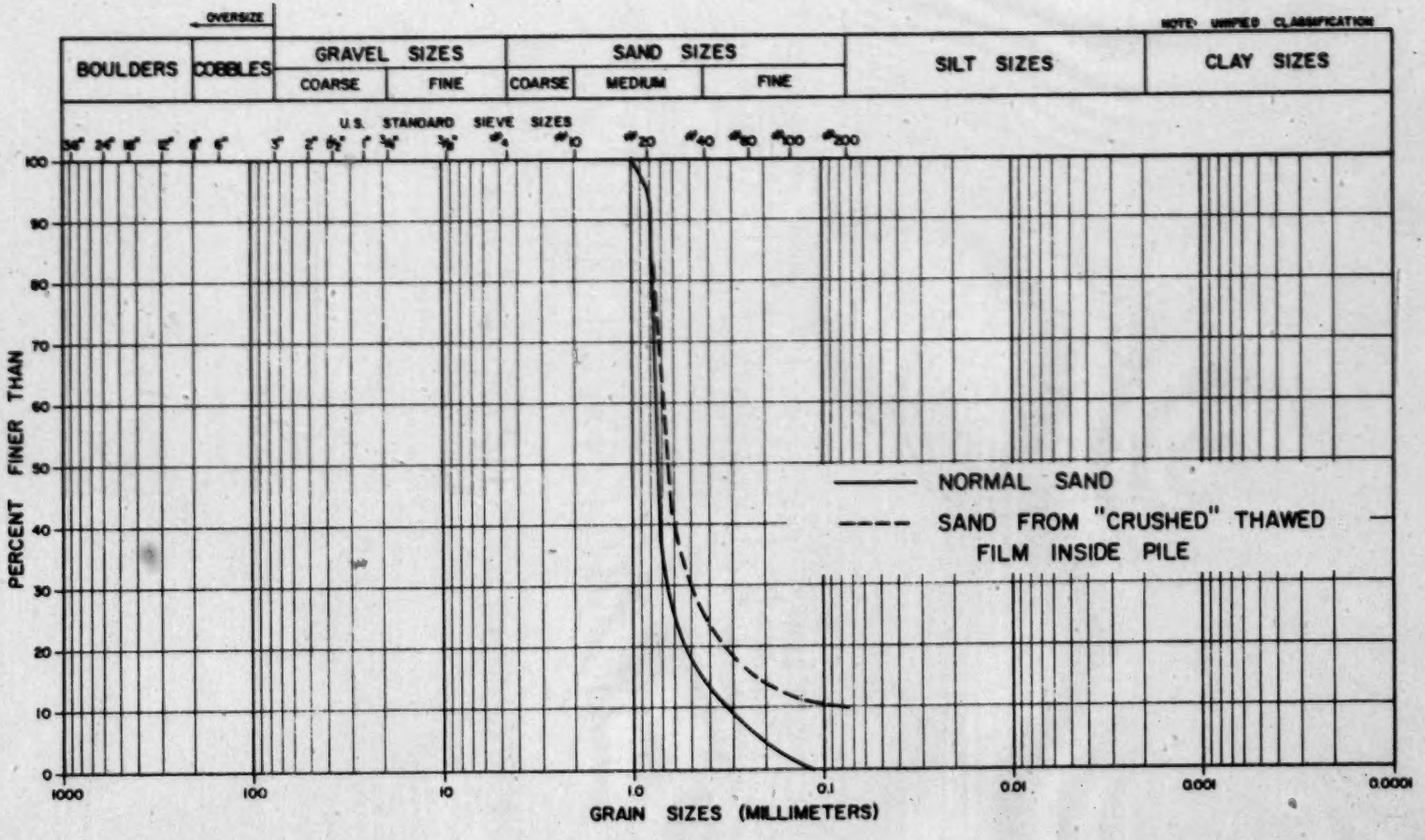

Figure 5.1 Grain size of sand in the thawed film

5.1.4 Pile Acceleration and Soil Response Load

During driving, the pile acceleration and soil load response were recorded and monitored on an oscilloscope (see Appendix A.7 and A.8 for details). In several cases the load signal had to be rejected because of an overloading of the load transducer. The shape of the rejected signals was the same as the shape of good signals but the voltage was beyond the linear range of the transducer. Hence, the signals were unreliable. In these experiments the test data was not all lost since sum of forces is equal to mass times acceleration. The mass of the pile and instruments attached to it is known and its acceleration measured. Hence, the sum of forces can easily be recovered.

The acceleration and load transducers were located at the top of the pile. Because of the very low driving frequency compared to the resonance frequency of the model pile, the pile behaved as a rigid body (refer to Sections 2.2 and 2.3). Therefore, what was measured at the top of the pile was equal to the response of the tip of the pile. Typical pile acceleration and soil response signals are shown on Plate 5.2. The load signal is basically composed of sharp impact peaks separated by periods of negligible force applied to the soil. The acceleration signal is also composed of sharp impact peaks that occur at the same time as the load peaks. Between acceleration impact peaks, there is a slightly distorted half sine wave. The distorted half sine wave corresponds to the upward motion of the pile

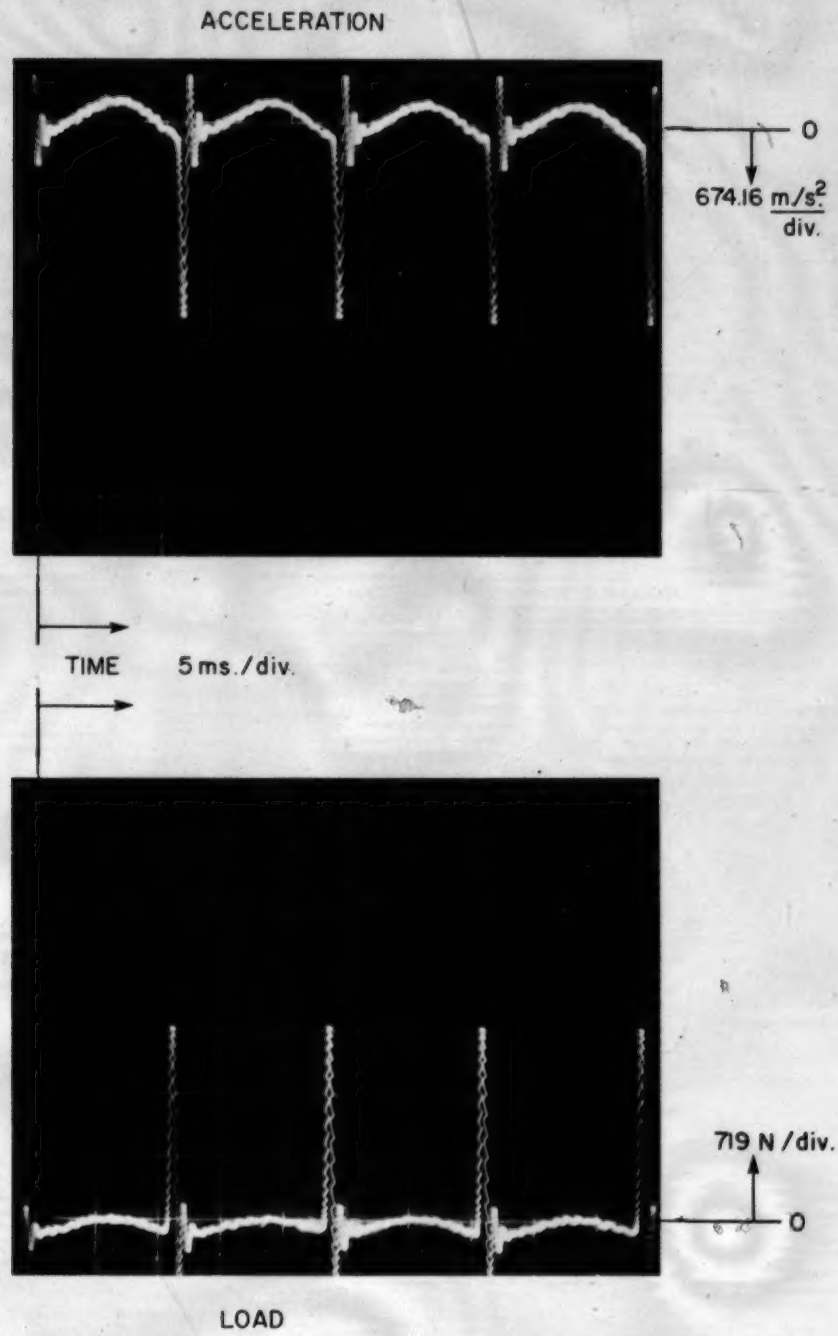

Plate 5.2 Typical recorded data

during which the pile looses contact with the soil. The two preceding wave forms are characteristics of the Instability Domain of driving force (see section 2.4.2). Therefore, the soil behavior was elasto-plastic. It should be added that on both traces, following the impact peak, there is a shorter peak opposed in sign to the impact peak. It is speculated that the small negative spike corresponds to the elastic rebound of the frozen material in which the pile was forced during the main impact of the driving process. This small spike probably represents only a small portion of the elastic rebound because of its small relative size. This small spike could also be upward force applied to pull the pile out of the material in which it was pushed during the main impact. The above observations convince us further that penetration is due to a plastic deformation rather than to melting.

Any driving apparatus has its limitations and there are no exceptions here. The vibrator can only take up to a certain amount of bias surcharge. This amount is determined by a combination of frequency and soil temperature. In a more specific way, one should say soil type rather than soil temperature. Since frozen soil changes physical properties with temperature, the same soil at different temperatures can be considered as different soils. When the capacity of the driver is exceeded, the moving internal core of the driver hits the bottom of its container. This repeated hitting results in a different type of loading on the soil.

Hence the recorded signals differ from the "normal" signals shown on Plate 5.2. Such distorted acceleration and load signals are shown on Plate 5.3. The load pushing the pile into the soil increases and as a result, the rebound spike previously introduced also increases. The real difference is the small spikes at mid-points between the main impact spikes. These small spikes are formed when the moving core of the driver is on its upward motion and abruptly stopped on the bottom of the core casing. The core is near the bottom of its casing because the high applied static load forces it to be there. The effect of such a condition is to reduce the amount of energy expended in the soil at the tip of the pile. Most of the energy is dissipated against the casing of the vibrator. This can also be seen from the acceleration trace itself. It is obvious that the area under the acceleration trace on either side of the axis is smaller than the area under an undisturbed trace. Since displacement is the second integral of acceleration and that an integral is the area under a curve, it is equally obvious that the displacement be less. Energy is a force times a displacement. Hence lower dispacement means lower energy transferred to the soil during the driving operation.

5.1.5 Penetration Rate

In this section, penetration versus time curves of each test will be discussed to clarify any oddity they might have. The reader will find all the penetration versus time

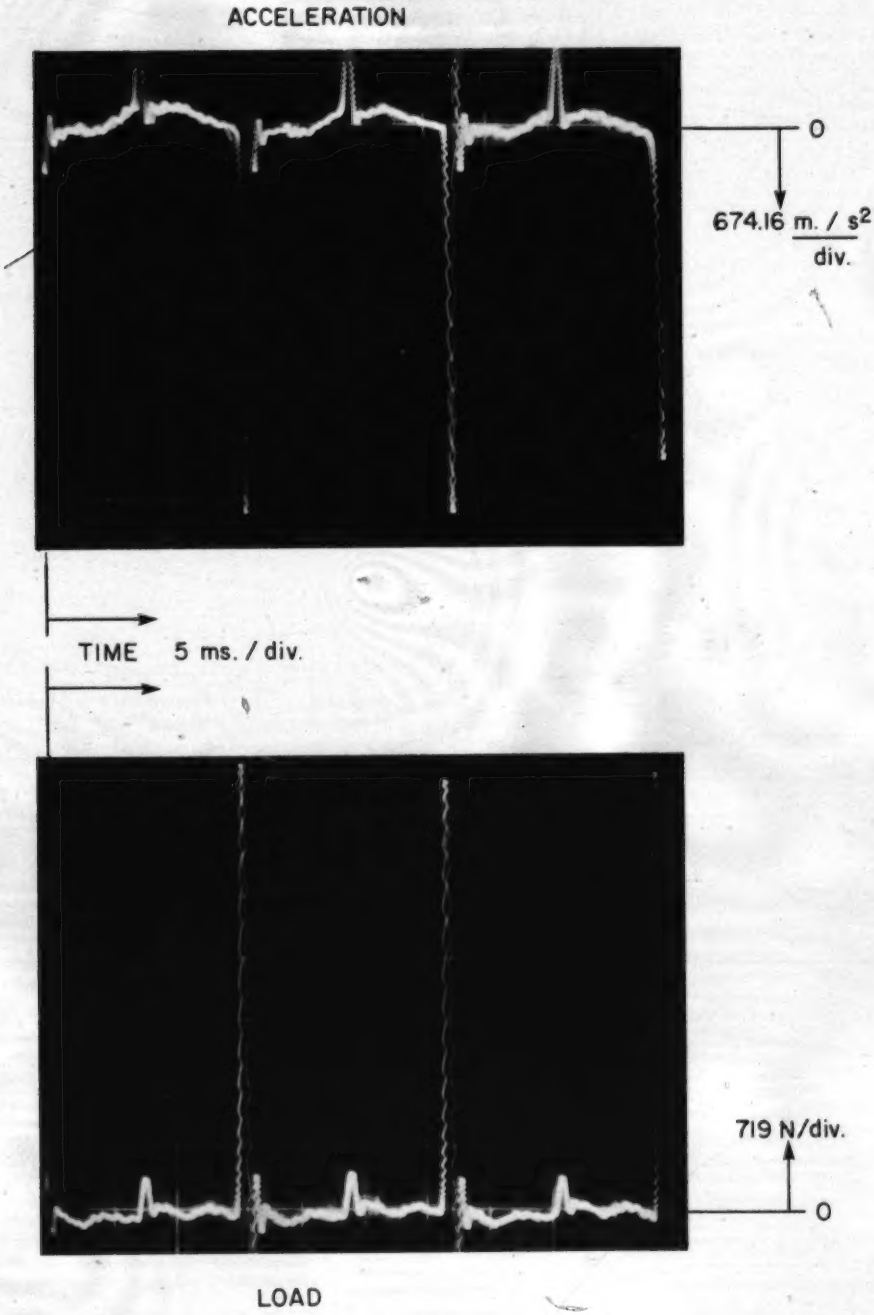

Plate 5.3 Typical signals when driver is overloaded.

plots in Appendix C. On these plots, the penetration rate at a point in time is given by the slope of the curve at that point. The steady penetration rates will be identified and any changes in penetration rate during the test will be discussed.

Test DS-1 shows three different penetration rates. The change from the first to the second penetration rate is due to an increase in shaft friction along the guiding piston. The reader should refer to Appendix A.2 for a complete description of the driver guiding system and its limitations. The second change in penetration rate is due to a release of some friction. These changes in frictional resistance along the guiding piston translate into changes in effective surcharge on the top of the model pile. It does not matter whether the real effective bias is known or not as it will be discussed in the next part of this chapter. The recorded signals give all the information needed to find what the consumed energy is at the tip of the pile. It is sufficient to say for now that the penetration rates are consistent with the acceleration and load records.

Test DS1-2 is highly linear. The small jump on the curve in the first part of the test is due to a disturbance of the penetration measuring instrument. At the end of the test, the pile jammed tightly in the frozen sand. From the recorded signals, it can be seen that the soil reaction was gradually becoming elastic. The impact peaks were slowly disappearing from the trace as the wave form became more

sinusoidal. A decrease in temperature of the thawed film could result from a decrease in oscillatory amplitude of the pile wall. Such a decrease in oscillatory amplitude is related to an overloading of the driver.

Tests DS1-3 behaved in the same manner as DS1-2.

Test DS1-4 started with a good penetration rate but slowed down considerably after 4 minutes of driving. The experiment went on for another 7 minutes without considerable penetration before it was stopped.

Tests DS1-5 behaved in the same manner as DS1-2.

Test DS2-1 was started with a bias surcharge of 17.14 kg. Note that the actual total surcharge is not necessarily the effective surcharge on the pile. The test was stopped after 1.5 minutes because the accelerometer was not working very well. The problem was fixed and the test restarted in the same hole under the same conditions. The restart was called DS2-2. Two minutes after the beginning of DS2-2, the bias surcharge was changed from 17.14 to 12.50 kg. The effect was to drastically reduce the penetration rate. The small increase in penetration rate near the end of DS2-2 is attributed to release of friction from the guiding piston.

Test DS2-4 has the strangest behavior of all. There are two increases in penetration rate and two time intervals with the same penetration rate. The changes are due to variations in friction in the guiding system.

Test DS2-5 has a normal behavior. There was a disturbance in the penetration measuring device after two

minutes of driving. An increase in effective surcharge on the pile almost made the pile jam in the sample.

Test DS2-6 was started with a surcharge of 19.98 kg. Because it overloaded the exciter too much, the surcharge was reduced to 17.69 kg. Near the middle of the test a small change in penetration rate is perceived. A second change is seen at the end of the test. It is likely due to a decrease in effective surcharge but could be due to another cause. The matter could not be investigated further since the driver had reached the end of its travel. The driver travel was not only limited by the piston guide but also by the sample container freeboard and carrying handles.

Test DS2-7 has a sudden change in penetration rate half way through. This change is once more related to a change in effective surcharge to the pile.

Test DS3-1 had an almost negligible rate of penetration. After 18.5 minutes of driving, penetration was only about 1.2 cm. Hence, the penetration curve was not plotted.

In test DS3-2, the impact spikes did not fully develop. Peaks were not all of equal magnitude. Every second peak was lower than the first. The phase period between a first and a second peak was different from the phase period between a second to the next first peak. No penetration was achieved in this test.

Penetration of test DS3-3 is steady from the start to the end. The test went to the maximum depth of the driving

system.

Test DS3-4 did not penetrate. It was conducted for about 15 minutes and only achieved an advance rate of 0.30 cm/min. The data of DS3-4 is not plotted because of the low penetration rate.

Test DS3-5 reached a steady penetration after some initial variations. At a depth of about 12 cm, the pile started to slow down toward another penetration rate. The change in rate of advance is associated with changes in sliding resistance along the guiding piston.

Test DS3-6 displays a steady penetration with a slight decrease near the end of the test.

Series LS1 tests was rejected because of problems associated with the sample preparation. This has been outlined in Chapter 4.

Test LS2-1 has a steady penetration and penetrated to the maximum depth of the system.

Test LS2-2 shows a continuous increase in penetration rate. The pile stopped when it jammed in the frozen material. The constant increase in penetration rate is due to a constant release of friction along the piston guide as the pile advanced. The constant release of friction is partly explained by a decrease in coefficient of friction with an increase in relative velocity of the two rubbing surfaces. Various scenarios are discussed in Appendix A and earlier in this section.

Test LS2-3 showed an initial increase in penetration rate before it reached a steady state. At a depth of 14 cm, the bias surcharge was reduced and the new set-up was called LS2-4. Penetration of LS2-4 never became steady in the short time interval the test was conducted. Hence no data can be used from that test.

Test LS2-5 also had an initial increase in penetration rate before it reached a steady state. At about 10 cm of penetration, the pile slowed down before it returned to close to its original rate at about 14 cm. This is again associated with the guiding system.

Test LS2-6 shows two different penetration rates. As far the test is concerned, everything seems to be in order.

Test LS3-1 jammed because of a considerable release in friction of the guiding piston.

Test LS3-2 also jammed because of too large load on the top of the pile.

Test LS3-3 did not have any penetration. Hence, no curve was plotted. Impact spikes did not develop clearly enough to allow sufficient transfer of energy to the soil. Only one spike every second period developed. The frequency was swept while the wave form was monitored on the oscilloscope. The maximum frequency at which impact spikes were fully develop (as on Plate 5.2) was approximately 75 Hz. The frequency was set at 75 Hz and a test carried out. The experiment at 75 Hz was named LS3-7. The very slow penetration rate at the beginning of LS3-7 is attributed to

the fact that the test was started with the pile being already in contact with the frozen material. A full impact situation developed quickly in the first millimeters of penetration. The following increase in rate is associated with an increase in effective surcharge on the top of the pile.

Tests LS3-4, LS3-5 and LS3-6 behaved like LS3-7 except for the initial slow penetration rate.

5.1.6 Influence of the Independent Variables

Five independent variables were identified in section 4.2. They are for a given pile: sample temperature, bias surcharge, driving frequency, ice content and sample density. It was also discussed that ice content and sample density were not truly independent from each other. For the experiments, only saturated samples were prepared. Hence, ice content and sample density become only one variable which may be called soil type. The influence of each of the four parameters will be discussed in the following paragraphs. Before the reader goes any further, he should be reminded that the variation in effective surcharge to the top of the pile caused a significant scatter in the data. Trends will be discussed when possible. Further analysis will shed more light on the data. That analysis is to be the object of another section.

5.1.6.1 Bias Surcharge

The effect of bias surcharge on penetration rate is summarized in Figure 5.2. Although there were problems associated with having a known effective surcharge to the top of the pile (see Appendix A.2 and section 5.1.5), the main trends can still be observed from the plot. There is a minimum surcharge below which no penetration can occur because impact peaks can not develop. Therefore, insufficient energy is delivered to the soil. If everything else is maintained constant, the energy delivered to the soil increases as the bias surcharge increases. Impact peaks grow steadily during that stage. After an optimum surcharge for the given soil-frequency combination is reached, a decrease in penetration rate is observed in Figure 5.2. This decrease is associated with a decrease in efficiency of the driver. The vibration amplitude becomes damped because the pile is pressed against the soil. Often much of the input energy is dissipated within the vibrator itself because the core comes in contact with the casing. The pile may even jam in the frozen soil under this condition.

The behavior discussed above is valid for dense frozen soils at all temperatures and driving frequencies. The behavior of loose frozen sand seems to be the same but is not as well defined in the test data.

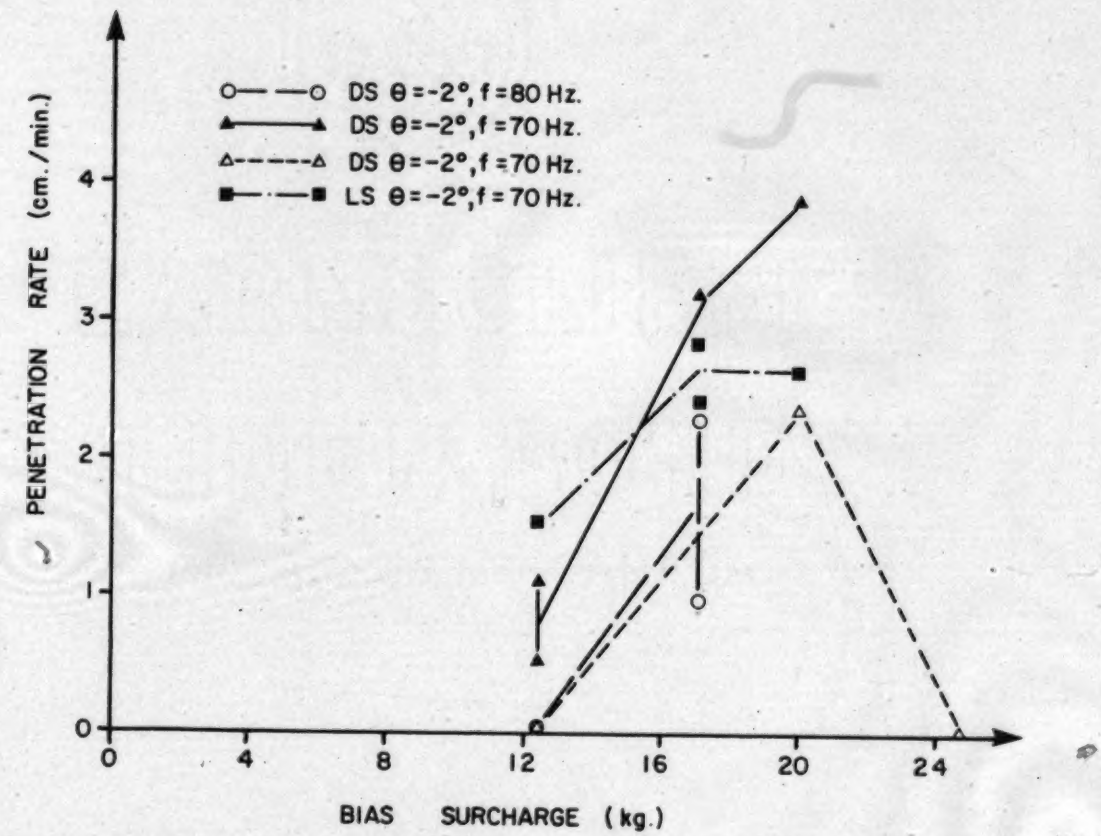

Figure 5.2 Effect of bias surcharge on penetration rate.

5.1.6.2 Soil Temperature

The effect of soil temperature on penetration rate is summarized in Figure 5.3. It can be seen that if everything else is kept constant as temperature is lowered, the penetration rate decreases. Soil strength increases with decreasing temperature. Hence, it gets stiffer and requires more energy to be thawed or to be displaced in the unthawed state.

In loose frozen sand, it is rather difficult to pick up any trend. It could be tentatively concluded that there is no solid evidence of temperature influence in loose soil at this point. However, there is a marked trend in dense soils.

5.1.6.3 Driving Frequency

The effect of driving frequency on penetration rate is summarized in Figure 5.4. There is a certain frequency below which no penetration will occur because the surcharge becomes too high for the displacement amplitude. Remember that displacement amplitude is inversely proportional to frequency (see section 2.3). As the frequency decreases, the displacement increases but the acceleration decreases. Hence, the load carrying ability of the driver is reduced since acceleration is proportional to force. This is also reflected in the fact that the force threshold described by Gharhamani (op. cit.) varies with frequency for a given soil and pile (see Section 2.4.2). If at the lower frequency

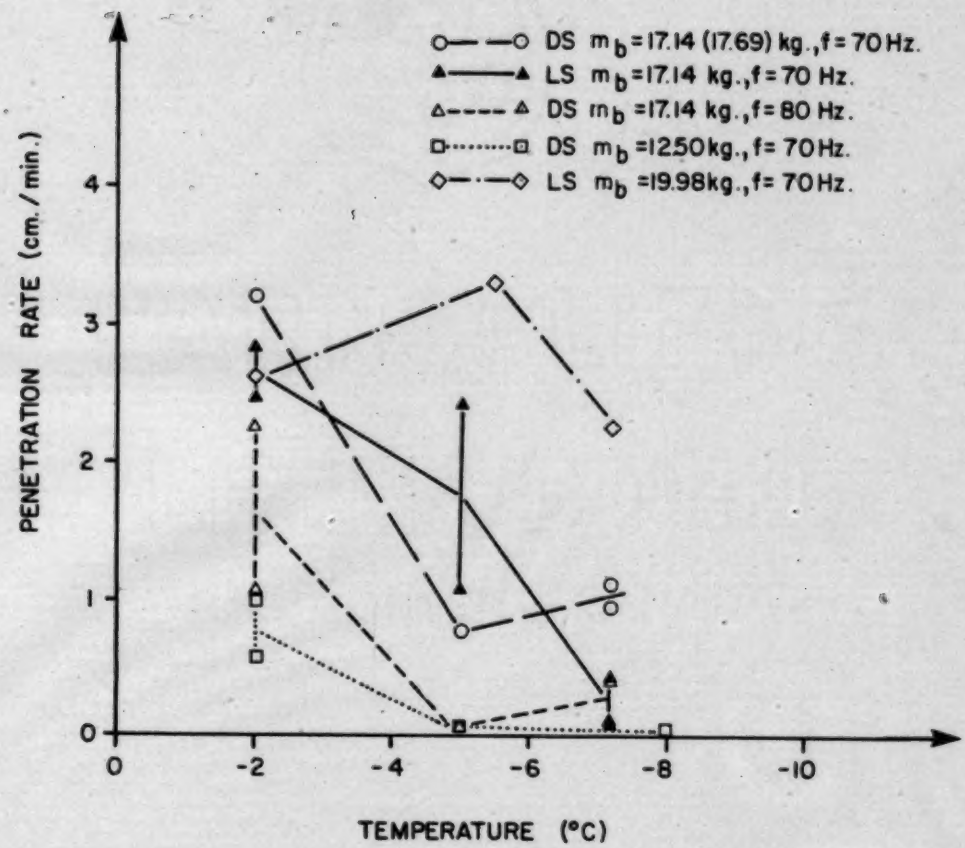

Figure 5.3 Effect of soil temperature on penetration rate.

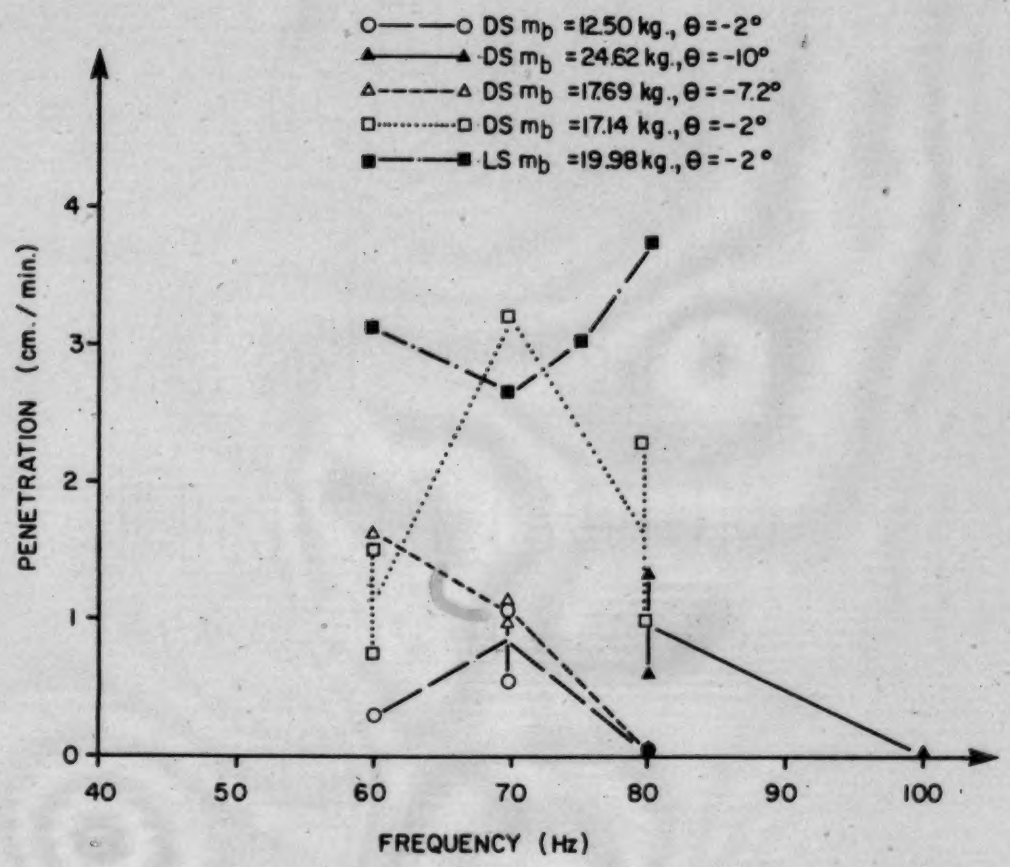

Figure 5.4 Effect of driving frequency on penetration rate.

threshold the surcharge is reduced to allow vibrations to occur, impact spikes in the load versus time plot do not develop and penetration does not occur. If all variables are held constant and the frequency is increased, the penetration rate will increase to a maximum and then decrease as the frequency increases further. Displacements at frequencies higher than this upper threshold are too small to allow transfer of sufficient energy to the soil and as a result, the pile will not penetrate. Also at higher frequencies, impact peaks do not fully develop or do not develop at all. Thus the elastic deformation of the frozen soil is not overcome and insufficient energy is available to weaken the soil.

5.1.6.4 Soil Type

The influence of soil type on penetration rate is shown in Table 5.1. In three cases, the penetration rate is larger in dense sand than in loose sand. It is tempting to attribute the difference to the different ice contents. Dense samples require less energy to melt a certain volume of soil than loose samples (see Table 5.4). This is due to a difference in ice contents. However, higher penetration rates in loose frozen sand at -5.5°C and at -2°C with a low bias suggest that there is a different penetration mechanism. It has to be said that there is not much difference in density between the loose and dense sand. The data could be within a normal scatter for these two close

Table 5.1 Influence of soil type on penetration rate.

TEMPERATURE °C θ	FREQUENCY Hz. f	BIAS SURCHARGE kg. m_b	PENETRATION RATE r_p cm/min.	
			LOOSE	DENSE
-2	70	17.14	2.86	3.21
-2	70	19.98	2.60	3.86
-2	70	12.50	1.53	0.52/1.07
-5.5	70	17.14	1.07/2.48	0.75
-7	70	17.14 17.69	0.43/0.077	0.92/1.10

densities. The influence of density will be further investigated in the analytical portion of this chapter.

5.2 Analysis of Results

5.2.1 Introduction

Observations of the previous section help in understanding the influence on penetration of each independent variable. The findings although interesting are not obvious. This is mainly due to the scatter of the data. As discussed several times in previous chapters and sections, the scatter is mainly due to the unknown effective bias surcharge applied at the top of the pile. Fortunately, the problem can be overcome by examining the tape recordings of the pile acceleration and soil response load signals. Changes in effective bias surcharge at the top of the pile are illustrated using these recorded signals. Hence differences in consumed power exist for the different slopes of the penetration versus time curves (see Appendix C).

In Chapter 4, three components of the energy balance were identified. They are:

1. Energy expended at pile tip to dislace the soil and make room for the pile;
2. Energy transferred to soil as heat in the thawed film;
3. Energy lost to soil as body waves.

It is obvious that the problem of energy transfer is greatly simplified by assuming only three energy "sinks". The limitations of such assumption will be discussed as each of these components are examined in this Section. Before the problem of energy is discussed, there are needs to discuss soil deformation at pile tip and soil dynamic response.

5.2.2 Soil Deformation at Pile Tip

The soil deformation at the pile tip is imposed by the pile tip itself. Hence, the soil deformation at the pile tip is equal to the displacement of the pile tip.

It is known that the soil reaction at pile tip is elasto-plastic(see Section 5.1.4). The accelerometer which was used measured the total displacement for each cycle. Because the permanent deformation for one cycle was very small, it can not be measured from accelerometer records. The permanent deformation for one cycle is illustrated on Figure 5.5. The permanent deformation (dp) can be easily back-calculated for each test since the penetration rate (rp) is known. The total soil deformation (e.g. pile tip displacement) can be obtained by integrating the pile acceleration records.

Because there are several technical problems associated with digitization of data, such as not having the capability of sampling enough points to define the impact spikes in an acceptable and reliable manner, two idealized models of

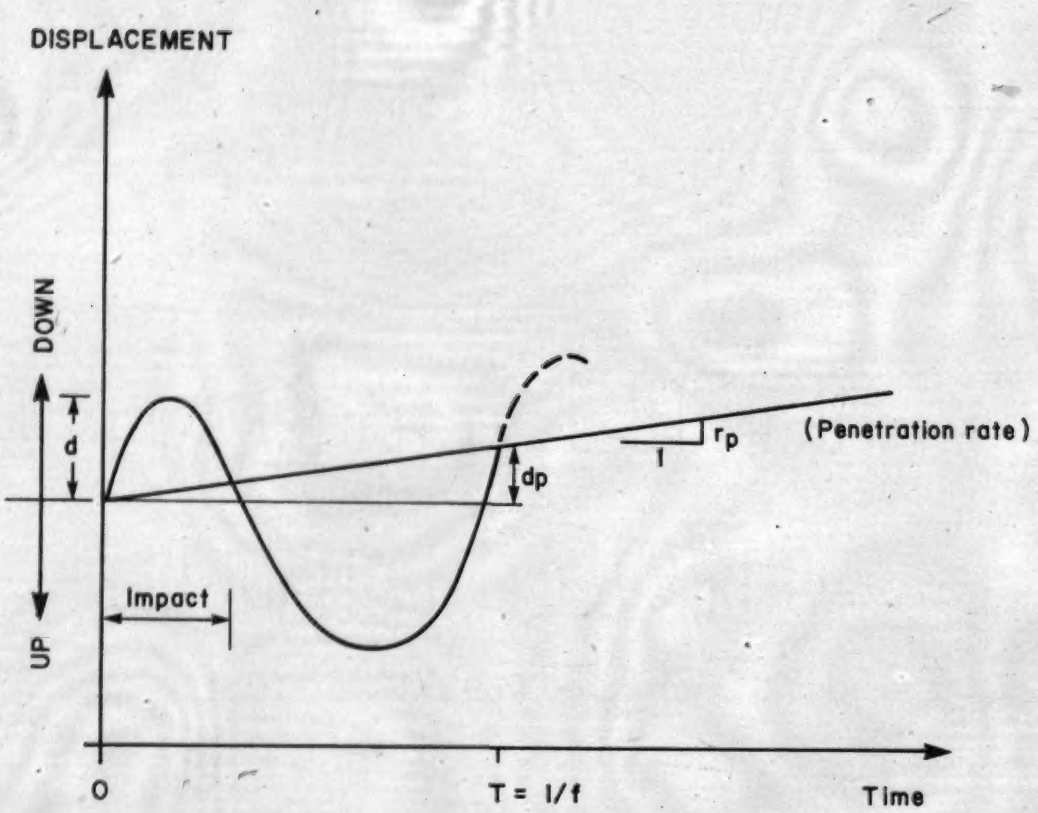

Figure 5.5 Permanent plastic deformation for one motion cycle

simple shape were designed to fit the two basic waveforms presented on Plates 5.2 and 5.3. These models are presented on Figure 5.6. The first model (a) of Figure 5.6 is for normal wave forms. This model was designed to fit the true signal with simple wave forms to facilitate integration. The second model (b) is for the damped vibration cases (see Plate 5.3). It appears appropriate to approximate the damped signals by a sharp triangular pulse preceded by an area of simple shape (triangle) to allow continuity of motion from one cycle to the next. The method used to perform the integration is discussed in detail in Appendix D.

Results of the integration of total pile tip displacement are compared to permanent soil deformation in Table 5.2. The soil permanent deformation has been back-calculated as per equation 5.4 found further in this Section. It can be seen from Table 5.2 that the permanent soil deformation is small when compared to the total pile tip displacement. This difference justifies the assumption that for integration purposes the permanent deformation can be neglected (see Appendix D). It also raises the question wether there is a loss of contact between the pile tip and soil during each motion cycle. This is raised because the ratio of elastic to plastic deformation is large. A simple answer to this question is difficult to give. The matter will be discussed in the Section which deals with dispersion of body waves generated at the pile tip.

Table 5.2 Comparison of total pile tip displacement and permanent soil deformation per motion cycle.

TEST No	d_p* mm/cycle	d** mm
DS1-1A	0.00277	3.89/2.10
1B	0.00125	2.75
1C	0.00229	1.34
DS1-2A	0.00824	5.03
2B	0.00824	2.25
DS1-3A	0.00562	4.24
3B	0.00562	2.81
DS1-4A	0.000067	1.72
4B	0.000067	0.43
DS1-5A	0.00331	0.63
5B	0.00331	0.94
LS2-1A	0.00750	4.37/4.00
1B	0.00750	3.87
LS2-5A	0.00536	2.00
5B	0.00536	1.83
LS2-6B	0.00102	2.07
6D	0.00018	2.02
DS2-6A	0.00219	1.94
6B	0.00219	1.78
6C	0.00262	1.84
6D	0.00262	2.40
DS2-7A	0.00085	1.20
7C	0.00027	1.51
7D	0.00027	1.14
LS3-1A	0.00255	1.43
1B	0.00255	0.75
1C	0.00590	1.93
1D	0.00590	1.75

*permanent soil deformation per motion cycle
**total pile tip displacement

Table 5.2 (foll'd) Comparison of total pile tip displacement and permanent soil deformation per motion cycle.

TEST No	d_p* mm/cycle	d** mm
LS3-2	0.00783	0.11
LS3-4	0.00861	1.21
LS3-5A	0.00681	0.104
5B	0.00681	0.174
LS3-6A	0.00364	0.90
6B	0.00364	1.10
LS3-7A	0.00667	1.65
7B	0.00667	0.145
DS3-1A	0.00016	1.06
1B	0.00016	1.56
DS3-2A	0.0	1.17/0.97
DS3-3A	0.00919	0.276
3B	0.00919	2.11
DS3-4	0.00083	2.21
DS3-5A	0.00422	2.65
5B	0.00422	4.21/4.56
5C	0.00208	1.93
DS3-6A	0.00458	0.22
6B	0.00458	3.07

*permanent soil deformation per motion cycle
**total pile tip displacement

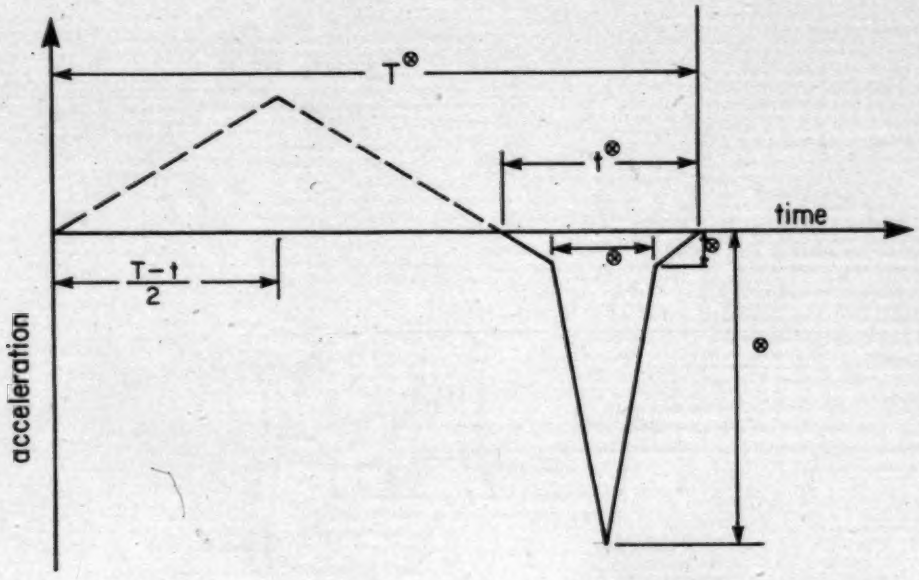

a) normal acceleration

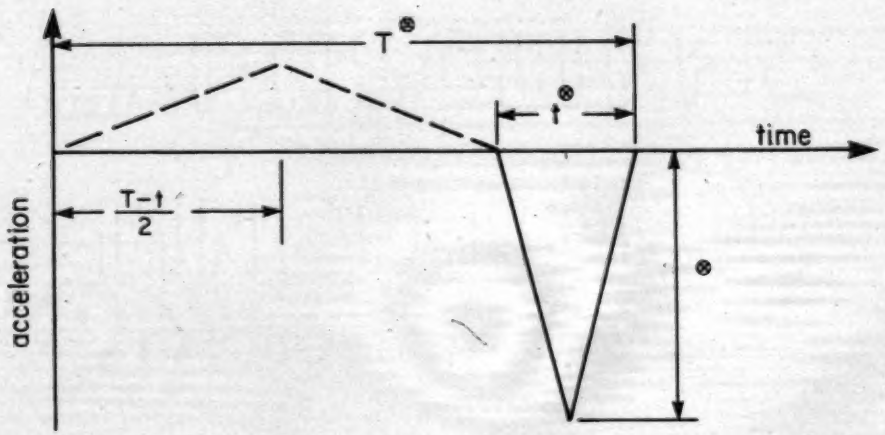

b) acceleration when driver is overloaded.

⊗ measurements taken from photographs.

Figure 5.6 Acceleration wave models.

5.2.3 Soil Dynamic Response

The soil dynamic response was measured at the pile top during the experiments, but in most tests, the data was lost because of overloading of the load transducer. Fortunately, not everything was lost. The pile acceleration records at the top of the pile were still available.

It is well known from Newton's second law that the sum of the forces in a system is equal to the acceleration of the system in the direction of the resultant force times the mass of the system. A free body diagram of the system used is shown on Figure 5.7. For obvious reasons, the soil dynamic resistance (J) only exists when the exciter force (Fe) is directed downward. Side resistance along the pile can be neglected because of the very low strength of the thawed film when compared to intact frozen soil. Newton's law for the situation illustrated in Figure 5.7 yields:

$$mp \times a = J - Fe \qquad (5.1)$$

where mp is the pile mass including masses of all adaptors and instruments between the top of the model pile and the bottom of the vibratory exciter. For all experiments of this research, mp was equal to 1.055 kg. (a) is the peak acceleration measured from the accelerometer records.

During the experiments, the exciter force (Fe) was not measured but it is known that:

1. its maximum is 267 N, from manufacturer's

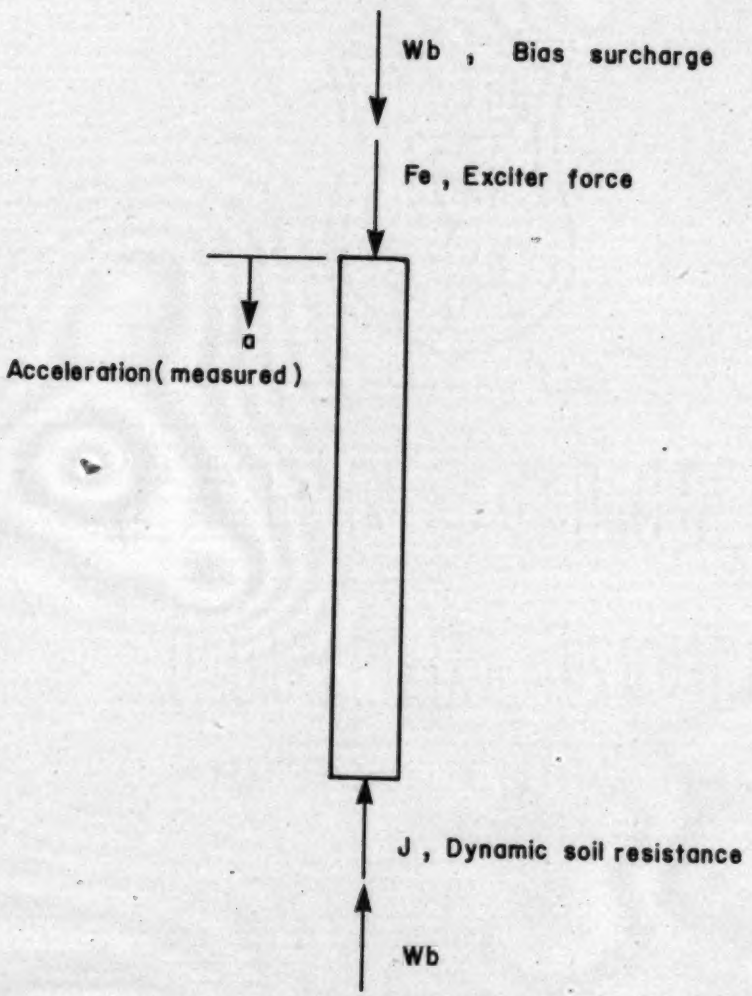

Figure 5.7 Free body diagram of the pile at a given time.

specifications, including corrections for altitude and temperature;

2. since the tip reactions were past the impact threshold in the instability domain, the phase angle between the exciter force and dynamic soil resistance lies most likely between 140 and 150° (Gharhamani (op. cit.)).

Hence, the exciter force in Equation 5.1 is 160 N. The dynamic soil resistance was calculated from the following formula:

$$J=1.055(a)+160 \qquad (5.2)$$

where (a) is the pile acceleration in m/s^2 and J the dynamic soil resistance in Newtons.

5.2.4 Distribution of Energy

5.2.4.1 Energy Required to Create a Permanent Deformation

It has been shown in past sections that penetration of the pile was due to an elasto-plastic deformation of the soil beneath the pile tip. If a force-deformation relationship is known or assumed, plastic work is easy to estimate.

Figure 5.8 shows a typical load-deformation curve for frozen Ottawa sand. The curve can be idealized to simulate a perfect elasto-plastic material requiring the same amount of work to deform plastically. Such an approximation

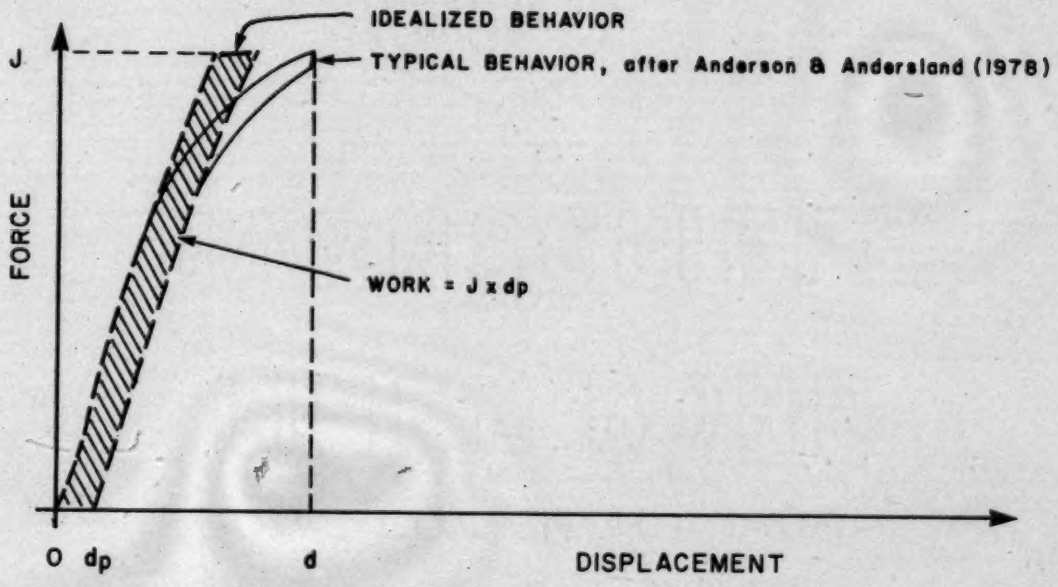

Figure 5.8 Deformation behavior of experimental material

constitutes an upper bound value for plastic deformation of the soil. From the idealized load-deformation curve, the amount of work done on the soil during one motion cycle (Ws) is:

$$Ws=J\times dp \tag{5.3}$$

where J is the soil dynamic response in Newtons and dp, the soil plastic deformation in meters. The soil plastic deformation is calculated as follows:

$$dp=rp/(600\times f) \tag{5.4}$$

where rp, the penetration rate is in cm/min and f, the driving frequency, in Hz. 600 is a constant to make units compatible.

The amount of energy spent to penetrate the pile 1 cm (E_1) is given by:

$$E_1=Ws\times f\times 6/rp \tag{5.5}$$

where 6 is a constant to make units compatible.

If Equations 5.3 and 5.4 are substituted into Equation 5.5, a simple equation is obtained:

$$E_1=J/100 \tag{5.6}$$

Equation 5.6 was used to calculate the amount of plastic work required to penetrate the pile 1 cm. The results are tabulated in Appendix E and illustrated on Figure 5.9.

It can be seen that dense frozen sand needs more energy to be deformed plastically than loose frozen sand. This behavior is perfectly normal since the matrix of a dense soil is stiffer than the matrix of a loose soil.

During the experiments it was observed, as earlier reported, that some 12% of the sand grains were crushed during driving. During high pressure, normal temperature tests conducted on the same material, grain crushing was also observed (Scott (1981)). At static stresses of 30 MPa, about 1.2% of the sand grains were observed to be crushed. The strain energy released during Scott's experiments was calculated to be 0.229 J/cm^3 from the stress-strain curve. This strain energy includes plastic work, most of which is lost by grain to grain slippage (frictional heat) and by grain crushing. Since the area of thawed film is known (about 4.769 cm^2), the volume of sand in which grains were crushed can easily be figured out. If the strain energy required to crush sand grains is directly proportional to the amount of grains crushed, the amount of energy expended to crush sand grains for 1 cm of pile penetration is 10.9 Joules.

Because strain energy includes all types of work done on the soil, this value constitutes an upper bound of work

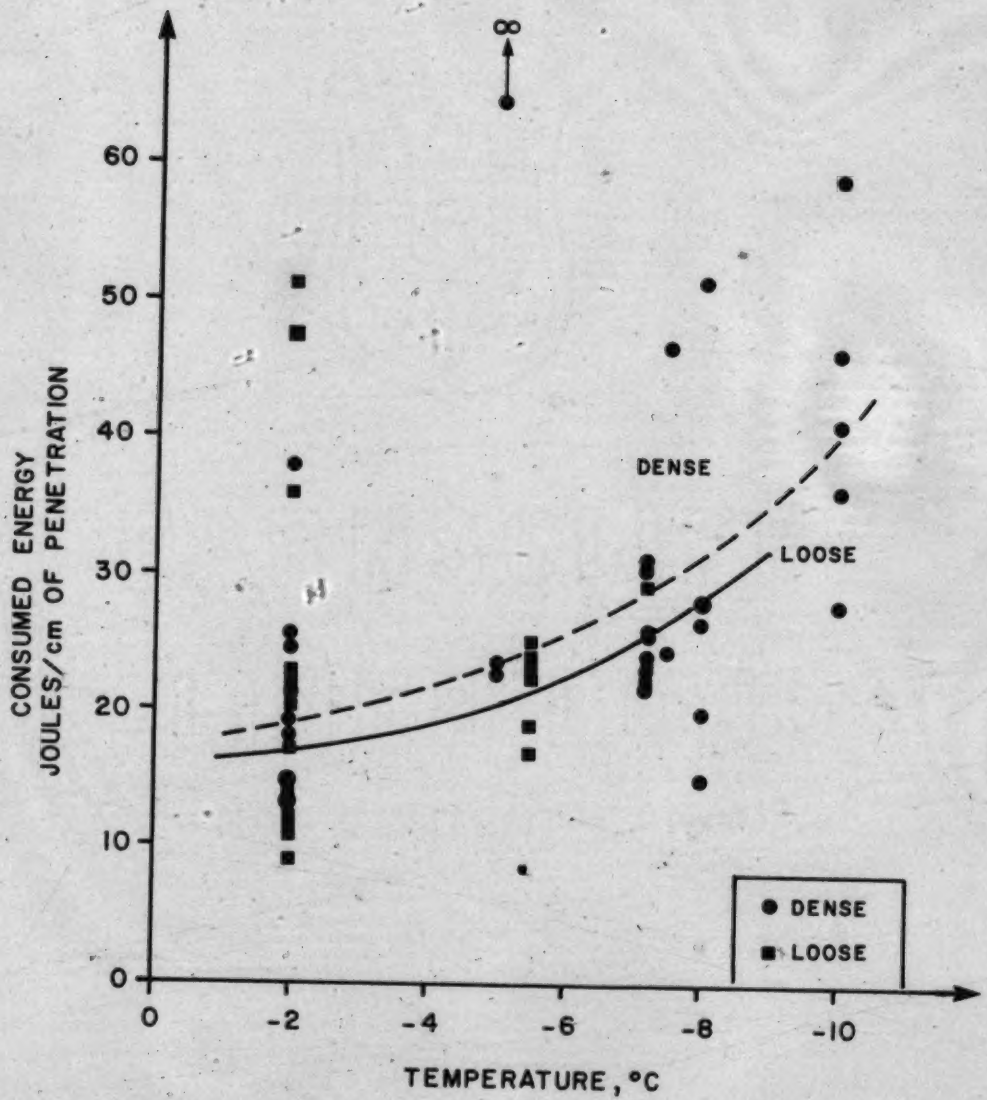

Figure 5.9 Plastic work done on soil to achieve 1 cm of penetration

done in grain crushing. It was also assumed that strain energy is proportional to the amount of grains crushed. This is certainly not the case. In fact, because of the already large stress level, strain energy probably increases more slowly than the number of crushed grains.

When the work required to crush sand grains and deform the soil matrix (10.9 J) is compared to the work calculated on Figure 5.9, it is in general lower. In frozen soils, more work goes to fail the ice matrix and displace confined material than to crush sand grains.

Analogy can be made to bearing capacity failure. If the bearing capacity of the soil is exceeded, plastic deformation definitely takes place. To fail in bearing capacity, frozen Ottawa sand at -3.85°C requires a pressure of about 16 MPa (Sayles 1973). With a mass of 1.055 kg and an area of 0.98 cm^2, the pile carried a pressure of 16 MPa every time the acceleration reached 1600 m/s^2. The model pile driver effectively accelerated the pile by that amount or more in all tests, see Appendix E. Moreover, the pile tip as reported in an earlier Section (5.1.2) wore much more on the outside than on the inside. This observation indicating an outward plastic flow, shows that a bearing capacity failure of the frozen material occurs.

To prove that bearing capacity needs to be exceeded, it was attempted to drive a 50.8 mm O.D. pile with a 1.6 mm thick wall (2.47 cm^2 in cross-section). Although higher loads were observed (they were beyond the capacity of the

load cell), no penetration was observed after several minutes of loading. The test was terminated to avoid detrimental overloading of the load transducer. Assuming the same force was transferred from the driver to the soil, the pressure applied on the soil at the pile tip was 2.5 times less than the pressure underneath the model pile which was successfully driven during the experimental program. Since pressure was lower, the ultimate bearing capacity of the soil was not surpassed and this larger pile could not be advanced.

Important points to remember from this section are:

1. Penetration is due to plastic soil deformation of frozen soil; the force and displacement requirements are dictated by the mateial strength in short term bearing capacity;
2. Dense frozen soils require more energy input than loose frozen soils for pile penetration because of their stiffer matrix, this is consistent with the above point;
3. The work expended in crushing sand grains is included in the calculated plastic work.

5.2.4.2 Energy Required to Create Thawed Film

From the discussion of section 5.2.4.1, it can be seen that distribution of energy is not that simple. To have a feeling for orders of magnitude, let us estimate the amount of energy required to create a thawed film.

If it is assumed that:

- the thawed film is uniform in thickness (2.5 mm) both inside and outside the pile wall;
- the film temperature is uniform and is +4°C during driving;
- the film advances at the same rate as the pile;
- the dense and loose samples have ice contents respectively of 11% and 19% with dry densities of 1.80 and 1.67 tonnes/m^3;
- the thermal properties of the two materials are as in Table 5.3;

then, the energy required to thaw a 1 cm long soil section as found around the model pile plus the area of the pile itself is given in Table 5.4. The energy required is obviously dependent on temperature. More energy is required for cooler initial materials. The difference required is small when compared to the magnitude of the power. This is due to the disproportionate part of latent heat in the energy equations compared to the part of specific heat. The data in Table 5.4 is the energy which must be supplied to the model pile to ensure melting of a ring of soil 1 cm long. This ring of soil has the thickness of the pile and both interior and exterior thawed films. The figures in Table 5.4 are given in Joules and do not include energy required to maintain the already formed slurry. The energy expended to maintain the slurry is considered insignificant.

Table 5.3 Thermal properties of loose and dense sand, after Andersland and Anderson (1978).

SOIL TYPE		THERMAL CONDUCTIVITY $\frac{W}{m.-°k}$	VOLUMETRIC HEAT $\frac{J}{cc.-°k}$	LATENT HEAT $\frac{J}{cc.}$
LOOSE	FROZEN	3.0	1.92	105.7
	UNFROZEN		2.58	
DENSE	FROZEN	3.2	1.77	66.5
	UNFROZEN		2.18	

Table 5.4 Energy (in Joules) required to thaw a soil volume equal to the thawed film area plus the pile area on a length of 1 cm.

SOIL TYPE	TEMPERATURE (°C)			
	-10	-7	-5	-2
LOOSE	645	617	599	571
DENSE	443	418	401	376

The amount of energy required to form the thawed film bears no resemblance whatsoever to the amount of plastic work done on the soil (compare Figure 5.9 to Table 5.4). Even the increase in requirement with temperature does not match, e.g. about 70 Joules/cm for the thawed film between -2 and -10°C compared to about 25 Joules/cm for plastic work done for the same temperature interval.

This can be explained in several ways. Firstly, some of the energy for thawing comes from release of strain energy or plastic work. Strain energy is released by grain to grain slippage within the soil mass and by grain crushing. The amount of heat hence released is probably small compared to the requirements for melting. Secondly, friction of pile walls on the highly confined material, especially near the pile tip is likely to be important. And thirdly, friction of the pile wall on the sand grains during upward motion of the pile is also likely to be an important factor.

Taking the above into account, pile penetration can definitely not occur because of thawing of the frozen soil. Thawing is a secondary effect occuring after or as a consequence of soil failure.

5.2.4.3 Energy Dispersed throughout Sample as Body Waves

At the pile tip, a deformation is imposed to the soil. A small portion of that deformation is non-recoverable while the rest is recoverable or elastic. This deformation is

periodically imposed on the soil.

The acceleration of elastically dispersed energy was measured in one of the samples (DS3) and is compared to the pile acceleration in Table 5.5. The z-direction was vertical or aligned with the longitudinal axis of the pile. The y and x-directions were mutually perpendicular and lying in a plane orthogonal to the z-direction. Only two directions were recorded at a time because of the lack of recording channels. Accelerations in the horizontal direction x and y are small and can be disregarded as noise due to transverse sensitivity of the transducers. Hence propagation of shear waves in the container appears unlikely. Accelerations in the z-direction lie between 2 and 10% of the pile acceleration. The average is 4.3%.

If the idealized model (b) for integration is used, the soil displacement at depth beneath the pile is found to be much smaller than the total pile tip displacement. However, it is similar, of the same order of magnitude, as the permanent deformation of the soil (compare Tables 5.2 and 5.5). This may lead to believe that there was a loss of contact between the pile tip and the soil and that, as a result, the soil deformation is not as large a multiple of plastic deformation as total pile tip displacement leads to believe.

For a wave travelling away from its source, there are two sources of damping: geometric damping and material damping. According to elastic theory, geometric damping of

Table 5.5 Measured acceleration of dispersed waves

TEST No	ACCELERATION			SOIL DISPLACEMENT mm
	Y_2 m/s^2	Z_2 m/s^2	PILE m/s^2	
DS3-1A	1.3		2060	
1B	1.0		2022	
DS3-2A	1.4/0.5	30	1835/1011	0.00056
2B	1.3/0.5	54/27	2097/1236	0.00101/0.00051
DS3-3A	1.8	130	3431	0.01047
3B	5.0	237	2247	0.00988
DS3-4A	1.2	24.4	1124	0.00046
DS3-5A		95	2172	0.00488
5B		77/90	1573/1873	0.00395/0.00462
5C	2.2(X)	122	1573	0.00508
DS3-6A	1.6		4270	
6B		87	2097	0.00447

the wave displacement amplitude at a relatively large distance from the source is inversely proportional to the distance from the source, Richart et al. (1970). According to Boussinesq, the static stress beneath a rigid footing resting on an elastic half-space drops to about 9% of the total load in the first 2.B of depth (B is the footing width). Hence, a "relatively large distance" could be defined as beyond a depth equal to 2.B. In a situation where scale effects are likely to be important because of the large size of the material grains compared to the pile size, the validity of such theories often becomes doubtful. Also, it should be kept in mind that the effective bearing area of the pile on the soil is very small and that the stresses imposed large enough to fail the soil. Nevertheless, if it is assumed that B is equal to the pile wall thickness, that the acceleration is measured 200 mm ahead of the pile tip and that deformation is directly proportional to force, the soil deformation 200 mm ahead of the pile tip should be in the order of 0.1% of the deformation at the pile tip.

If it is assumed that integration of the acceleration signals give a true picture of the deformation, then comparison between soil displacement in Table 5.5 and pile tip displacement in Table 5.2 show that the difference is of the same order of magnitude as mentionned above (e.g. about 0.1%). Acceleration records do not show convincingly that amplitudes get larger as the pile gets closer to the

embedded transducer. Lack of precise information on the distance between pile tip and embedded accelerometer inhibits more detailed analysis. Since the scope of this measurement was only to verify that all the energy is used efficiently, it is left to others to make detailed studies of the various factors involved in the elastic deformation of frozen soil beneath a vibrating footing.

Present practice of estimating material damping using dimensionless mass ratio (Richart et al. (op. cit.)) can not handle problems on such small scale as it was developed for full size footings.

Geometric damping can account for the difference in amplitude between the pile tip and the embedded transducer. There still is material damping but its effects are shadowed by larger geometrical damping and probably by scale effects. There does not appear to be any significant amount of energy propagating away from the pile tip without having participated in soil deformation, hence in the penetration mechanism.

5.2.5 Conclusion of Analysis

The analysis reveals that the distribution of energy in the soil-pile system is not simple. Input from the driver is used for strain energy, plastic work, grain crushing, thermal loss through grain to grain and grain to steel friction and for elastic excitation of the soil mass. One phenomenon is always the cause of another. Hence, the

energy associated with any of the sinks (users of the driver's energy) overlaps with the energy associated with another sink.

It has been shown than penetration of piles by vibration in frozen soils is due to plastic deformation of soil at pile tip and not to melting of soil as previously believed.

5.3 Recent Field Tests

Field driving tests were conducted in frozen granular soils on two open-ended pipe piles, Morgenstern (1980). Both low frequency and resonant drivers were used. The piles were fully instrumented for force and acceleration at both their top and tip. The piles were 600 mm in diameter with a wall thickness of 19 mm. Both piles were steel and made of up to three sections about 12.5 m long welded on as penetration allowed. Both pile tips were reinforced by a driving shoe 75 mm long and 12.7 mm thick. The driving shoe increased the tip area to 591 cm^2.

The procedure adopted was to drive the piles to refusal with an impact hammer, then to refusal again with a low frequency vibratory hammer and finally, to refusal with a Bodine Resonant Driver.

The site stratigraphy was as follows: 39.6 m of brownish, grey, fine to medium frozen sand, traces of gravel, gravel seams and clay pockets, underlain by 4.6 m of

frozen silty clay followed by frozen sand and sandy silt. Ground ice description is not available and ground temperature was not measured. Ground temperature is estimated to be a minimum of -2°C near the surface and around -0.5°C at 50 m depth.

5.3.1 Field Observations

During driving, a thawed film was observed both inside and outside the pile. It was observed that the grain size distribution of the thawed film slurry was much finer than that of the natural material, Weaver (1980).

These field observations agree very well with the phenomenon observed during the laboratory tests. It is a good indicator of the pile to ground pressure at the tip of the pile.

5.3.2 Low Frequency Driving

The use of the low frequency driver did not prove very successful.

After nearly two hours of vibrating the pile at a frequency of 18 Hz did the pile start to move. Its penetration rate was in the order of 1.9 cm/min. This is a good rate compared to tests in the laboratory research but poor as a field performance.

The acceleration signal was not very clear but the force at the tip of the pile, the soil dynamic response, appeared to be in the Impact Domain. The force peak

magnitude was about 500 kN, producing a tip stress on the soil of about 8.5 MPa. This stress is around the lower bounds of bearing capacity for the soil. Pile acceleration was around 100 m/s^2 at that time.

Shortly after the above measurements were taken, the driver output was increased. This resulted in an increase in penetration rate to 4.1 cm/min. The soil dynamic response was increased to about 890 kN (pressure on soil of 15.1 MPa). However, it should be noted that every second peak did not develop an impact spike as large as the first one. This is attributed to insufficient bias surcharge being applied to the top of the pile. The exciter frequency was around 16.3 Hz at the time of these measurements. Again, the acceleration signals contained a lot of noise. Much of it can be attributed to transverse sensitivity of the transducers. The acceleration for that part of the test was around 80 m/s^2. The lower acceleration is attributed to a larger contribution of the driver force to the soil dynamic resistance (see Equation 5.1).

In all acceleration and force records where no penetration was achieved, tip acceleration and force were within the Elastic Resistance Domain where no permanent deformation is imposed to the soil. Damping along the sides of the pile which was embedded about 12 m, caused dissipation of energy before it reached the pile tip.

All the observations from the raw data are in good agreement with the experimental program conducted in the

laboratory.

5.3.3 Resonant Driving

If the equations recommended in Chapter 2 to predict pile resonance frequency are used, it is found that the piles were not excited at resonance during the field program.

The first test pile was driven for 10 m at frequencies ranging from 83 to 90 Hz when its resonance frequency was 70 Hz and its length 24.1 m. Then its length was increased to 36.9 m and the resonance frequency became 46 Hz. The pile was excited at frequencies ranging from 63 to 110 Hz. It penetrated 12.2 m before another section was added. Best penetration rates were obtained at frequencies between 66 and 68 Hz. After the third section was added, the pile length and resonance frequency were respectively 47.9 m and 35 Hz. Driving until refusal at a depth of 46.0 m was carried out at a frequency of 98 Hz.

The Bodine Driver started on the second test pile as it was 24.8 m long and had a resonance frequency of 68 Hz. Driving took place at 97 to 100 Hz. After about 1.5 hours of cumulative driving on the second test pile, the hammer offset roller bearing housing broke and the project had to be cancelled because of the long delays for replacing that part.

Acceleration and force records show that measured tip forces are low (<30 kN) and that acceleration is high (peaks

over 300 m/s² in the direction of penetration). There appears to be a contradiction: high acceleration with low force. The tip force record does not show any sign of impact. Not all the records were available, this is true only for three sampling points taken during the first 20 min of driving the second test pile. It was observed that the bottom instrumentation of the second pile started to fail near the end of the test. The possibility of instrumentation disturbance prior to that has to be considered.

Observed penetration rates ranged between 6.1 and 18.3 cm/min for lengths driven with the Bodine Driver. Although the piles were not driven exactly at resonance, they still behaved as deformable bodies. Such behavior is very complex and requires more analysis before any conclusions can be drawn. Unfortunately, because of the lack of availability of data, analysis can not proceed at this point in time. Incomplete data also inhibits any definite conclusions about the penetration mechanism in high frequency driving. However, the author remains highly skeptical as to the existence of low forces at the tip of piles excited at high frequencies.

5.3.4 Conclusion

The behavior of piles driven at low frequencies in permafrost is in perfect agreement with the behavior observed during laboratory tests. Lack of data does not

allow any conclusion about high frequency driving. It is felt that the efficiency of the Bodine driver could have been increased by driving at the pile's resonance. The soil resistance at pile tip has to be carefully evaluated for the Bodine driven piles.

5.4 Summary

In this Chapter, the test data was presented and analysed. It was compared to field data.

It was found that slow vibratory driving took place. Tip reactions were elasto-plastic. The factors which led to this conclusion are:

1. Enough plastic work is done on the soil for penetration; the soil dynamic resistance exceeds the soil elastic range;
2. Excessive wear of the pile tip;
3. Visual inspection of the pile hole after driving did not reveal any thawed bulb ahead of the pile;
4. Crushing of the sand grains occurs; very high grain to grain pressures generate high grain surface temperature during slippage, with pile side friction, this contributes to soil thaw after its failure (or yielding);
5. Piles driven in dense frozen sand required more energy than piles driven in loose frozen sand to penetrate. If melting was the cause of penetration, the opposite would

be because of the large difference in ice content.

The influence of each independent parameter was discussed. For each soil type and temperature, there is an optimum surcharge-frequency combination for penetration.

Field data for piles behaving as rigid bodies, although limited, was in very good agreement with the laboratory findings. Lack of data for piles behaving as deformable bodies does not allow valuable comments. Penetration was observed to be higher for high frequency driving but force at the pile tip to be lower. Defective instrumentation or soft clay pockets are suspected. Further examination of records may provide some answers once the data becomes available.

CHAPTER 6

CLOSURE

6.1 Recommendations for Future Laboratory Tests

In order to study pile driving behavior on other material and to investigate some points more deeply to confirm the present findings are applicable to all cases, the following changes to the testing program and equipment shall be made.

- A well graded sand should be used to increase the density contrast between loose and compact sand.
- The sample containers should be fitted with false bottoms containing a large diameter copper tube coil through which a very cold fluid could be circulated. There could be a similar coil on the outside of the container burried in dry ice for cooling. This system would allow more reliable and more uniform freezing of samples. To speed up freezing, liquid nitrogen could be used as a fluid.
- A higher capacity load cell should be used, at least 450 kg preferably 900 kg.
- Pile penetration, load, acceleration, driving force (current output from driver) and body waves in the x, y

and z directions should all be recorded on the same magnetic tape to synchronize the signals.

- The above data should be recorded at high speed and played back at low speed on a strip-chart recorder.
- The testing program should concentrate on two extreme temperatures only, say -2°C and -8 or -10°C.

6.2 Recommendations for Future Field Tests

The following objectives should guide any future field tests of vibratory driving in permafrost:

1. Improve present driveability prediction methods for vibratory pile drivers;
2. Develop or verify a soil resistance model for vibratory pile drivers;
3. Rate the performance of drivers for future studies.

To achieve these objectives, a thorough testing program with complete instrumentation is required. It should not be forgotten to measure the ground temperature profile as it is a determining factor of the soil mechanical properties. A thorough site investigation shall be carried out to determine the soil mechanical properties.

As far as the driving is concerned, it should be carried out at either the calculated resonance or at the field-tuned resonance. Critical spare parts should be readily available on site to avoid long delays. Finally, the pile sizes should be such that the driver has enough

power to be effective. Several pile and driver combinations could be investigated.

6.3 Recommendations for Analytical and General Background Research

Any analytical work initiated on vibratory pile driving in permafrost should have for aim:

1. Development of a proper soil rheological model;
2. Incorporation of an adequate soil model in driveability predictions;
3. Development of a damping or energy-dispersing model accounting for pile misalignment and eccentricity during driving;
4. To take into account deformability of the pile;
5. To take into account change in soil properties with depth.

As far as general background is concerned, the following areas are considered pertinent to the driving problem and lacking in data:

1. Dynamic properties of frozen soils in the 50-150 Hz range;
2. Requirements for impact crushing of soil particles with respect to bearing capacity strength;
3. Plastic flow under high confinement (e.g. at pile tip);
4. Effects of pile buckling or lateral deformation during driving on effective tip force.

6.4 Conclusion

The most important finding of this research program is that penetration of the pile is due to a plastic deformation of the frozen soil rather than to melting of the latter as previously believed. The influence of various factors which influence this tip elasto-plastic reaction was also examined. Only one requirement transpires from it all: the strength of the material has to be overcome.

The energy distribution at the pile tip is not an easy problem to solve. All phenomenons are inter-related and each can not be taken apart from the others. However, it has been shown from experimental results, analysis and discussions that no other energy than that required to fail the soil is dispersed through the soil. Also, the energy used for melting the permafrost surrounding the pile comes from both plastic work and side friction of the pile walls on the confined material. It was concluded that energy used to crush the sand grains was included in plastic work.

Field tests carried out by private industry were examined and despite their lack of data, agree well with the present findings.

Recommendations for future research in the laboratory, in the field and in related areas were made in the first parts of this Chapter. The purpose of further research is to ultimately provide good engineering prediction methods for vibratory pile driving in permafrost. A theoretical model which would allow prediction of wether or not there

will be penetration would allow design of large machinery for large scale piling in offshore conditions for example. Understanding of the mechanics of penetration is now sufficient to allow work on a theoretical basis. However, the importance of gathering more experimental data should not be overlooked. Every possible case needs to be studied to provide a wider base to the present understanding of vibratory driving in permafrost.

BIBLIOGRAPHY

Andersland, O.B., Anderson, D.M., (1978), Geotechnical Engineering for Cold Regions, McGraw-Hill Inc., U.S.A., 566p..

Bernhard, R.K., (1967a), "Resonant Curve Analysis", United States Army Cold Region Research Engineering Laboratory, SR 97, Hanover, N.H..

Bernhard, R.K., (1967b), "Fluidization Phenomena in Soils During Vibro-Compaction and Vibro-Driving and -Pulling", United States Army Cold Region Research Engineering Laboratory, SR 106, Hanover, N.H..

Bernhard, R.K., (1968), "Pile-Soil Interaction During Vibro-Pile-Driving", Journal of Materials, American Society for Testing Materials, Volume 3, Number 1, pp. 178-209.

Catoire, B., (1963), "Théorie soviétique du fonçage des pieux", Annales des Ponts et Chaussées, Volume 133, numéro 1, pp. 63-88.

Davisson, M.T., (1965), "Estimating Resonant Frequencies for Piles Driven with the BRD", Internal Report at the University of Illinois, October, 19p..

Eastwood, W., (1955), "Model Investigations Concerned with Driving Piles by Vibration", Civil Engineering, Volume 50, Number 589.

Fawcett, A., (1973), "The Peformance of the Resonant Pile Driver", Proceedings 8th International Soil Mechanics and Foundation Engineering, Volume 2.1, Moscow, pp. 89-96.

Ghahramani, A., (1967), Vibratory Pile Driving, Ultimate Penetration and Bearing Capacity, Ph.D. Thesis, Princeton University, Princeton, N.Y., 106p..

Griggs, F.E.Jr , (1967), The Pile Problem with Special Emphasis on the Vibratory Placement Technique, Dr Eng. Thesis, Reensselaer Polytechnic Institute, Troy, N.Y., 113p..

Halliday, D., Resnik, R., (1967), Physics, parts I and II, 2nd edition, John Wiley and Sons, Inc., New-York, N.Y., 1214p..

Hayley, D.W., (1979), "Site Evaluation for Artificial Drilling Island in the Beaufort Sea", 1st Canadian Conference on Marine Geotechnical Engineering, Calgary, Canada.

Huck, R.W., Hull, J.R., (1971), "Resonant Driving in Permafrost", Foundation Facts, Volume 7, Number 1, pp. 11-15.

Hull, J.R., (1977), "Placing Piles in Permafrost", World Construction, December, pp. 64-67.

Hunter, A.H., Davisson, M.T., (1968), "Measurements of Pile Load Transfer", American Society for Testing Materials, Symposium on Deep Foundations, San Francisco, 21p..

Kovacs, A., (1966), Unpublished Data on Resonant Pile

Studies at United States Army Cold Region Research Engineering Laboratory, Hanover, N.H., Cited by Kovacs and Michitti (1970).

Kovacs, A., Michitti, F., (1970), "Pile Driving by Means of Longitudinal and Torsional Vibrations", United States Army Cold Region Research Engineering Laboratory, SR 141, Hanover, N.H., 17p..

Littlejohn, G.S., Rodger, A.A., (1980), "A Study of Vibratory Pile Driving in Granular Soils", Geotechnique, Volume 30, Number 3, pp. 269-293.

Morgenstern, N.R., (1980), Private Communication.

Rayleigh, Strutt, J.W., Baron, (1926), Theory of Sound, Volume 1, 2nd edition, Macmillan, London, 480p..

Rayner, J., (1974), "Vibration Pile Driving Dints Costs", Engineering Contract Record, Volume 87, Number 9, pp. 15,16,55,74.

Reseigh, A.S., (1961), "Sonic Waves Drive Piles", Providence Sunday Journal, Reprint, October 29, 4p..

Richart, F.E. Jr, Hall, J.R. Jr, Woods, R.D., (1970), Vibrations of Soils and Foundations, Prentice-Hall, Englewood Cliffs, N.J., 414p..

Sayles, F.H., (1973), "Triaxial and Creep Tests on Frozen Ottawa Sand", Permafrost: the North American Contribution to the 2nd International Conference, Yakutsk, National Academy of Science, Washington, D.C., pp. 384-391.

Schmid, W.E., (1969), "Driving Resistance and Bearing

Capacity of Vibro-Driven Model Piles", in Performance of Deep Foundations, American Society for Testing Materials Special Technical Publication 444, American Society for Testing Materials, pp. 362-375.

Scott, J.D., (1980), Private Communication.

Smart, J.D., (1969), Vibratory Pile Driving, Ph.D. Thesis, University of Illinois, Urbana, Ill., 184p..

Vyalov, S.S., Targulyan, Yu.O., (1968), "Boring and Pile Driving into Permafrost", Osnovaniya, Fundamenty i Mekhanika Gruntov, Number 2, pp. 24-26, English Translation in Soil Mechanics and Foundation Engineering, pp. 115-118.

Vyalov, S.S., Targulyan, Yu.O., Vsorskiy, D.P., (1969), "Interplay of Frozen Ground with Piles during Vibratory Driving", Technical Translation FSTC-HT-23-944-68, U.S. Army Foreign Science and Technology Center, 13p..

Weaver, J.S., (1980), Private Communication.

APPENDIX A

DRIVING APPARATUS AND LABORATORY FACILITIES

In this appendix, the laboratory equipment and facilities will be described. The description details the general facility and specific equipment used in this laboratory program.

A.1 Cold Room

The tests were conducted in a 3.35 x 4.0 m insulated cold room. The room is kept cool by two fan operated refrigeration units capable of maintaining the temperature within half a °C of the required temperature. The room can be kept at temperatures as low as -20°C. A 24-hour electrical alarm system prevents accidental defrosting of the facility. Access to the cold room is through a double door air lock which reduces inflow of warm air from outside in order to minimize the temperature variation within the cold room.

The electronic controls for the vibratory exciter and the thermocouple chart recorder are kept outside of the cold room. A double thermal pane-window gives visual access to the test set-up. This allows for visual control of the test from the instrument controls. Some measuring instruments have to be recorded by a data acquisition system which is

located in the next room. In those cases, the lines go from the cold room to the acquisition system over the false ceiling.

The vibratory exciter is a heavy piece of equipment and has to be supported adequately. The samples are equally heavy and also have to be supported. Hence, modifications were carried out to the existing cold room in order to provide such support. A buttress support system and a sample pedestal needed to be supported on the concrete slab of the laboratory rather than on the insulated false floor of the cold room. The insulated floor of the cold room was not designed to withstand dynamic loads and it would have acted like a spring under the test set-up. A 12.5 mm thick aluminum plate was placed on the concrete pedestal to ensure a smooth surface. And, finally, a copper pipe coil was placed inside the concrete pedestal near its surface. It is intended to circulate a refrigerant fluid to form a barrier to the heat flow coming upward through the concrete slab and sample pedestal. This measure was necessary because of the high heat conductivity of the pedestal compared to the insulated false floor in the cold room. Details of the driver support are discussed and illustrated in the following section.

A.2 Driver Support and Guiding System

Figures A.1 to A.3 show details of the driver support and guiding system. Plate A.1.a shows the driving apparatus and Plate A.2.b shows a close-up of the guiding system. All of the guiding system herein explained was designed and built for this research at the University of Alberta.

The main feature of the set-up is indeed the column and its buttress support piles as were discussed in the previous section. To the column is attached the exciter support. Two rollers made from linear bearings are mounted on the exciter support. The guiding system consists of a "piston" passing through a guiding box coated with teflon to reduce the friction. The exciter is bolted upside down to the bottom of the piston. A 76 mm wide webb belt is attached to the top of the piston on one side and, after travelling over the two rollers, to a counterweight support. The details of the system are contained in Figure A.2.

The exciter support is well braced to minimize the deflections caused by the heavy weight of the exciter.

In spite of all precautions taken some friction remains in the system. Its main source comes from the temperature shrinking of the piston guide. Although enough tolerance has been given to ensure good movement at temperatures as low as -10°C, other factors such as the machining tolerance of the piston itself become important. Another factor likely to greatly influence the friction is the verticality of the whole apparatus. No reliable means of measuring the

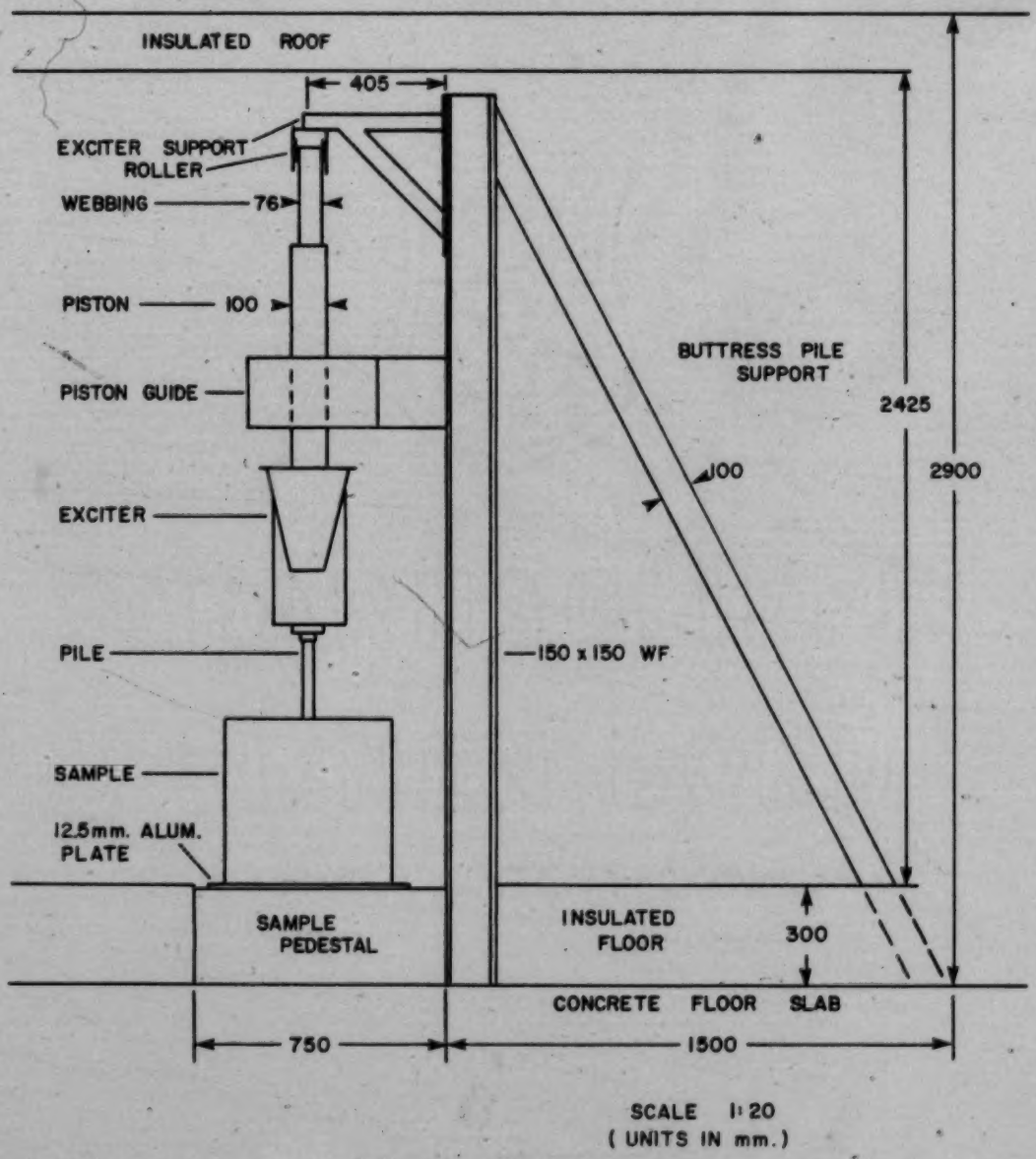

Figure A.1 Side view of the testing apparatus

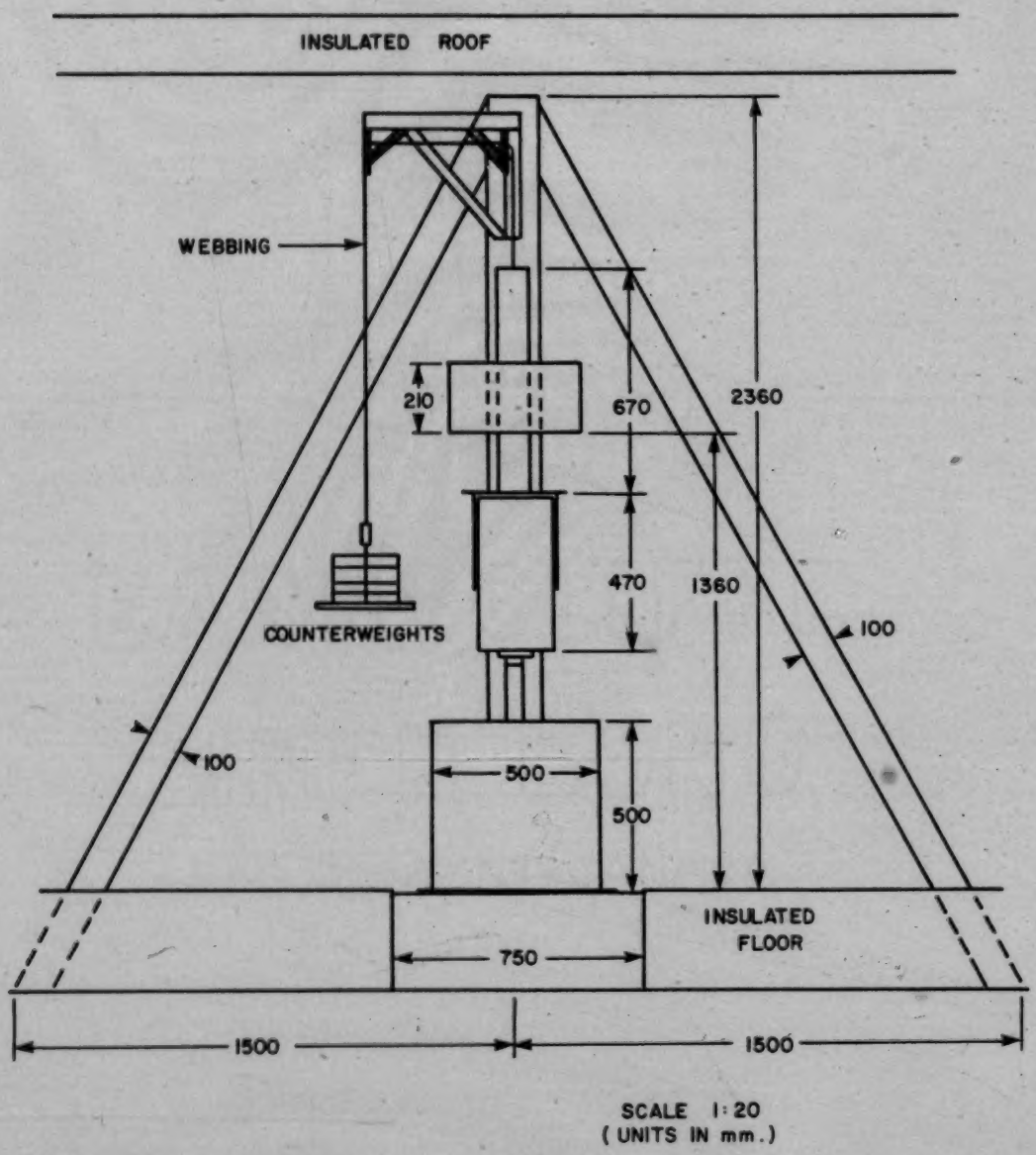

Figure A.2 Front view of the testing apparatus

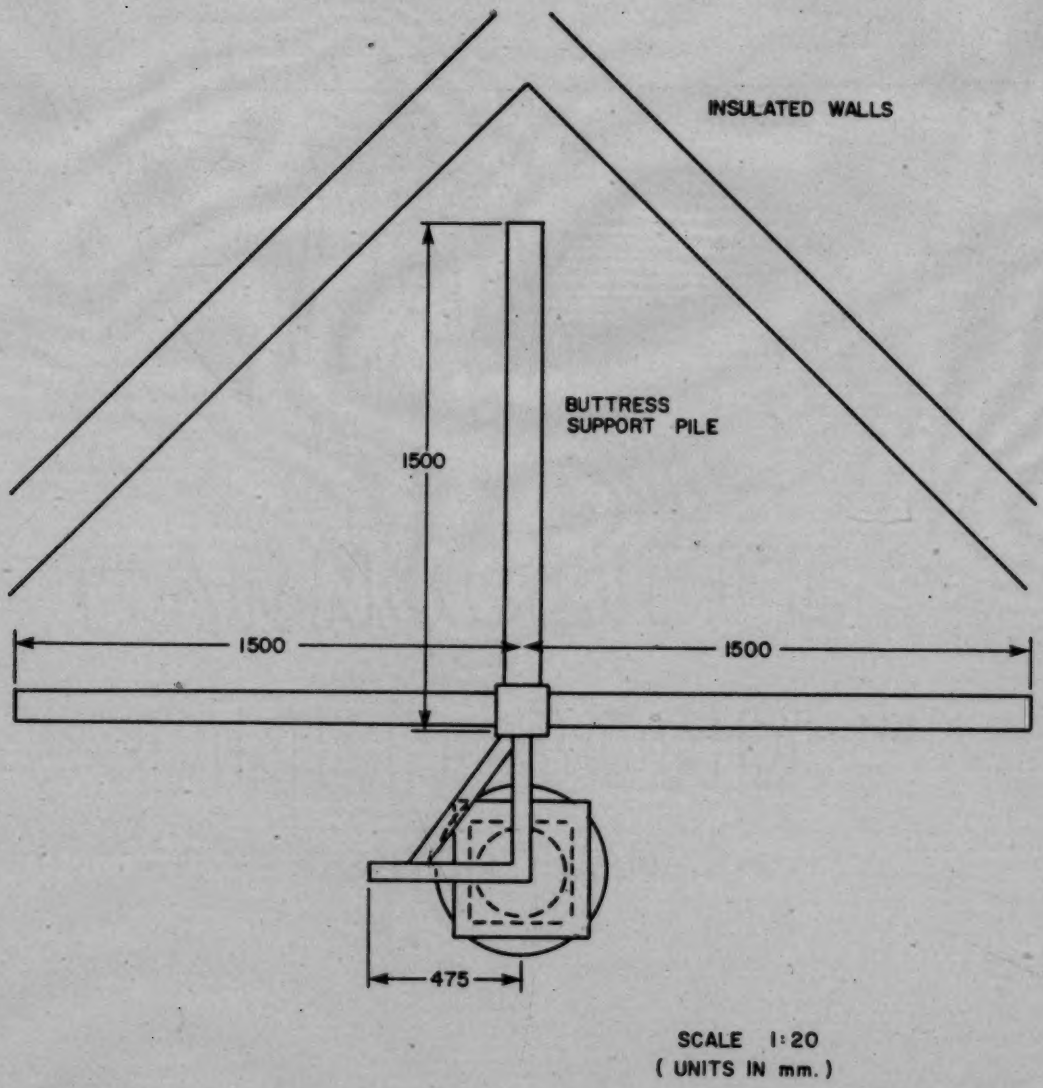

Figure A.3 Top view of the testing apparatus

a) Driving apparatus.

b) Exciter control and temperature chart recorder.

Plate A.1 General view of test facilities.

a) Pile attachment and instrumentation.

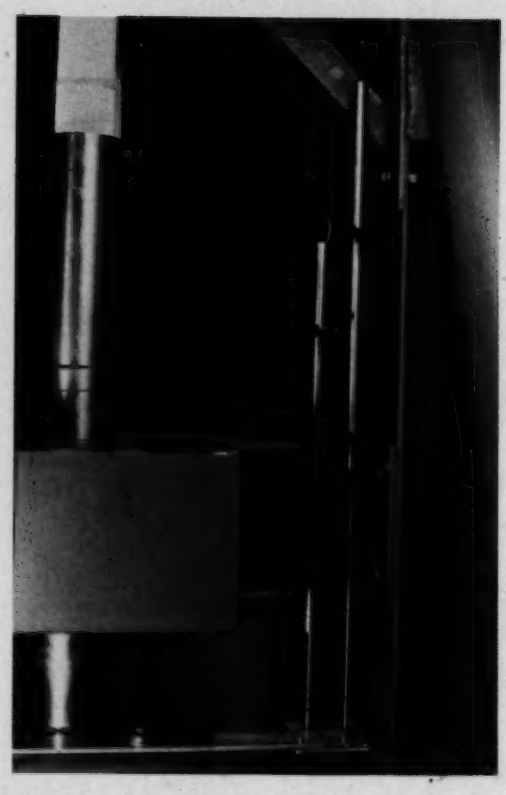

b) Displacement transducers.

Plate A.2 Detailed view of test facilities.

losses in friction has yet been found, given the complexity and variability of the governing factors. Friction, as discussed in the main text, has had an important influence on the test results but one of the important goals of the research is to point out trends and the relative importance of various parameters rather than to produce absolute results on penetration rates.

A.3 Pile Attachment

The pile attachment is shown in Figure A.4 and Plate A.2.a. The same arrangement is usable for either exciter (B&K 4808 or 4812) with a minor modification for the small exciter (4808). The exciters are described in a later section.

The device consists of an adaptor cap welded to the top of the tubular pile, a load cell, an aluminum plate and a rubber pad to minimize the flexural loads on the exciter magnetic core. The pile cap has an air bleeding hole to eliminate the potential cushion effect while driving. The adaptor cap is screwed into a load cell which in turn is fixed to the aluminum plate by a set screw. Manufacturer's specified inserts go through the aluminum plate and rubber pad to the exciter table. When the small exciter is used a load cell adaptor has to be used to allow the inserts to be placed. Because of the small size of the pile, the accelerometer is placed near the edge of the aluminum plate.

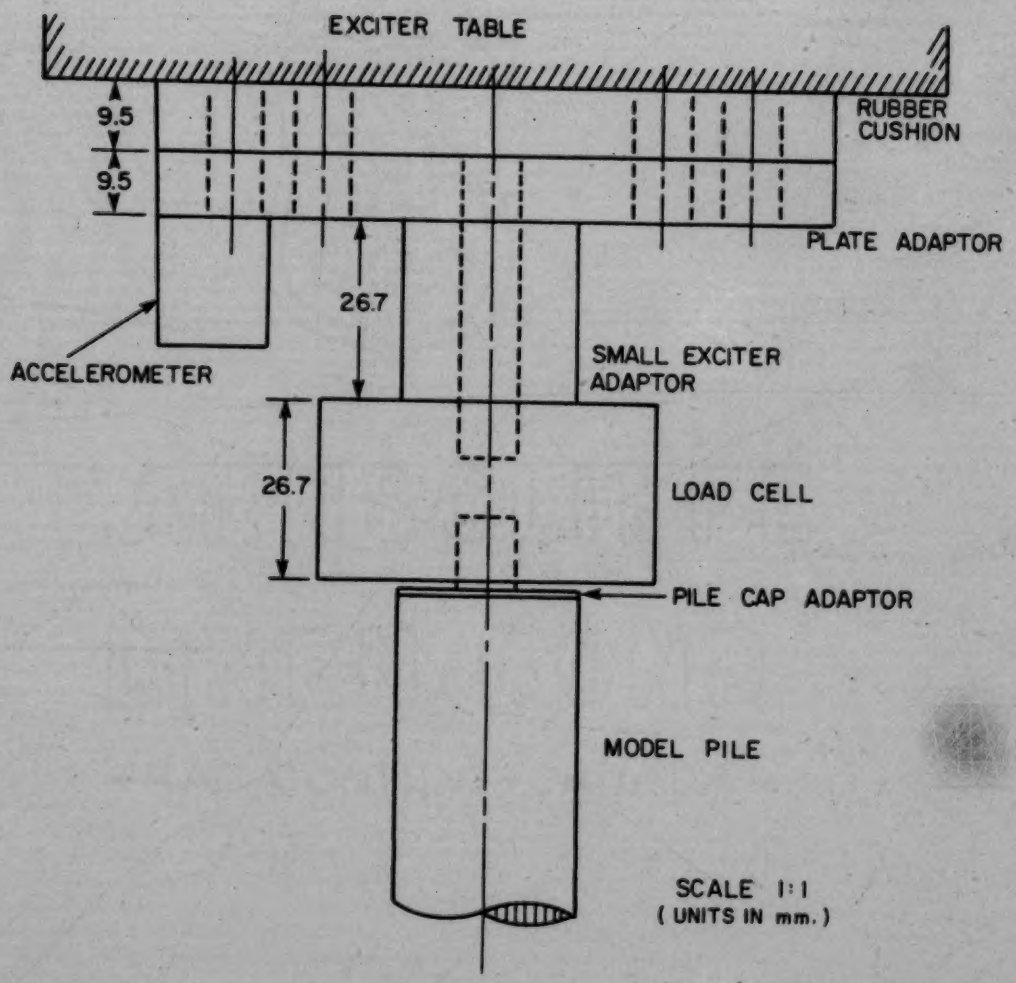

Figure A.4 Pile attachment to the driver

A.4 Sample Container

A sample container was designed for this research project. It is cylindrical and allows for a sample of 50 cm in diameter and 50 cm high. The container wall is made of 3.2 mm thick rolled aluminum. The bottom was first made of a 3.2 mm thick plate but later reinforced with 12.7 mm thick aluminum plate to resist frost heaving pressures when sitting on the freezing apparatus. Aluminum was selected because of its light weight and because of its excellent thermal conductivity. Gharamani (op. cit.) used a plastic container to reduce wave reflections in his experiments. Plastic would certainly be inadequate to hold a sample of the desired size or to resist the frost heave pressures. Plastic also looses most of its ductility in cold environments.

The container has four carrying handles near the top. the estimated mass of a full sample container lies between 190 and 200 Kg.

Another container first intended for the preparation of polycrystalline ice was used. Its dimensions are slightly different from the first one. It has a diameter of 505 mm and a depth of 540 mm. This container features a perforated false bottom to allow flooding of the sample from the bottom. This feature was not used as the samples were pre-saturated during preparation.

The first mould was always used for the dense samples while the second was always used for the loose samples.

A.5 Freezing Stand

The samples have to freeze as quickly as possible to reduce the preparation time and avoid uncontrollable freezing in three dimensions. Uncontrolled freezing from the surroundings would certainly lead to the formation of a unfrozen zone in the center of the sample. Such a zone would delay sample freezing and may cause the sample to crack due to the build-up of pressure within the thawed central zone. For the forementioned reasons, a freezing stand was designed. It allows one dimensional freezing from the bottom under a high temperature gradient. The apparatus was designed to hold either dry ice (solid carbon dioxide) which has a temperature of -78°C or liquid nitrogen which has a temperature of -195°C. The apparatus is shown in Figure A.5.

Once the unfrozen sample is placed on top of the filled apparatus, the sample container is wrapped in fiberglass insulation wool to ensure a minimum amount of heat transfer occurs through the sides of the sample container. The top is insulated by a styrofoam cover.

When dry ice is used, 24 to 48 hours are required to freeze the sample, depending upon the water content. At least another 12 hours is given to the sample to equalize to room temperature once the insulation is removed and the sample container is removed from the freezing stand.

Liquid nitrogen has not yet been used to freeze a sample since the dry ice method produces a sample of

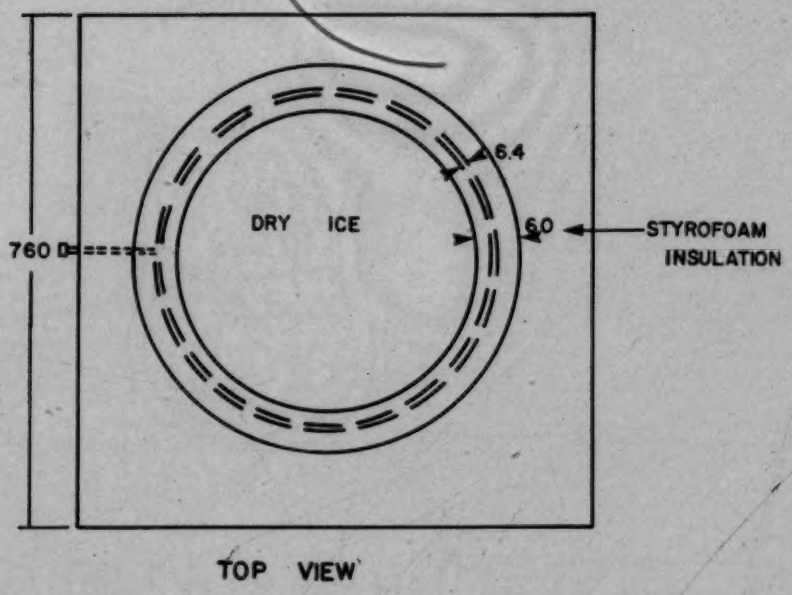

TOP VIEW

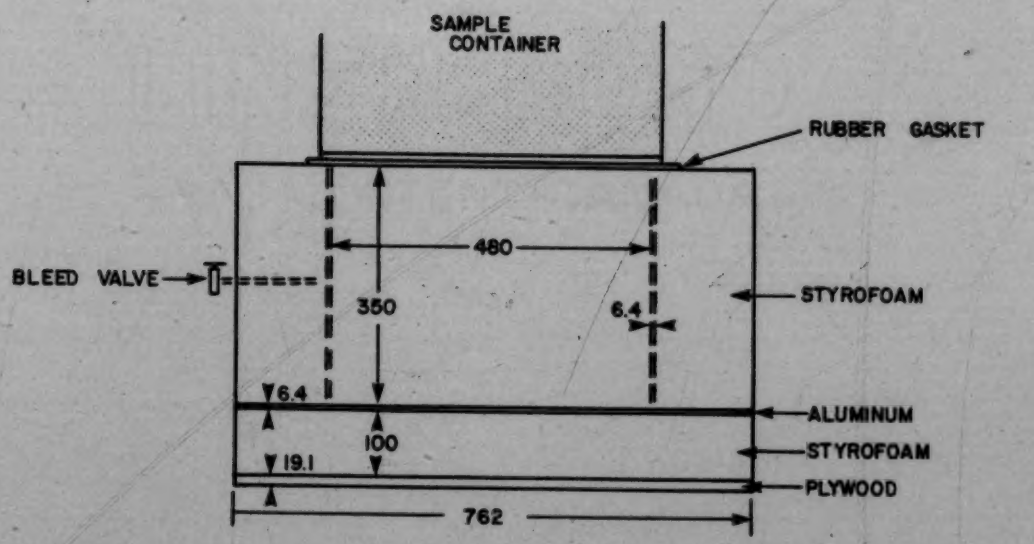

FRONT VIEW SCALE 1:10 (UNITS IN mm.)

Figure A.5 Freezing stand for samples

acceptable quality and within the required time. Liquid nitrogen would decrease the preparation time and may improve the quality of the sample. It would be advantageous for mass production of samples. The actual cycle for making and testing one sample is five days if all the tests are carried out at the same temperature. Another day must be counted for every temperature change. As far as cost is concerned, the volume of liquid nitrogen required to fill the apparatus is slightly cheaper than the required volume of dry ice.

A.6 Driver and Controls

Two electromagnetic vibration exciters are available for model studies at the Department of Civil Engineering. They are the type 4808PM and type 4812 mounted on body 4801S exciter made by Bruel and Kjaer.

Figures A.6 and A.7 show schematically the controls for exciters 4808PM and 4812 respectively. Plate A.1.b shows the exciter control with power amplifier below.

Exciter 4808PM is controlled by the exciter control 1047 whose signal is amplified by the power amplifier type 2707A. The exciter draws its power directly from the power amplifier as it only requires 115 volts. The signal from the accelerometer (4366S) can be sent to the exciter control for closed loop operation or simply for visual monitoring on a vibration meter. The accelerometer signal has to go through a signal conditioner and amplifier before it can be

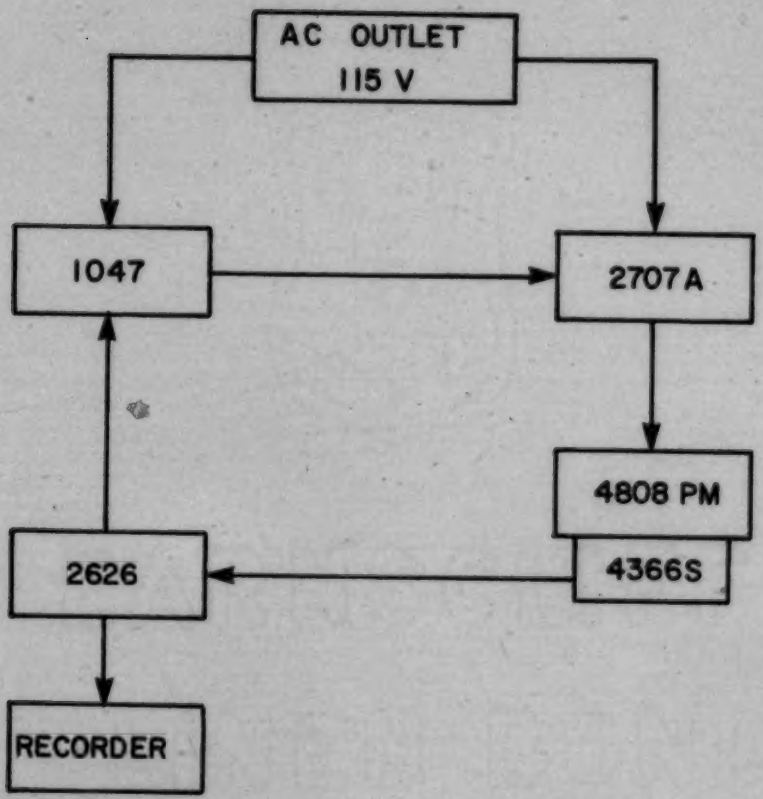

Figure A.6 Controls of the small exciter, 4808PM.

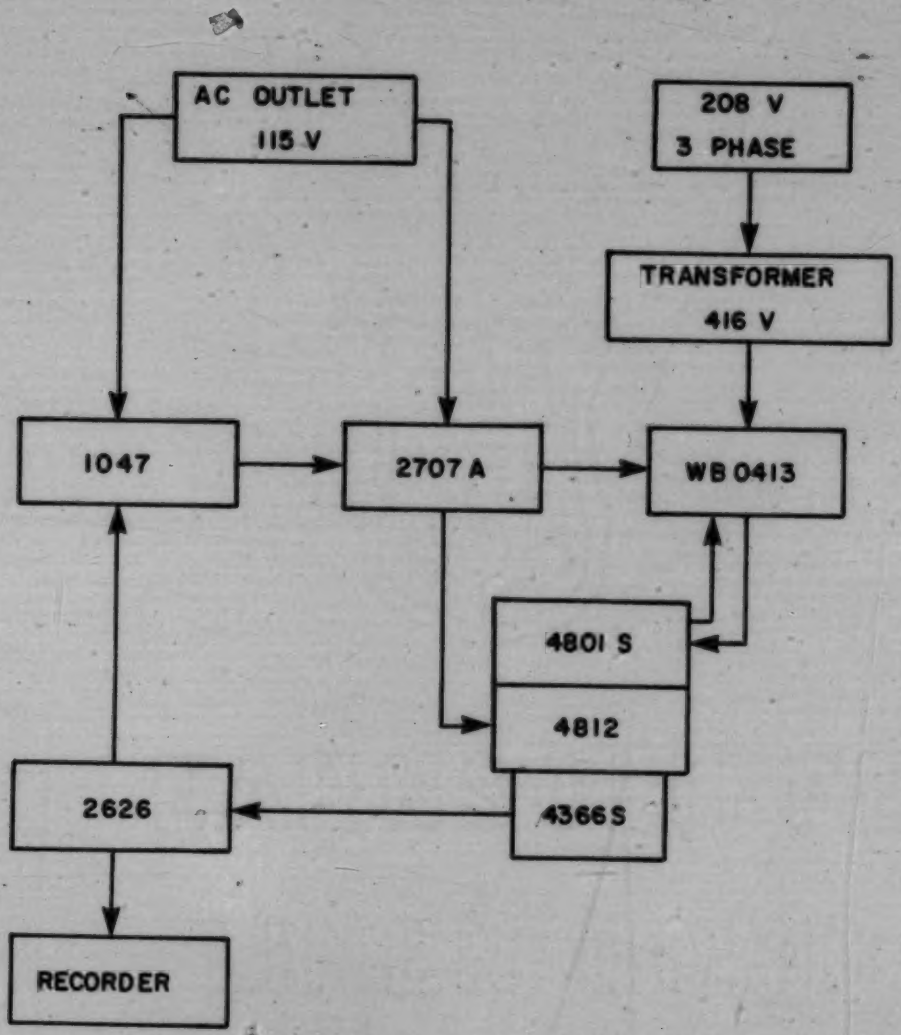

Figure A.7 Controls of the large exciter, 4812.

decoded. Exciter body 4801S needs 416V 3 phases power to operate. Because it was not available in the building, a 208V, 3 phases outlet was brought in the room and a transformer built to upgrade the voltage. The 416V current is sent to a transfer box (WB0413). From the transfer box, the power supply is amalgamated to a signal from the power amplifier 2707A and sent to the exciter body. Simultaneously, a signal is sent to the exciter head from the power amplifier. And, as in the case of exciter 4808PM, an accelerometer signal can be sent back to the exciter control 1047 via a signal conditioner (2626).

The operation of both systems is similar except for a couple of settings on the power amplifier and exciter control. One just has to ensure all the proper hook-ups are made before operating any one of the two set-ups.

Only the type 4812 exciter was used in this research project. The type 4808PM does not quite have the required force nor energy specifications to drive these piles.

A.7 Accelerometers

Two types of accelerometers were used: type 4366S and type 4321 triaxial. They are both made by Bruel & Kjaer. A Bruel & Kjaer type 2626 signal conditioner was used for the 4366S transducer and three type 2635 conditioners were used for the triaxial transducer. Three of these four signals were recorded on a field portable Bruel & Kjaer tape

recorder. The signals were analysed in detail after the experiments were carried out.

A.8 Load Cell

A Kulite TC-500 load cell was purchased by the University but had to be returned to the manufacturer because of technical problems. Months later it was decided to move the experimental program ahead with a Transducer Inc. 18 series, model 182 load cell with a capacity of 233 kg in both tension and compression. The Transducer failed in fatigue after the second series of tests. The Kulite was selected because of its overcapacity rating and smaller size. The high capacity provides protection against fatigue during repeated loading. The small physical size gives more room between the driver and the sample for adjustments.

The first tests showed that the load sporadically exceeded the nominal capacity of the load cell. Hence, a TC-1000 which has twice as much capacity (466 kg) was ordered but still has not arrived.

The signal from the load cell was recorded with the acceleration data. Before it is recorded, the signal from the load cell was amplified. Hence, the electronics shop of the Civil Engineering Department designed and built an amplifier compatible with both the load cell and the recorder. The signal from the load transducer is fed into the amplifier which directs the amplified signal to the

recorder.

A.9 FM Recorder

As previously stated, a recorder was used to save the signals for subsequent analysis. It was a Bruel & Kjaer recorder type 7003. The recorder has four channels and can handle signals of up to 50 Volts either alternative or continuous. Two channels were used to pick up the body waves within the sample, one to monitor the pile acceleration and the last one to monitor the pile load. The recorder also allows the signals to be monitored on another device as they are recorded. An oscilloscope was the device used to monitor the waves during the tests.

The Civil Engineering electronics shop designed and built a switch to feed a voltage to one channel of the Fluke 2240A Datalogger while the recorder is on. This allows to relate the recorded signals to the penetration data recorded on the Datalogger (see the section about displacement transducers).

A.10 Temperature Measurements

To monitor the temperature within the samples during freezing and during the tests, thermocouples were embedded at various locations in the first samples to be made. A Honeywell Electronik-15 temperature chart recorder (see Plate A.1.b) was used to record the temperatures. It has a

capacity for 24 channels. The scan of all channels takes 125 seconds.

Temperatures at the pile face were recorded by the Fluke 2240A Datalogger using platinum resistance thermal devices (RTD's) model F2105, series F1, by Omega Engineering Ltd. The RTD's are 1 mm thick and 2.0 x 2.3 mm in size.

A.11 Displacement Transducers

The penetration of the pile was measured by the Fluke 2240A Datalogger using linear voltage displacement transducers (LVDT's). The LVDT's have a total travel of 25 cm. Two of them were used in series when displacements exceeded that figure. An overlap of at least 30 mm was provided to ensure continuity of the measurements. Plate A.2.b shows the two LVDT's overlapping.

The LVDT's are made by Schaevitz Engineering Ltd. and designated model 5000 HR-DC.

A.12 Sample Preparation

A Monarch concrete mixer was acquired to mix the sand and water. The mixer is driven by a 1/4 HP electric motor to avoid fumes in non-ventilated working areas. The mixer has a capacity of about 70 litres. Other accessories used such as shovels, scoops or else are standard items found within the department.

A.13 Oscilloscope

A Tektronik 564B two-channel oscilloscope was used to monitor the load and acceleration of the pile during the tests. With the help of a special adaptor, a Polaroid Land camera was used to take photographs of the waves directly from the oscilloscope screen. The photographs were taken at some time after the test at selected locations on the recorded tape. Polaroid type 47 film was used to take photographs.

A one-channel oscilloscope was used in the first half of the experimental program and had to be replaced because of its very high degree of unreliability. The two-channel oscilloscope gave much more satisfactory results.

APPENDIX B

TESTING PROCEDURE

The most important step in the testing procedure is the sample preparation. Two density states were created: the loosest possible and the densest possible states. As the techniques to produce those densities are quite different, they will be treated under separate headings. A third section of this appendix will explain the steps followed to carry out the experiments.

B.1 Loose Samples

To create a sample in the loosest possible state, sand was thoroughly mixed with water and allowed to saturate in two plastic containers for a minimum of one day.

The sample mould was then filled with 50 to 70 mm of water. A scoop was used to place the saturated sand in the mould. The sand in the scoop was submerged before being poured in the water. It was also insured that the current surface of sand was flat at all times.

When the sample reached the desired height, usually a freeboard of approximately 13 cm on the 540 mm container (see Appendix A), the excess water was removed first by bailing and, after the level lowered, by siphoning.

After the above operations were executed, the sample was placed on the freezing stand. It is needless to say that the freezing stand had previously been filled with dry ice. The sample was wrapped in fiberglass wool insulation. A styrofoam lid was placed on top to stop convection. Samples were allowed to freeze for two days.

B.2 Dense Samples

To create a sample in a very dense state, sand was thoroughly mixed with water and allowed to saturate as in the previous case. The wet sand, with as little excess water as possible, was placed in the mould in lifts of 75 mm. The material was hand-compacted as much as possible. That is about three passes covering the whole area and using as much energy as one can reasonably deliver. The hand tamper has a diameter of about 20 cm. A concrete vibrator was used in the early stages of the research to simulate field vibro-flotation processes. The idea was quickly abandoned as it did not produce the desired effects. About 10 cm of freeboard were allowed in the 50 cm high mould (see Appendix A).

Following its preparation, the sample was placed on the freezing stand and wrapped in fiberglass wool insulation as in the case of the loose sample. A styrofoam lid was put on the top. Forty-eight hours were allowed for the samples to freeze.

B.3 Test Procedure

The following steps were executed to conduct the experiments:

- the sample is unwrapped and removed from the freezing stand;
- at least twelve hours are allowed for the sample to equilibrate at room temperature;
- initial sample temperature readings are taken if thermocouples were placed in the sample;
- the sample is placed on the pedestal under the vibrator;
- proper instrumentation setting is ensured: the scan interval on the Datalogger is 30 seconds, the calibration factors of the tape recorder are verified, the accelerometer charge amplifiers are checked as well as all the exciter controls;
- the transformer, the power amplifier, the charge amplifiers, the tape recorder power source and the oscilloscope are all plugged in and switched on (the vibrator head is not activated);
- the sample surface is cleared of the excess ice, produced by the volume expansion of freezing water, with a sharp scraper;
- the pile is brought in contact with the soil surface by removing counterweights;
- a zero reading of the LVDT is taken with the pile sitting on the surface of the sample;
- the pile and driver are lifted by putting back removed

counterweights to make certain there is no contact with the sample;

- the pile is set in motion at the desired frequency;
- counterweights are taken off to allow the desired net downward bias force on the pile. The pile is held back as weights are removed and slowly lowered by hand until full contact with the sample is made. At that time a second person whose watch is synchronized with the first turns the Datalogger on in the next room;
- penetration of the pile should occur. Vibration meters and the oscilloscope monitor are carefully watched to ensure everything is normal;
- the tape recorder is turned on 30 seconds or one minute after the start of the test. Ensure the coordination switch is also turned on so that the recorded data can be matched with the penetration data;
- after full penetration is achieved, the pile is retracted from the hole and then and only then the vibrations are stopped;
- all the recording equipment is turned off.

If the pile is stopped vibrating while still embedded, the soil and pile freeze together in a matter of seconds. Hence, some tests have to stop before full penetration is achieved because the vibrations become too damped and there is a danger of freezing the pile in the frozen soil.

In some instances, when the retrieved core is of good quality, sample are taken to measure the water (ice)

content.

APPENDIX C

PENETRATION VERSUS TIME CURVES

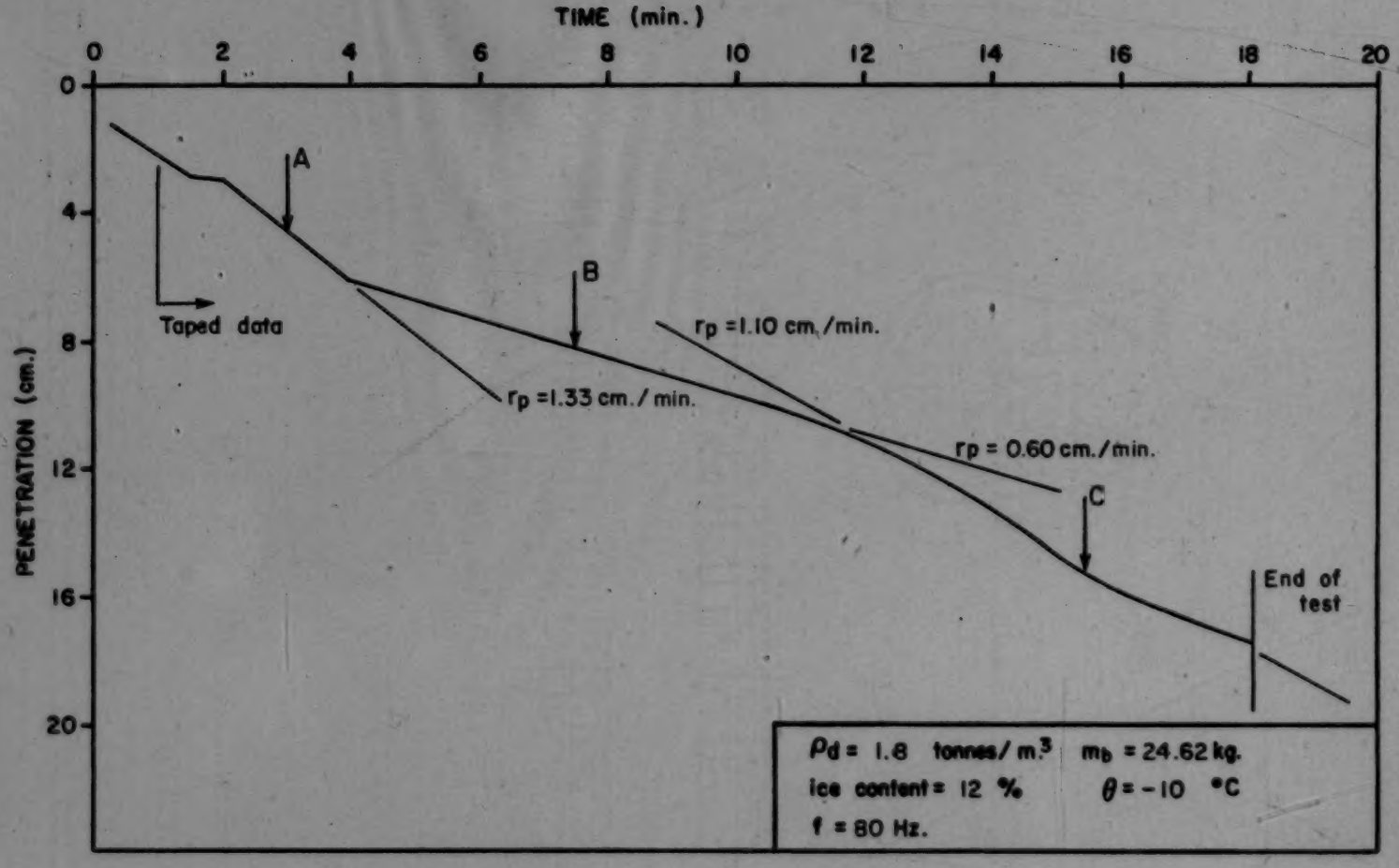

FIGURE C.I PENETRATION vs. TIME CURVE, TEST NO. DSI-1

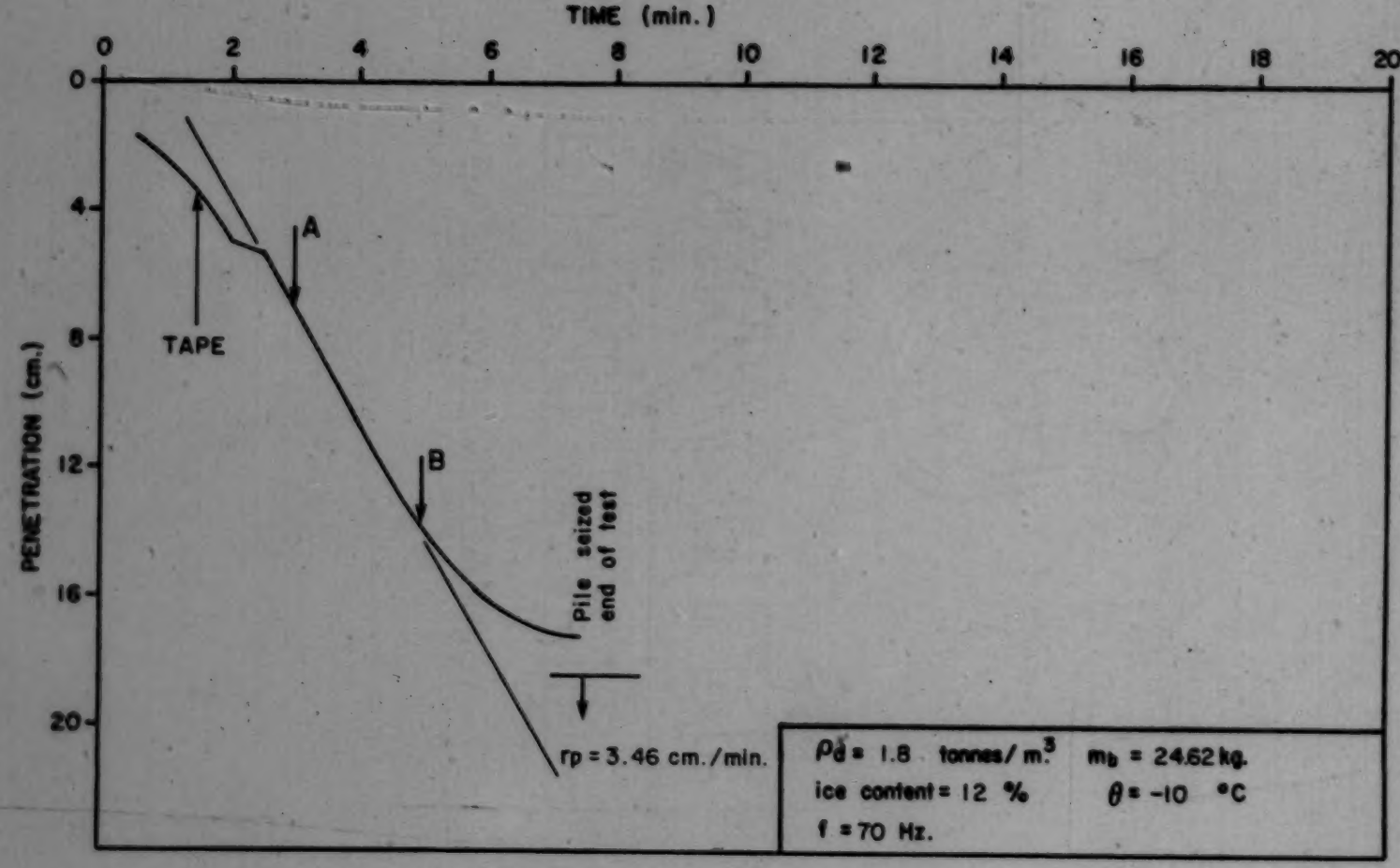

FIGURE C.2 PENETRATION vs. TIME CURVE, TEST NO. DS1-2

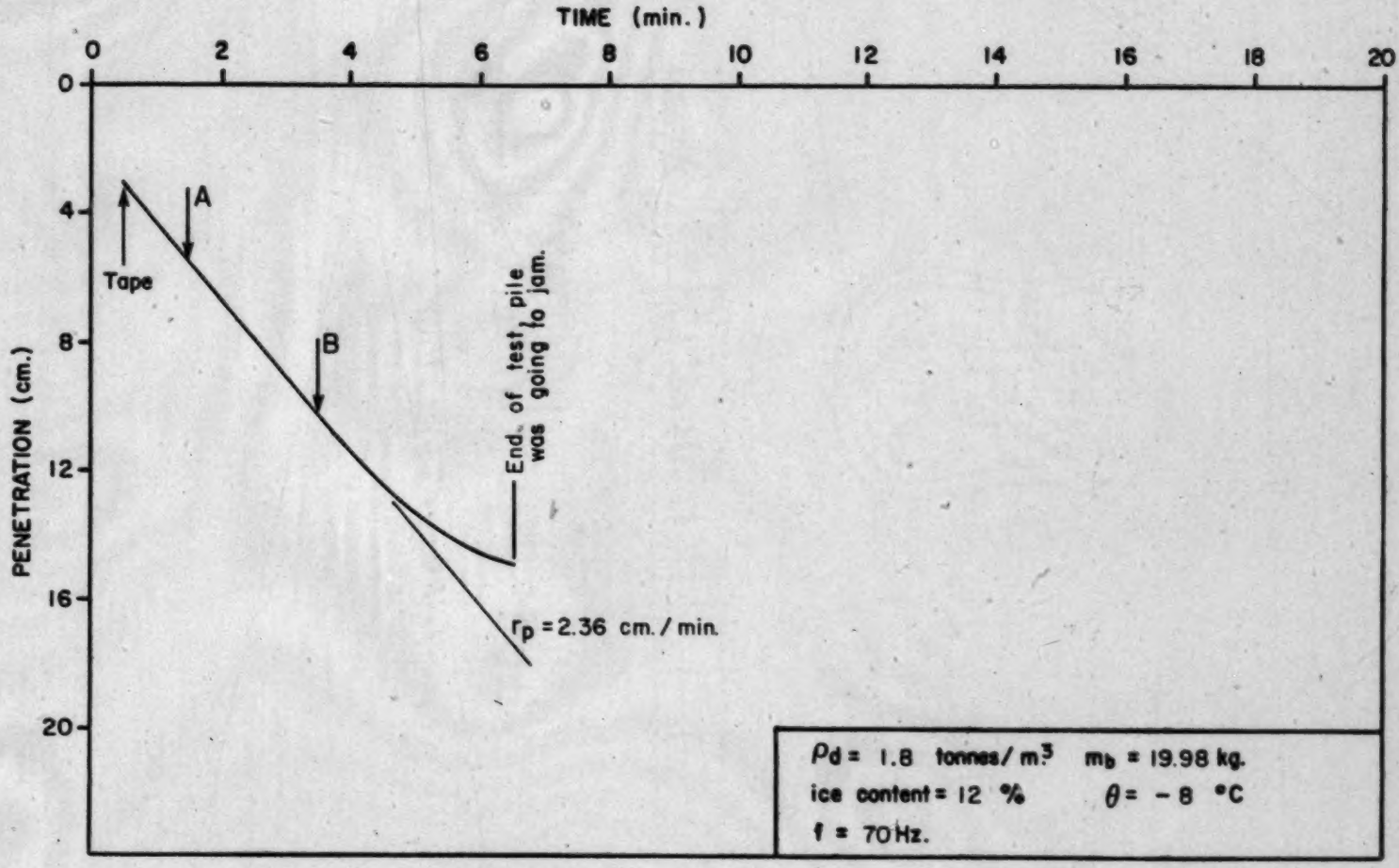

FIGURE C.3 PENETRATION vs. TIME CURVE, TEST NO. DS1-3

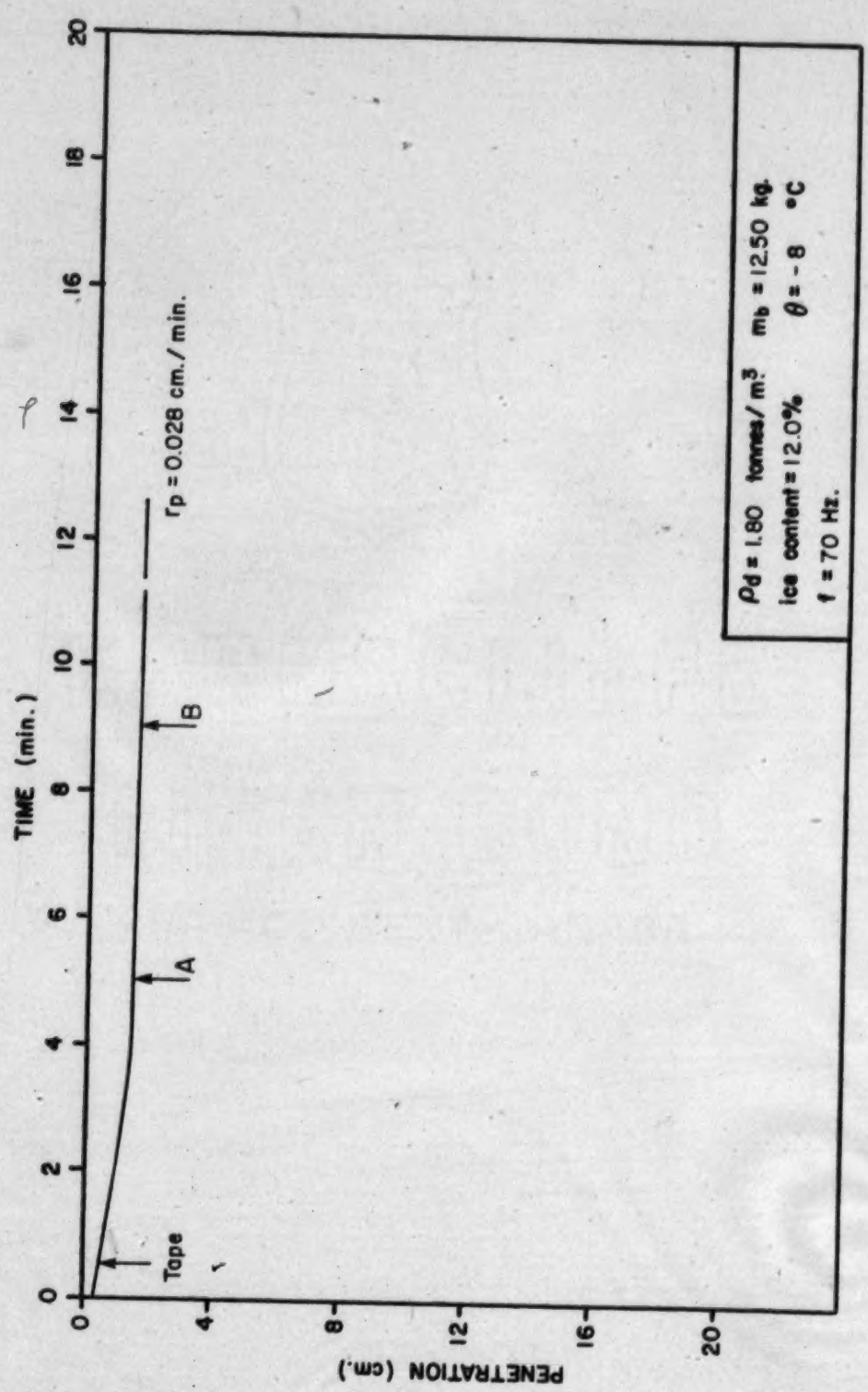

FIGURE C.4 PENETRATION vs. TIME CURVE, TEST NO. DS I-4

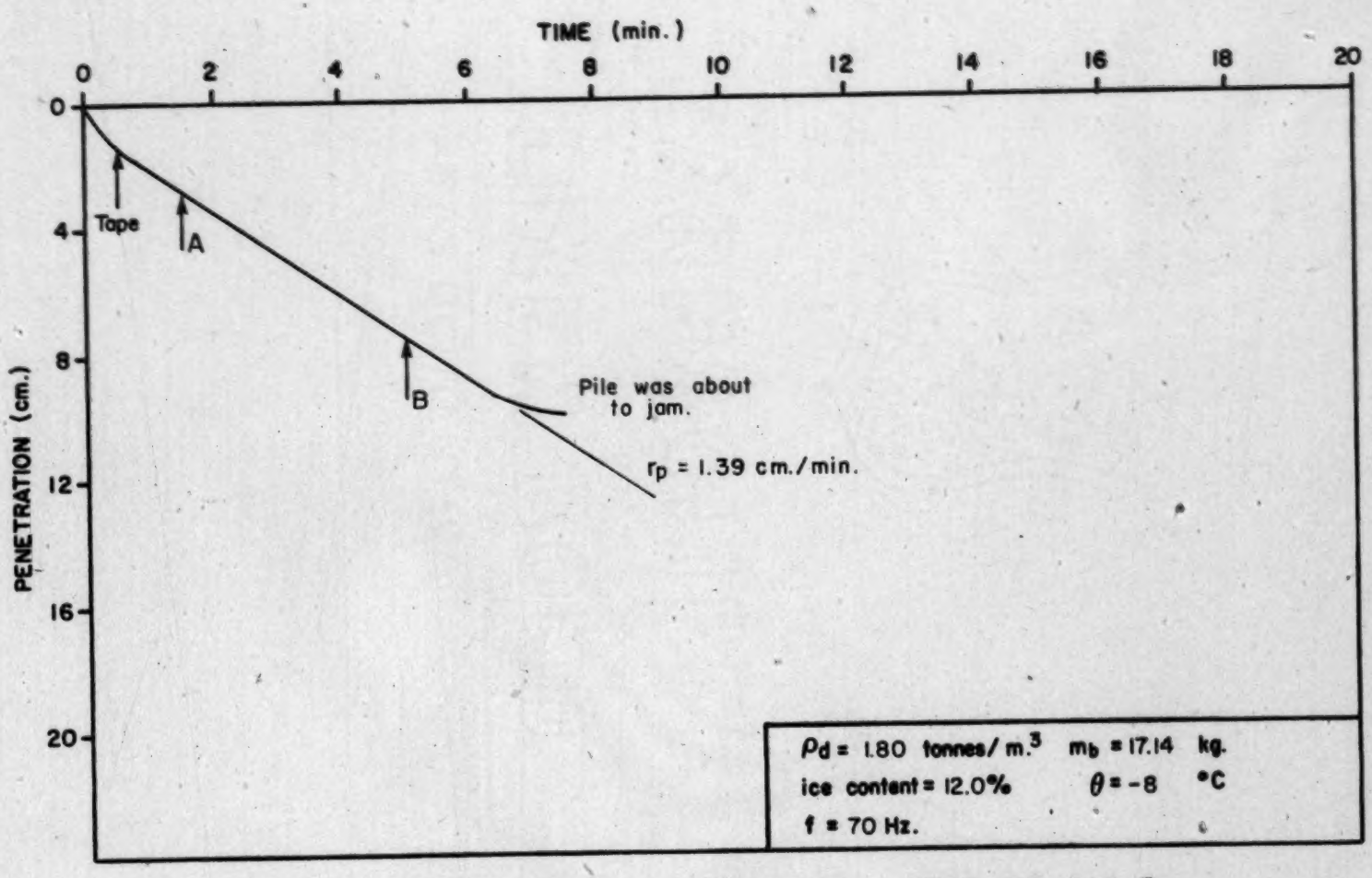

FIGURE C.5 PENETRATION vs. TIME CURVE , TEST NO. DS1-5

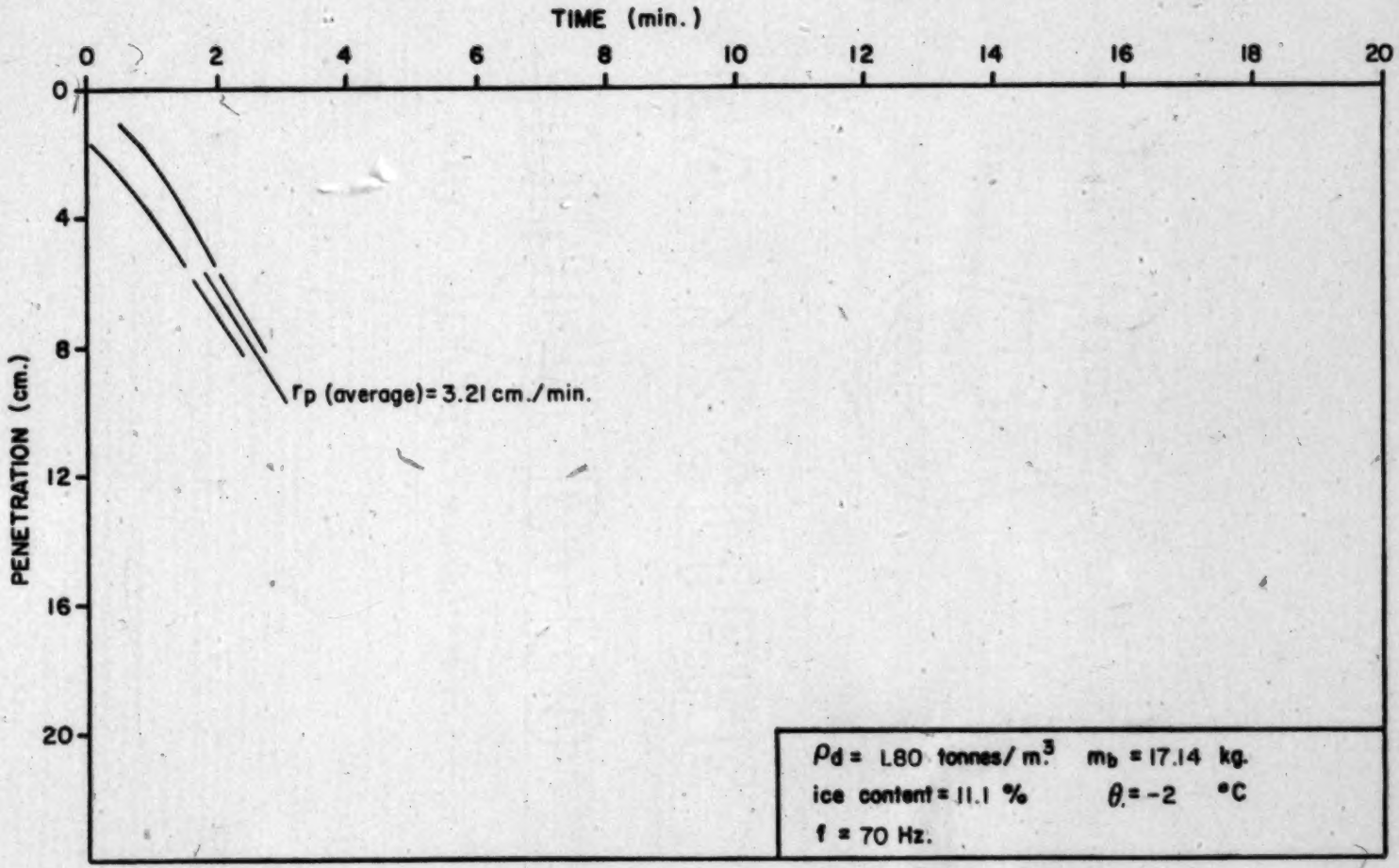

FIGURE C.6 PENETRATION vs. TIME CURVE, TEST NO. DS 2-1

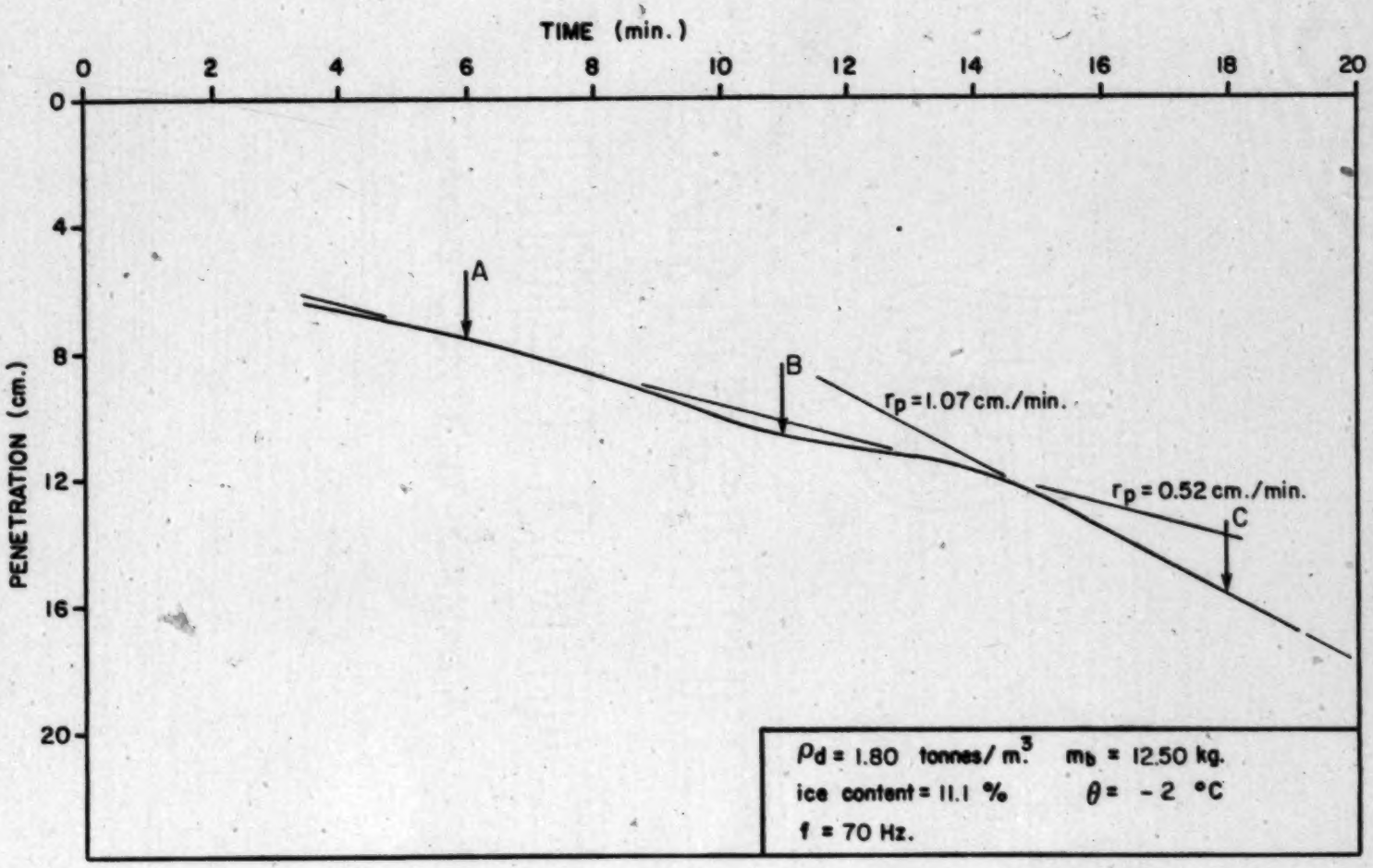

FIGURE C.7 PENETRATION vs. TIME CURVE, TEST NO. DS 2-2

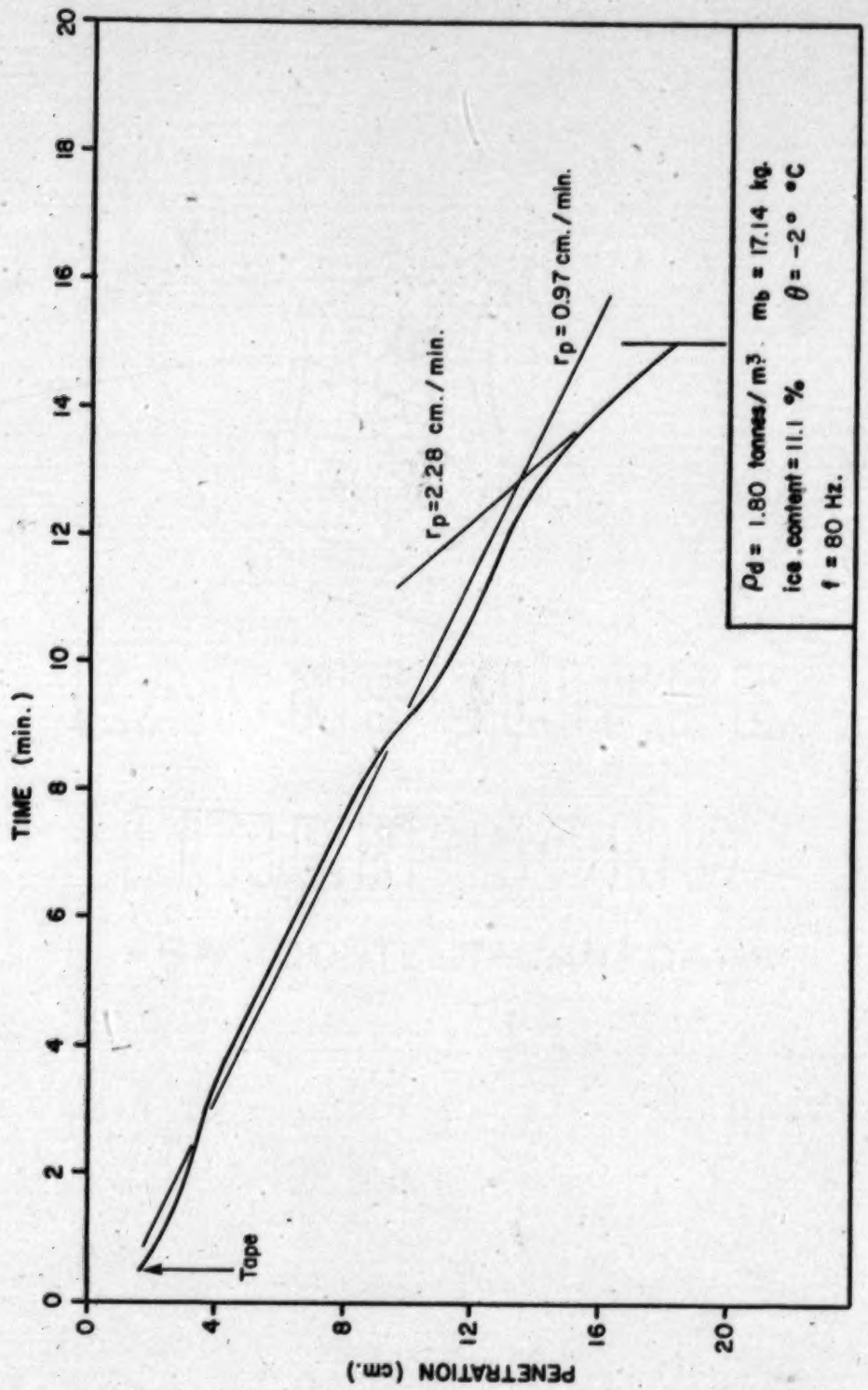

FIGURE C.8 PENETRATION vs. TIME CURVE, TEST NO. DS 2-4

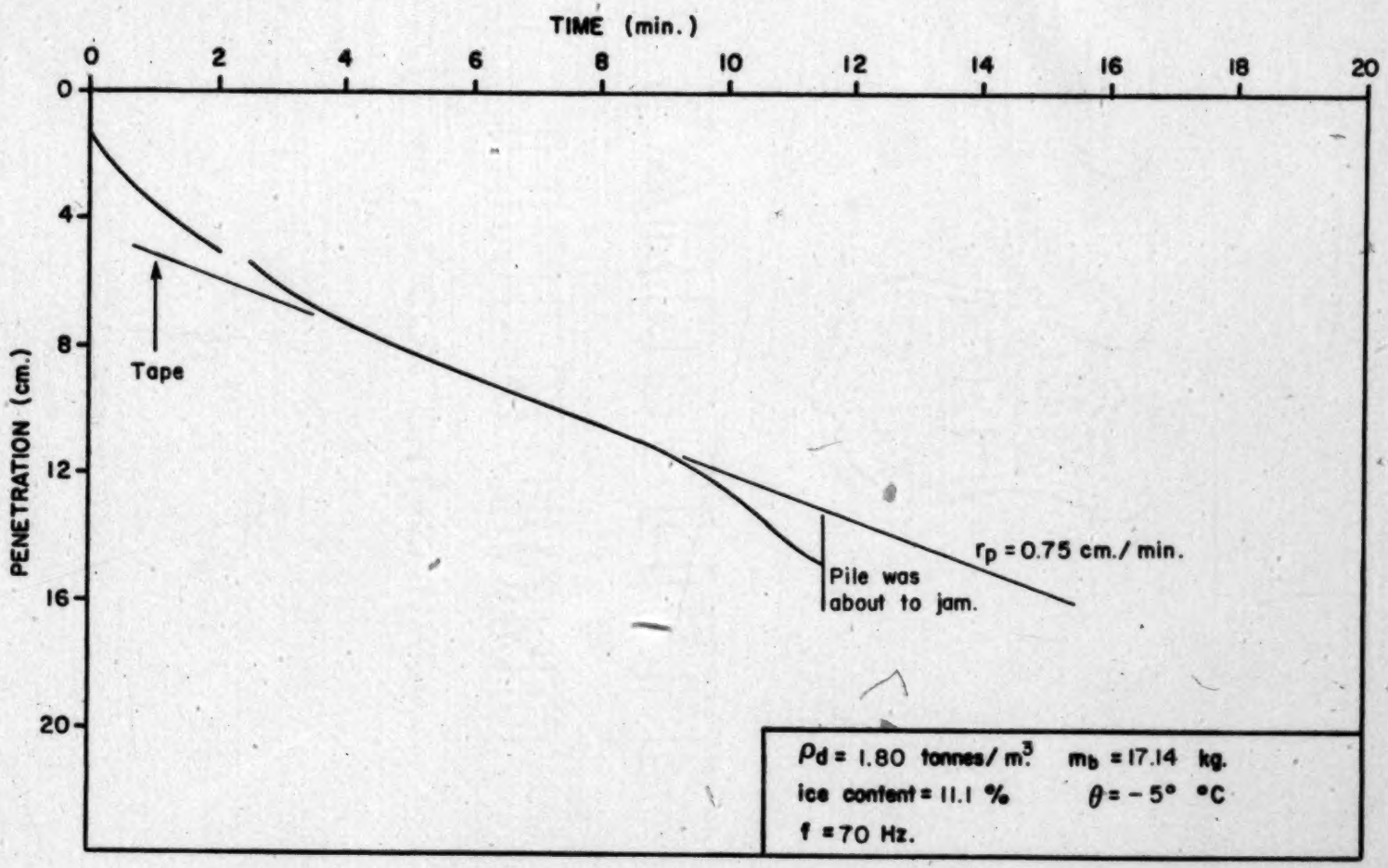

FIGURE C.9 PENETRATION vs. TIME CURVE, TEST NO. DS 2-5

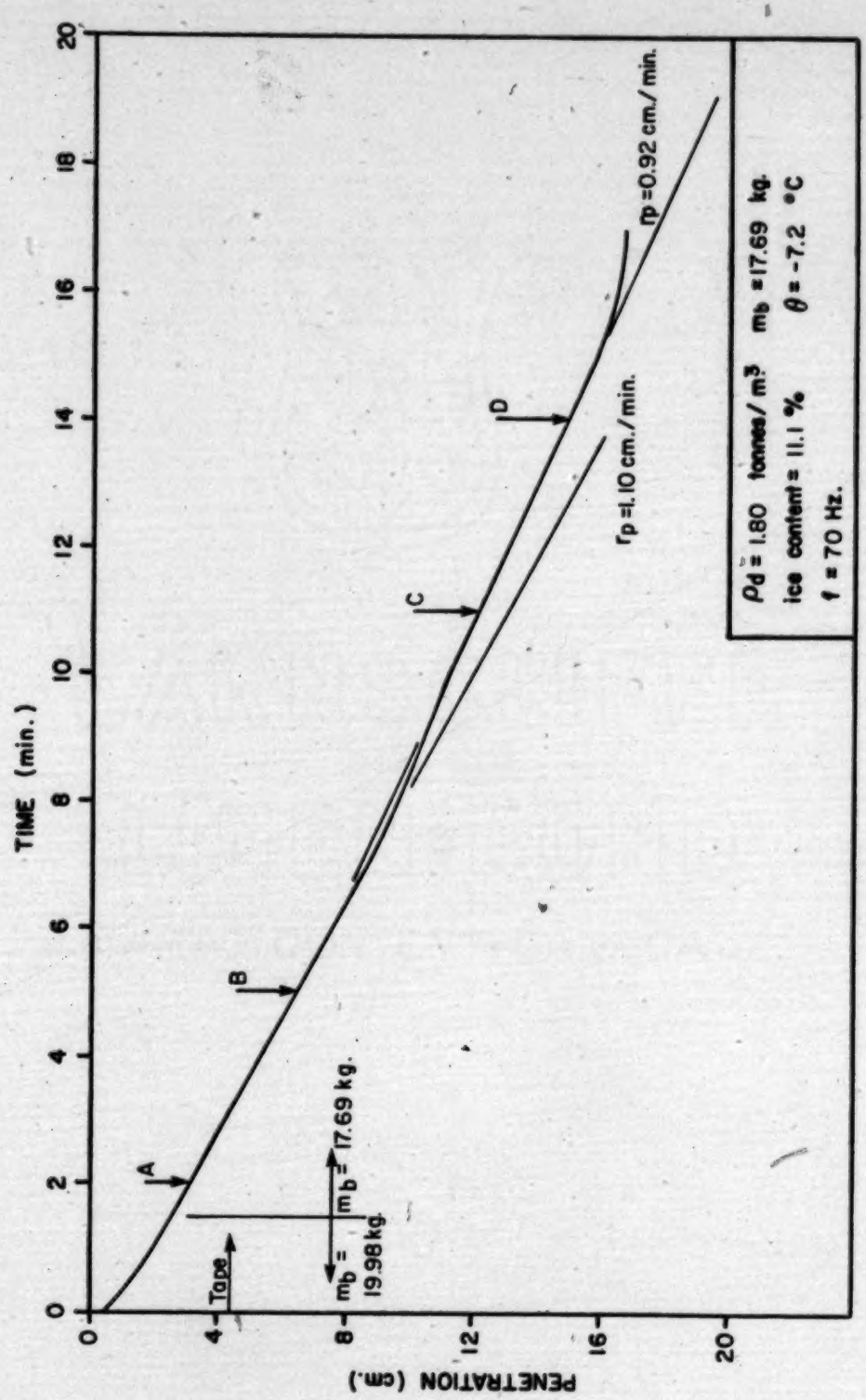

FIGURE C.10 PENETRATION vs. TIME CURVE, TEST NO. DS 2-6

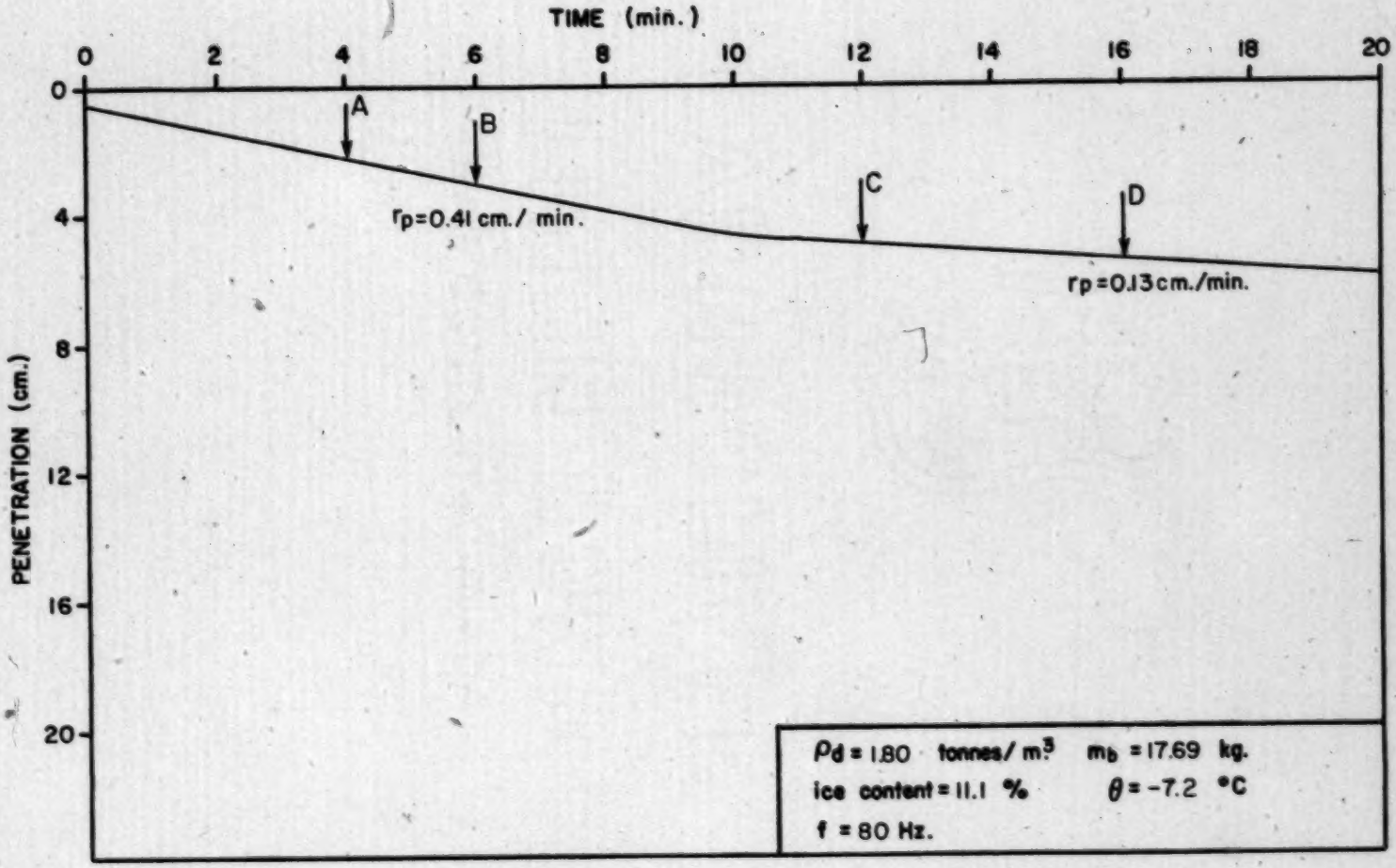

FIGURE C.11 PENETRATION vs. TIME CURVE, TEST NO. DS 2-7

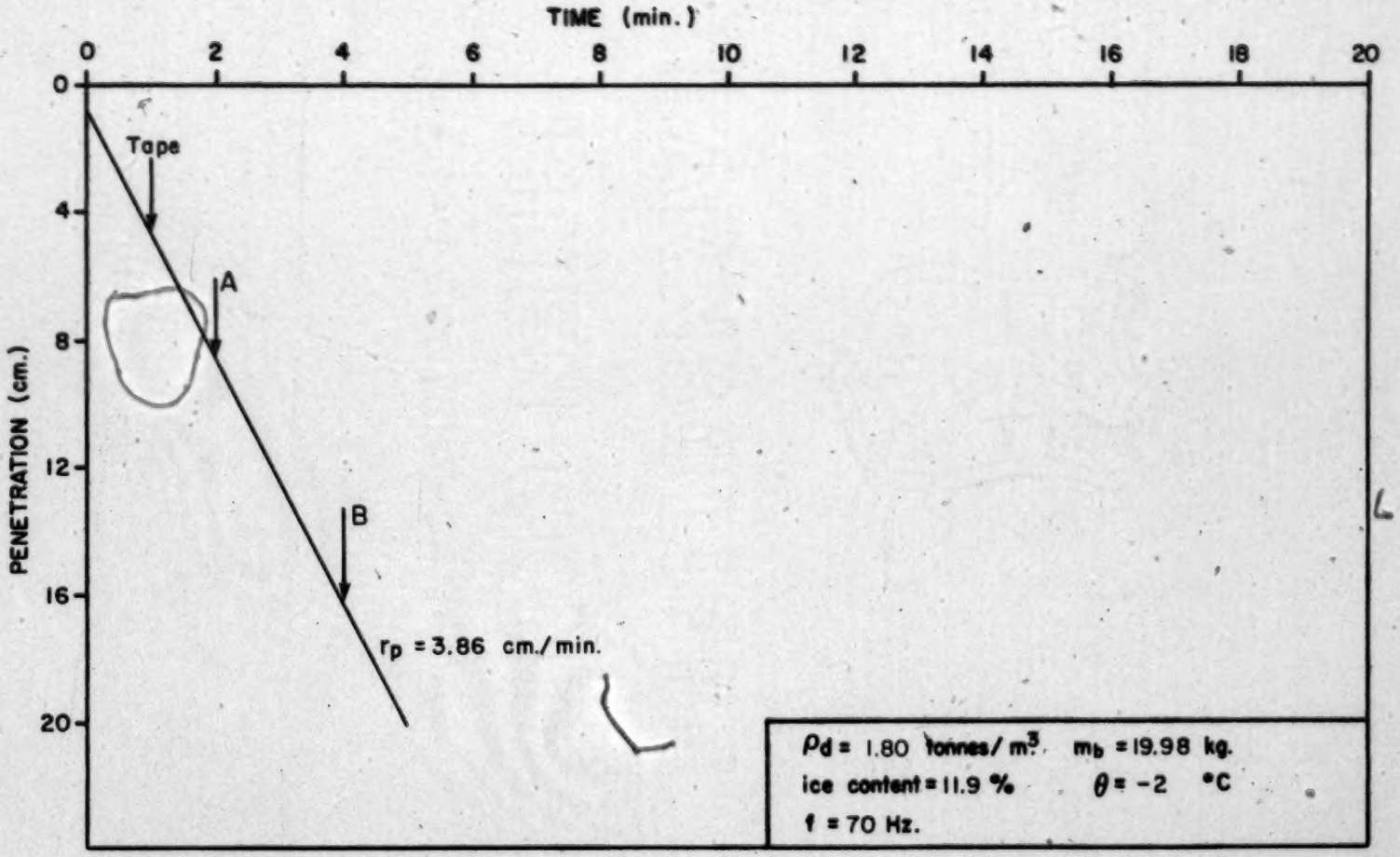

FIGURE C.12 PENETRATION vs. TIME CURVE, TEST NO. DS 3-3

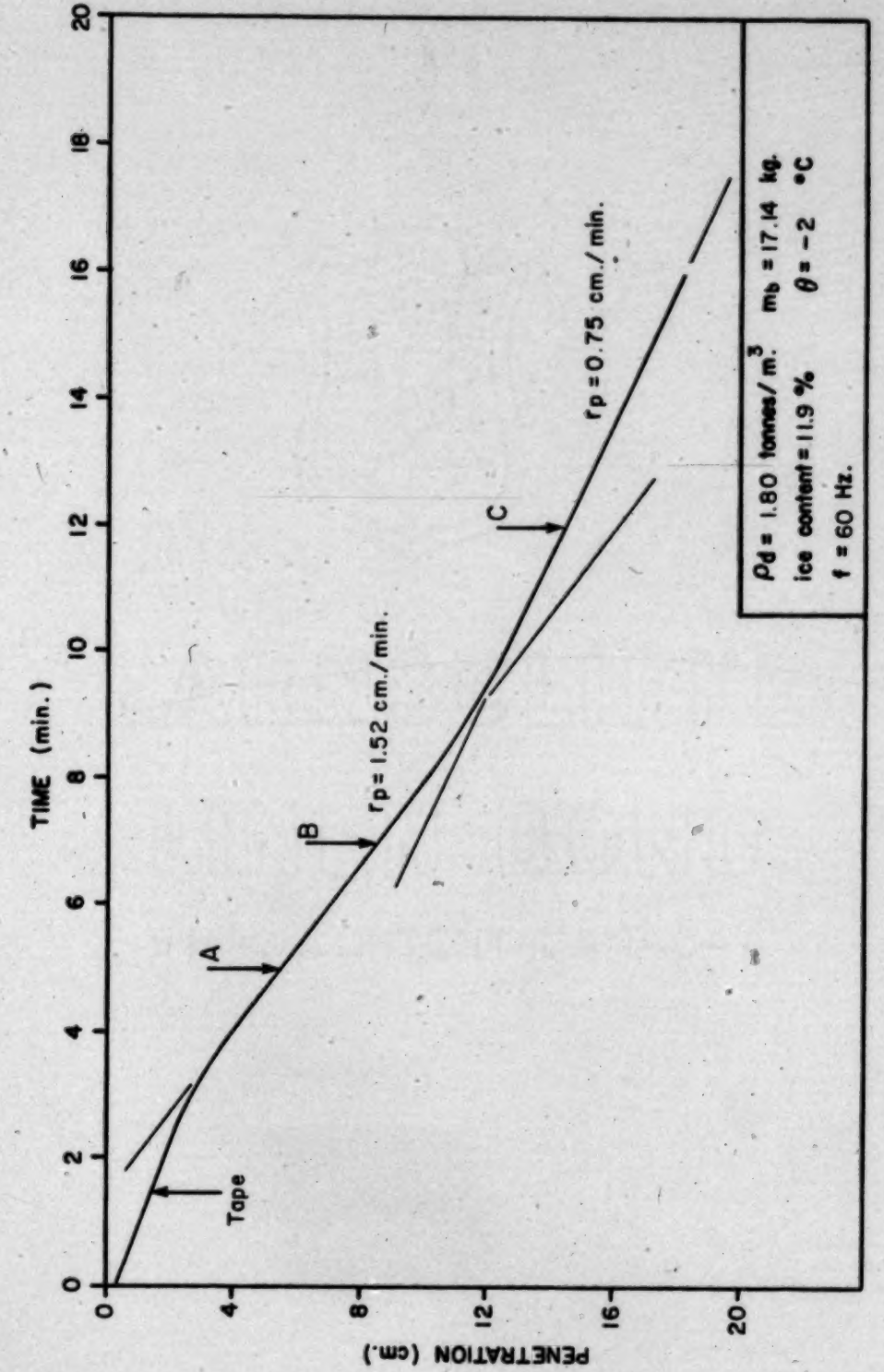

FIGURE C.13 PENETRATION vs. TIME CURVE, TEST NO. DS3-5

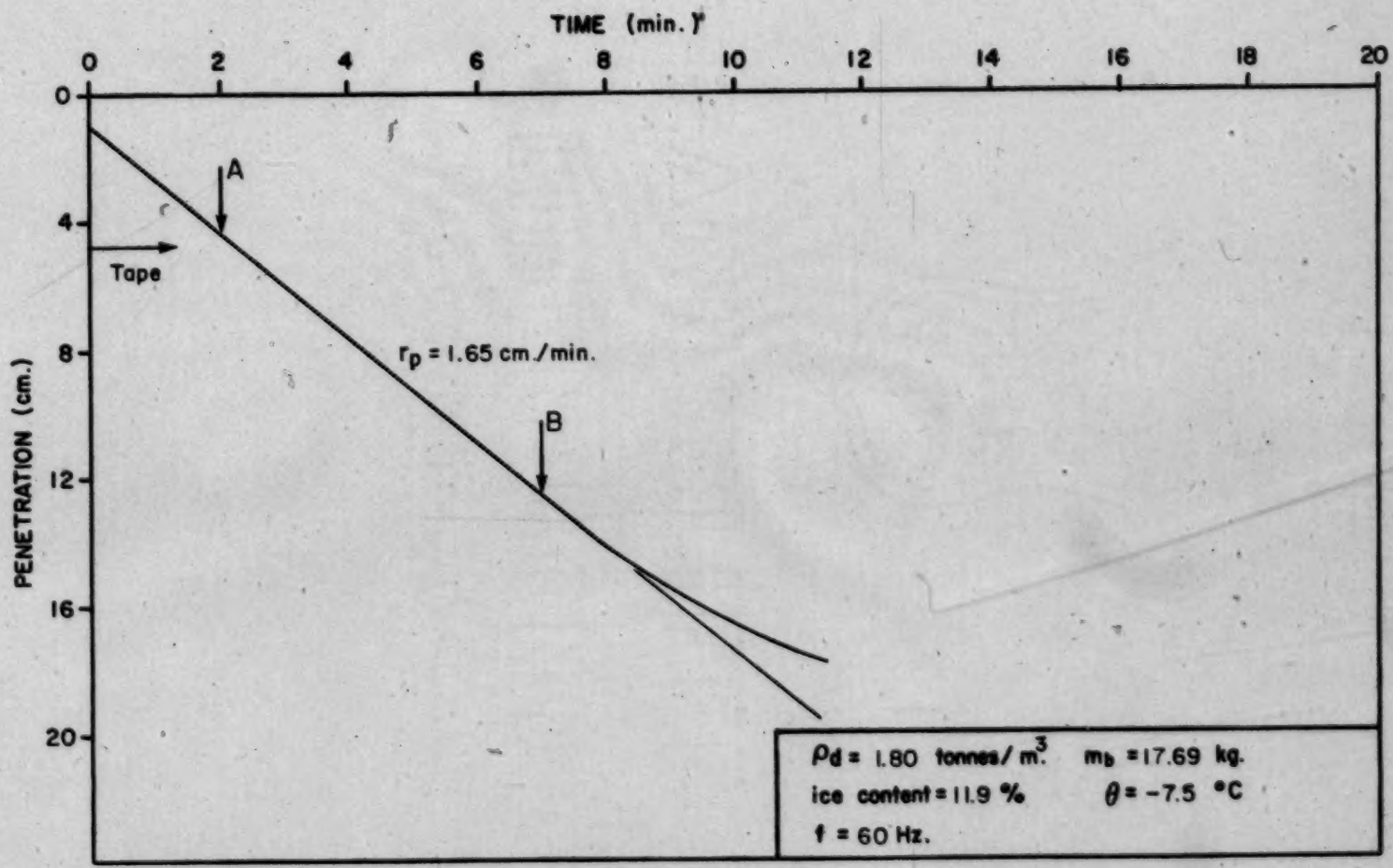

FIGURE C.14 PENETRATION vs. TIME CURVE, TEST NO. DS3-6

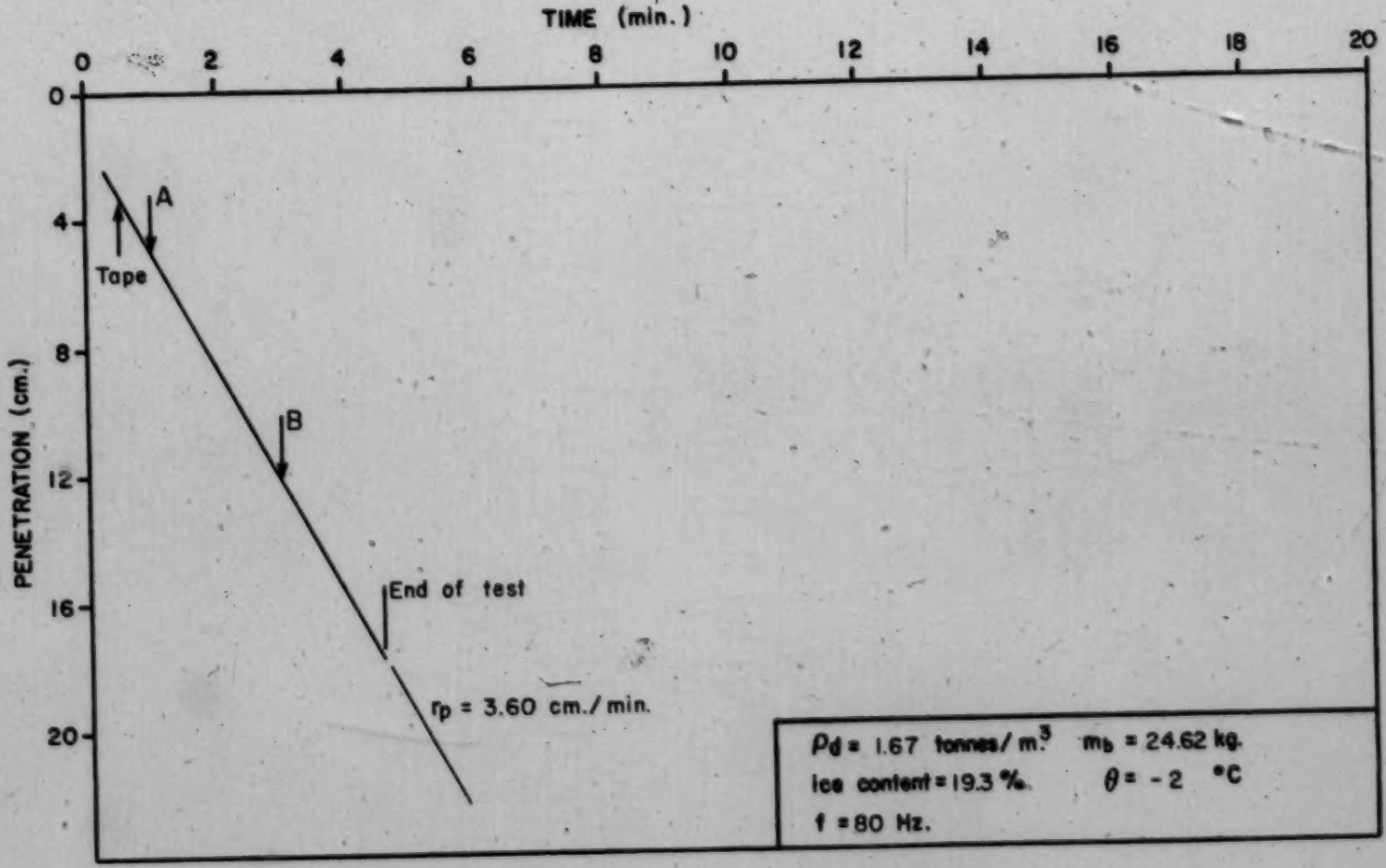

FIGURE C.15 PENETRATION vs. TIME CURVE, TEST NO. LS2-1

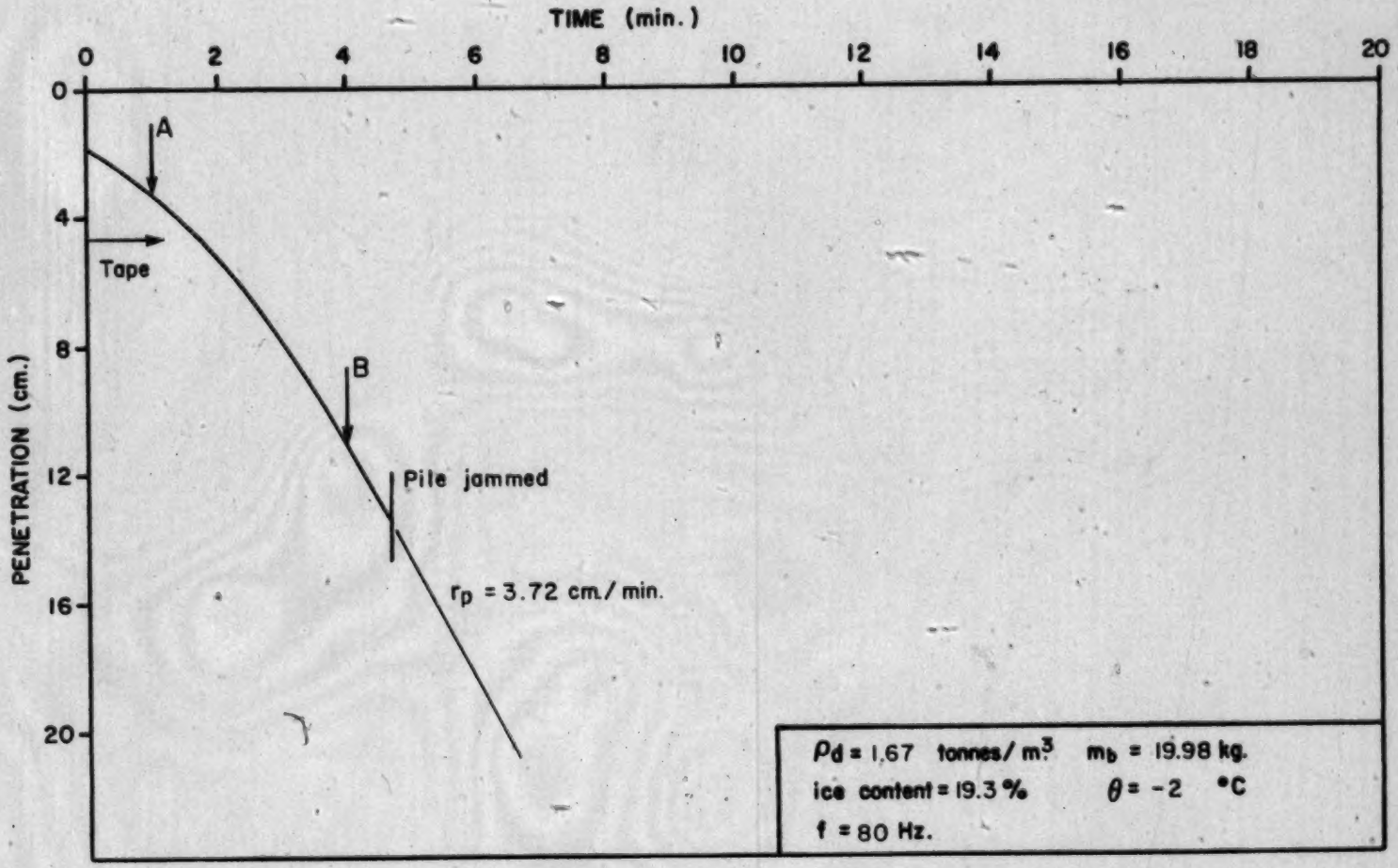

FIGURE C.16 PENETRATION vs. TIME CURVE , TEST NO. LS 2-2

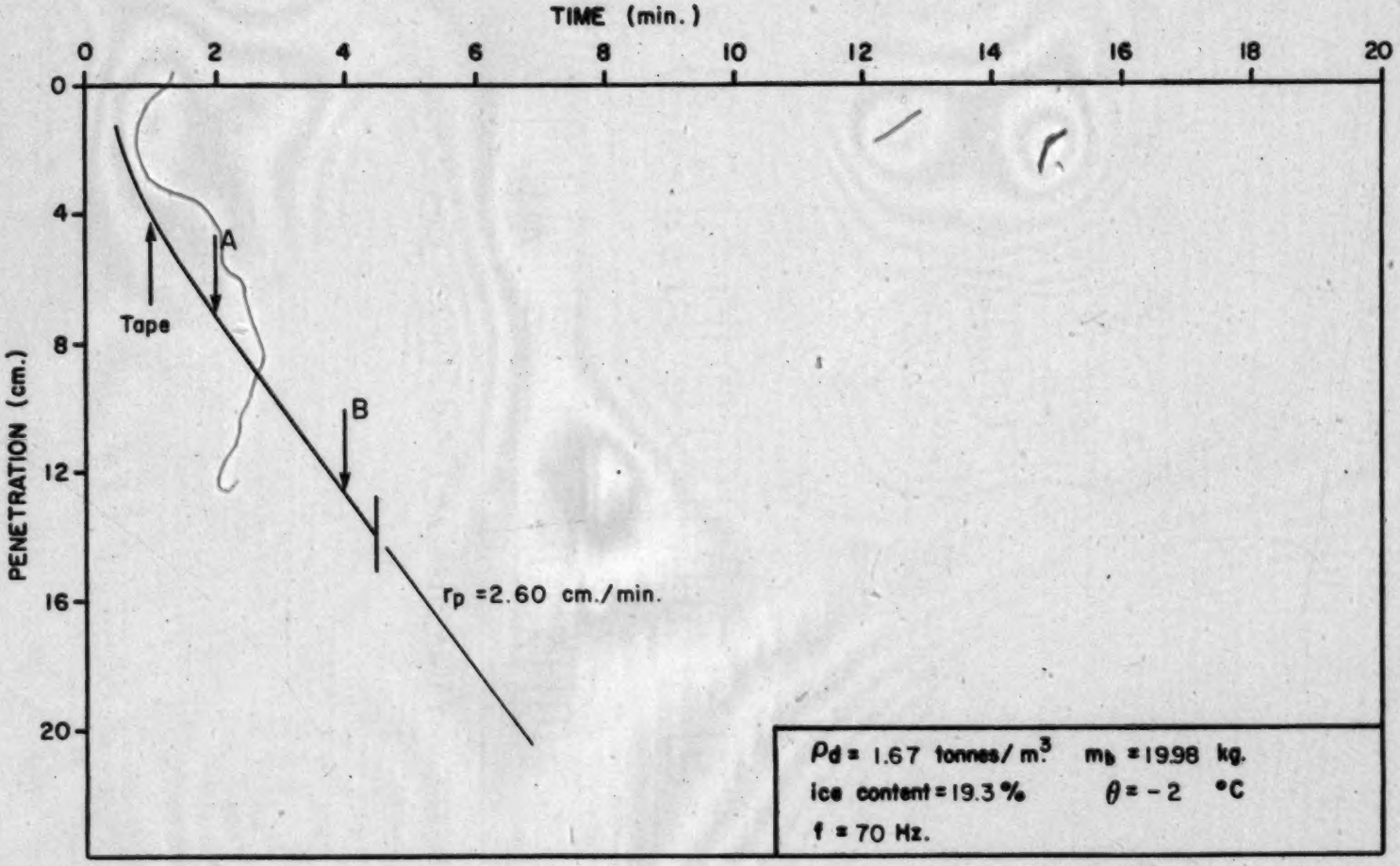

FIGURE C.17 PENETRATION vs. TIME CURVE, TEST NO. LS 2-3

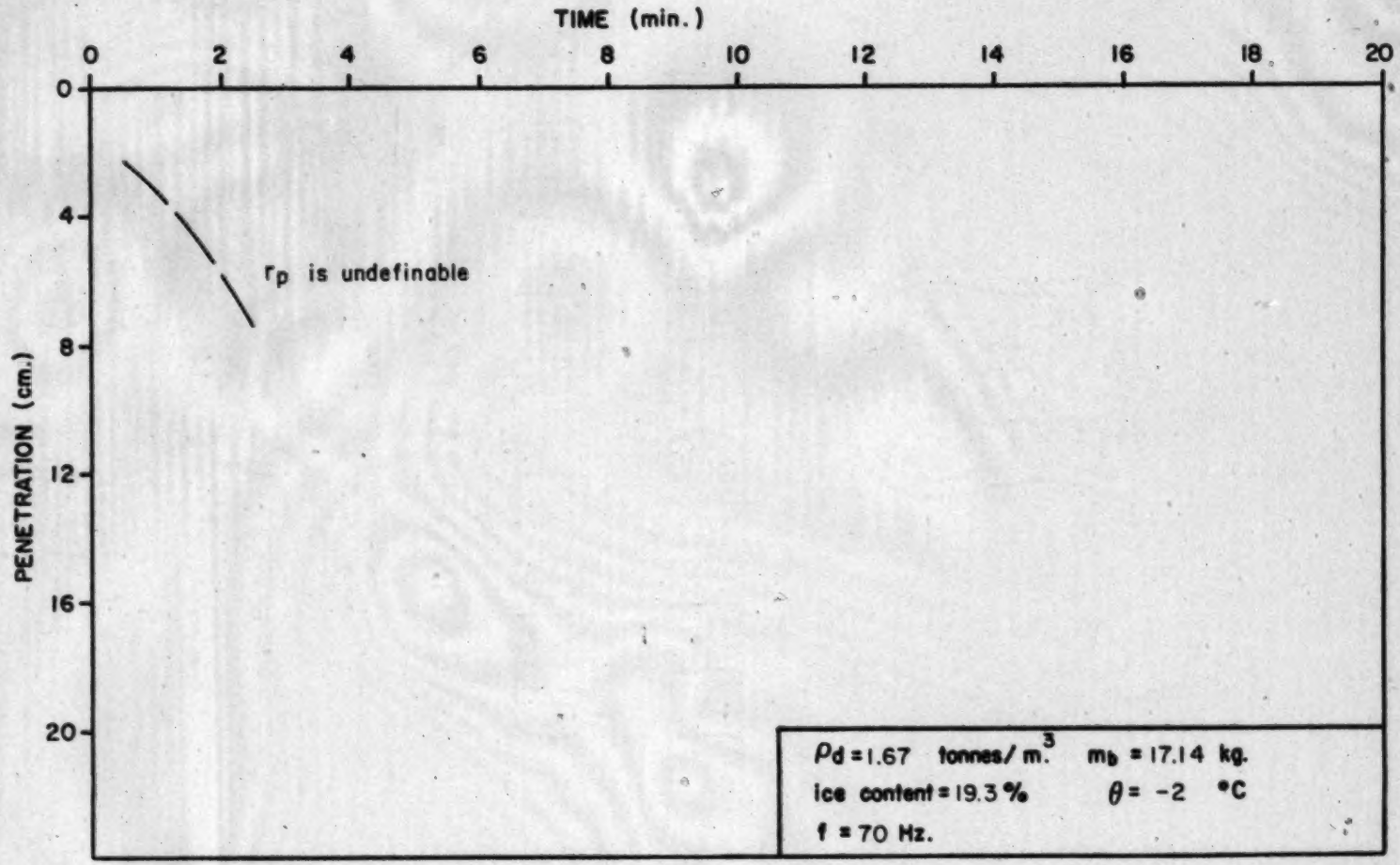

FIGURE C.18 PENETRATION vs. TIME CURVE, TEST NO. LS 2-4

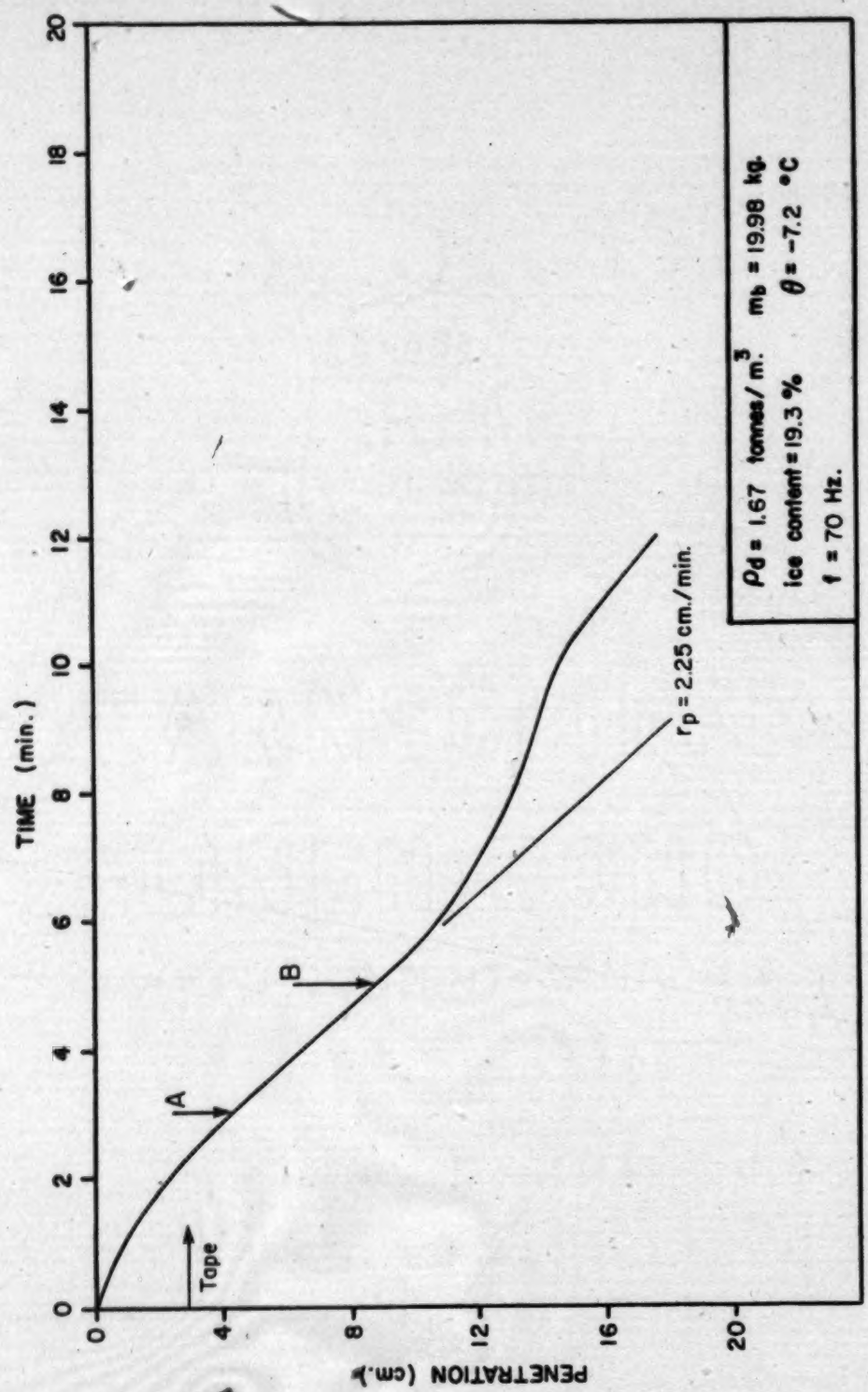

FIGURE C.19 PENETRATION vs. TIME CURVE, TEST NO. LS 2-5

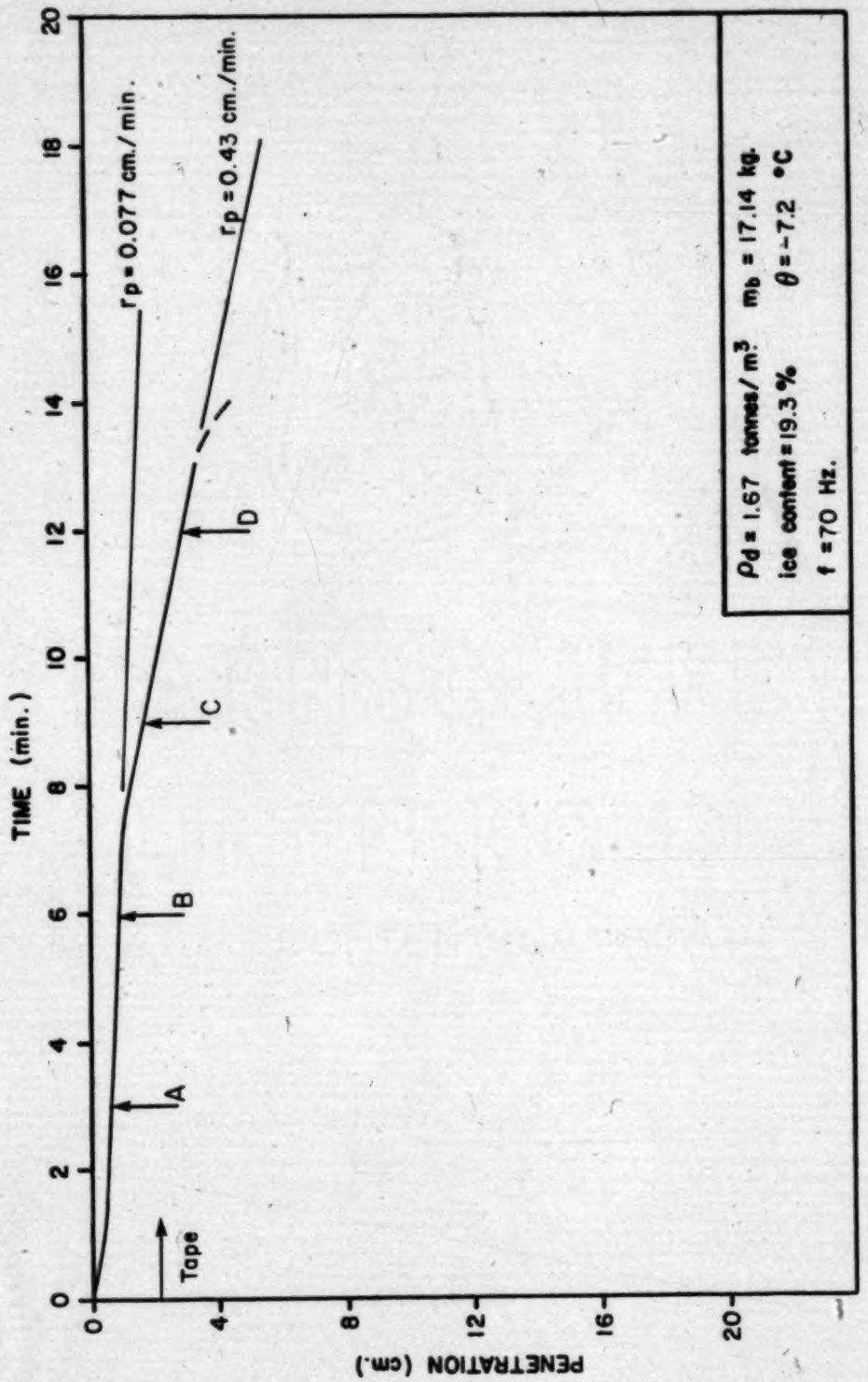

FIGURE C.20 PENETRATION vs. TIME CURVE, TEST NO. LS 2-6

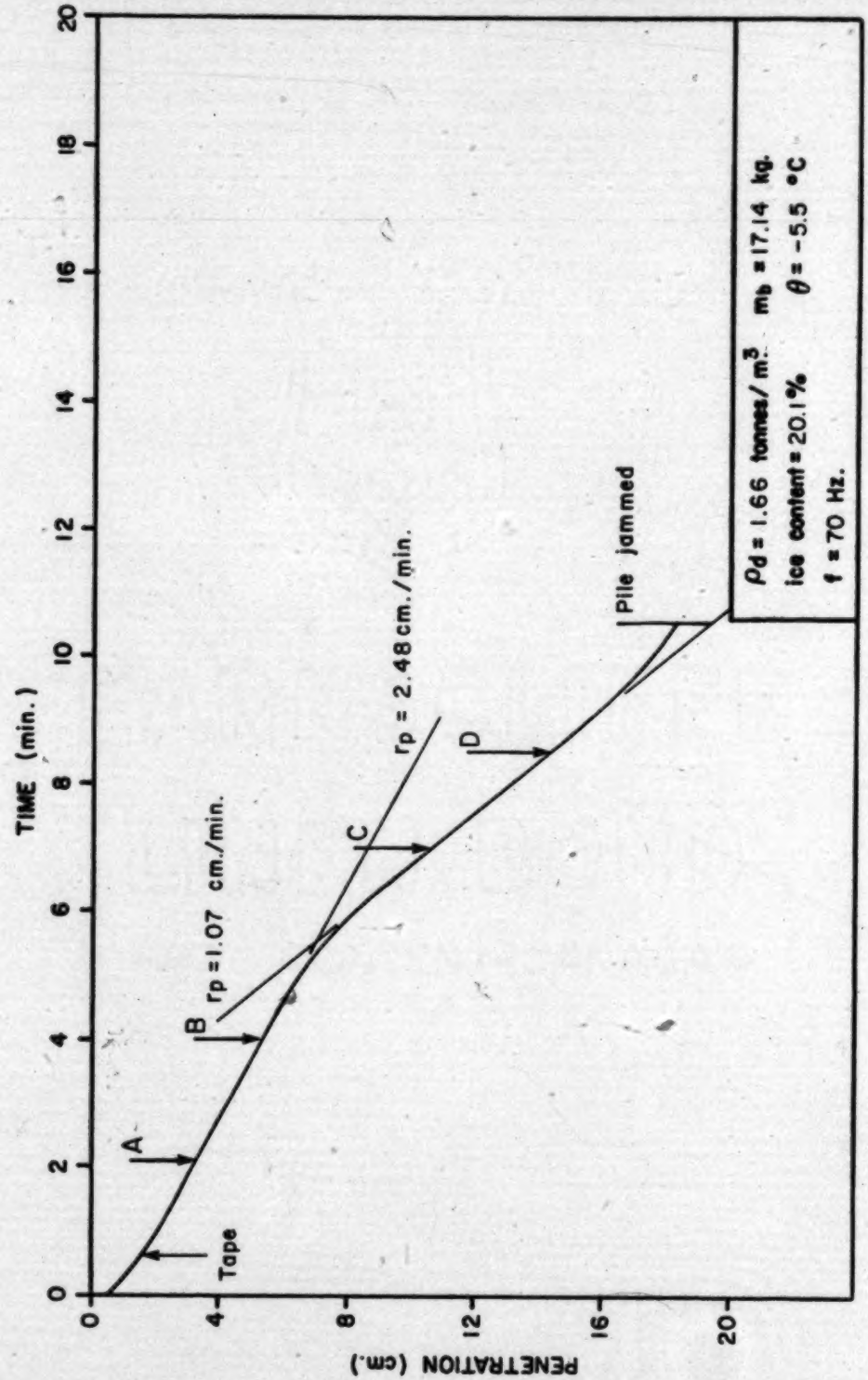

FIGURE C.21 PENETRATION vs. TIME CURVE, TEST NO. LS 3-1

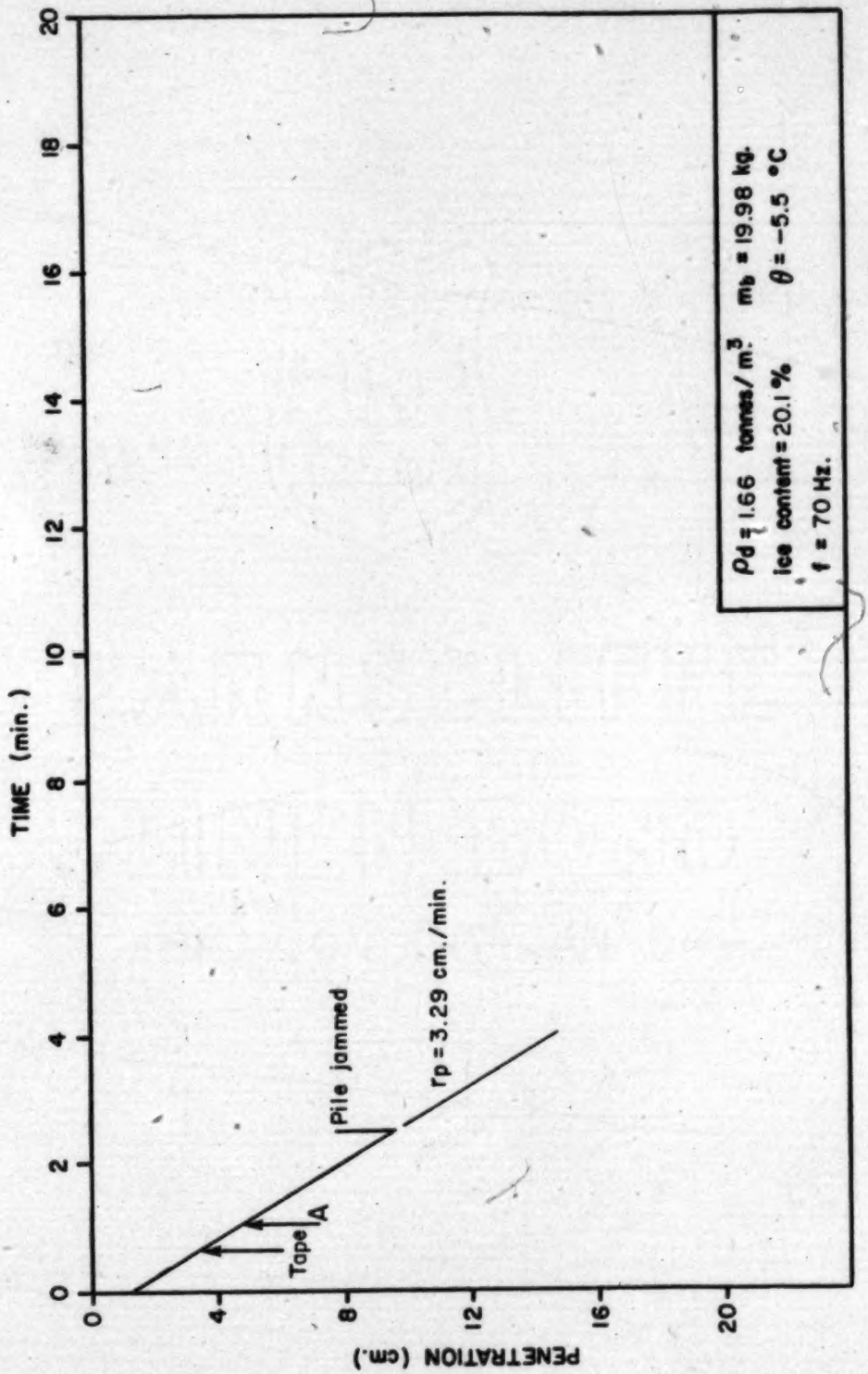

FIGURE C.22 PENETRATION vs. TIME CURVE, TEST NO. LS 3-2

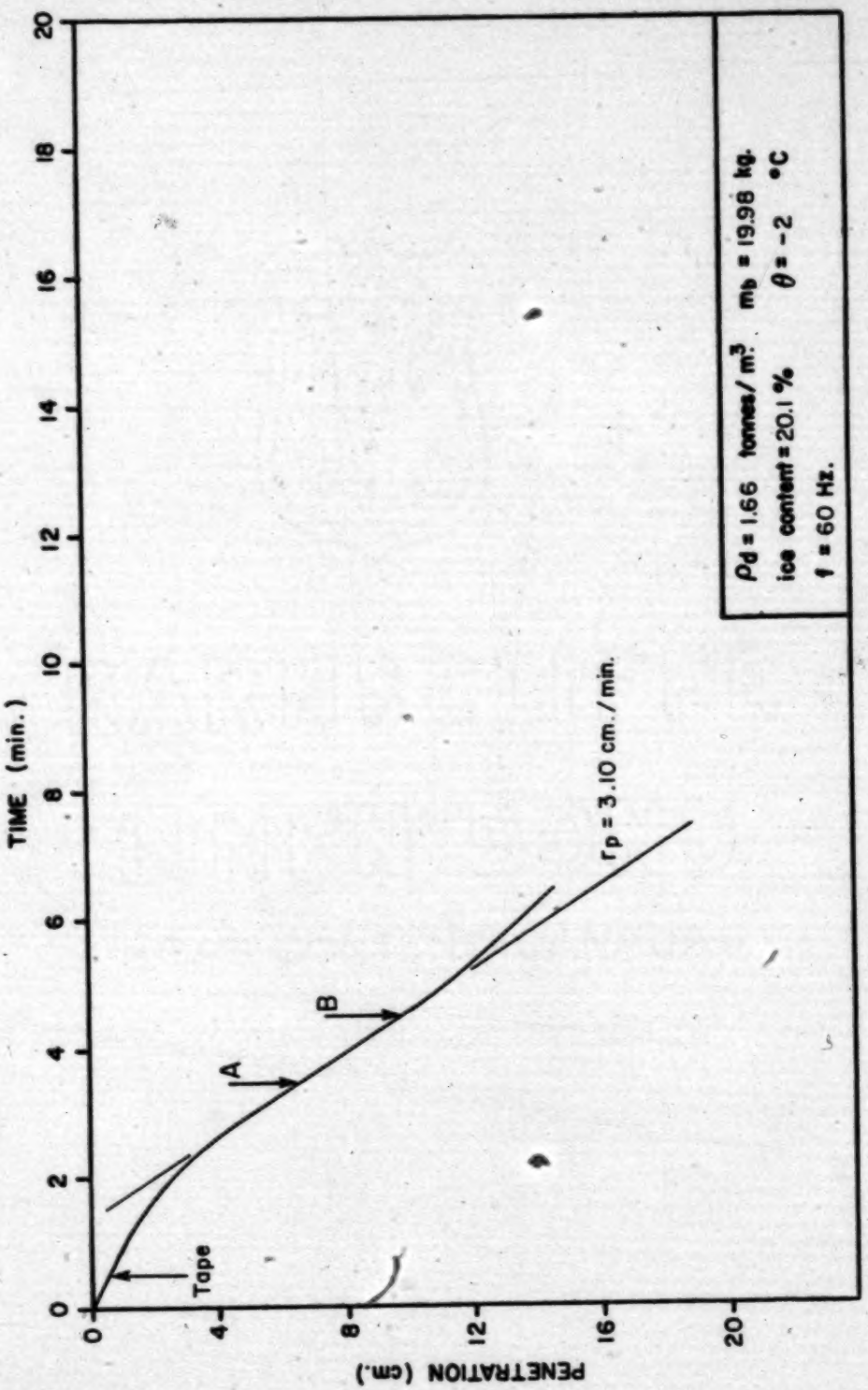

FIGURE C.23 PENETRATION vs. TIME CURVE, TEST NO. LS3-4

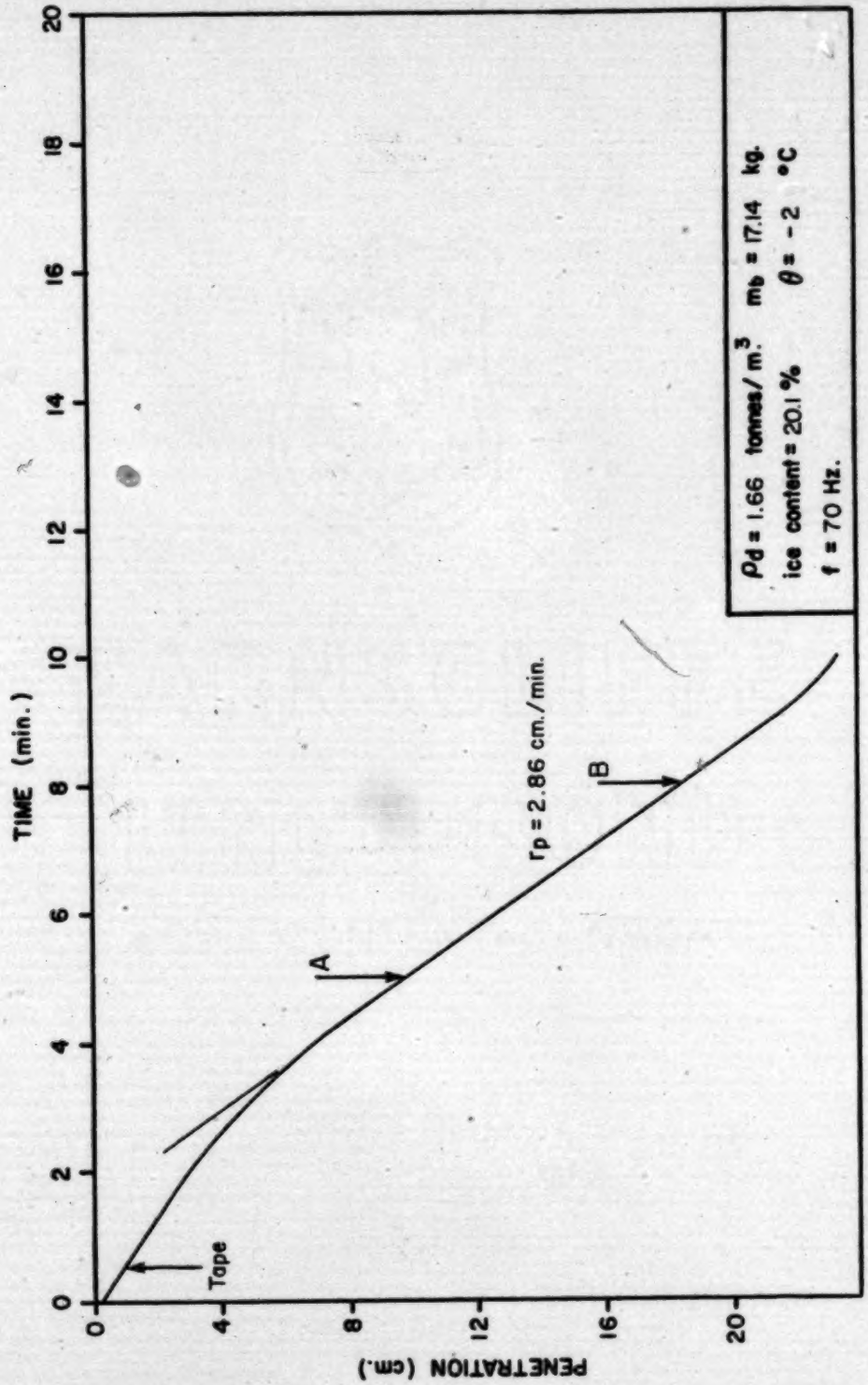

FIGURE C.24 PENETRATION vs. TIME CURVE, TEST NO. LS3-5

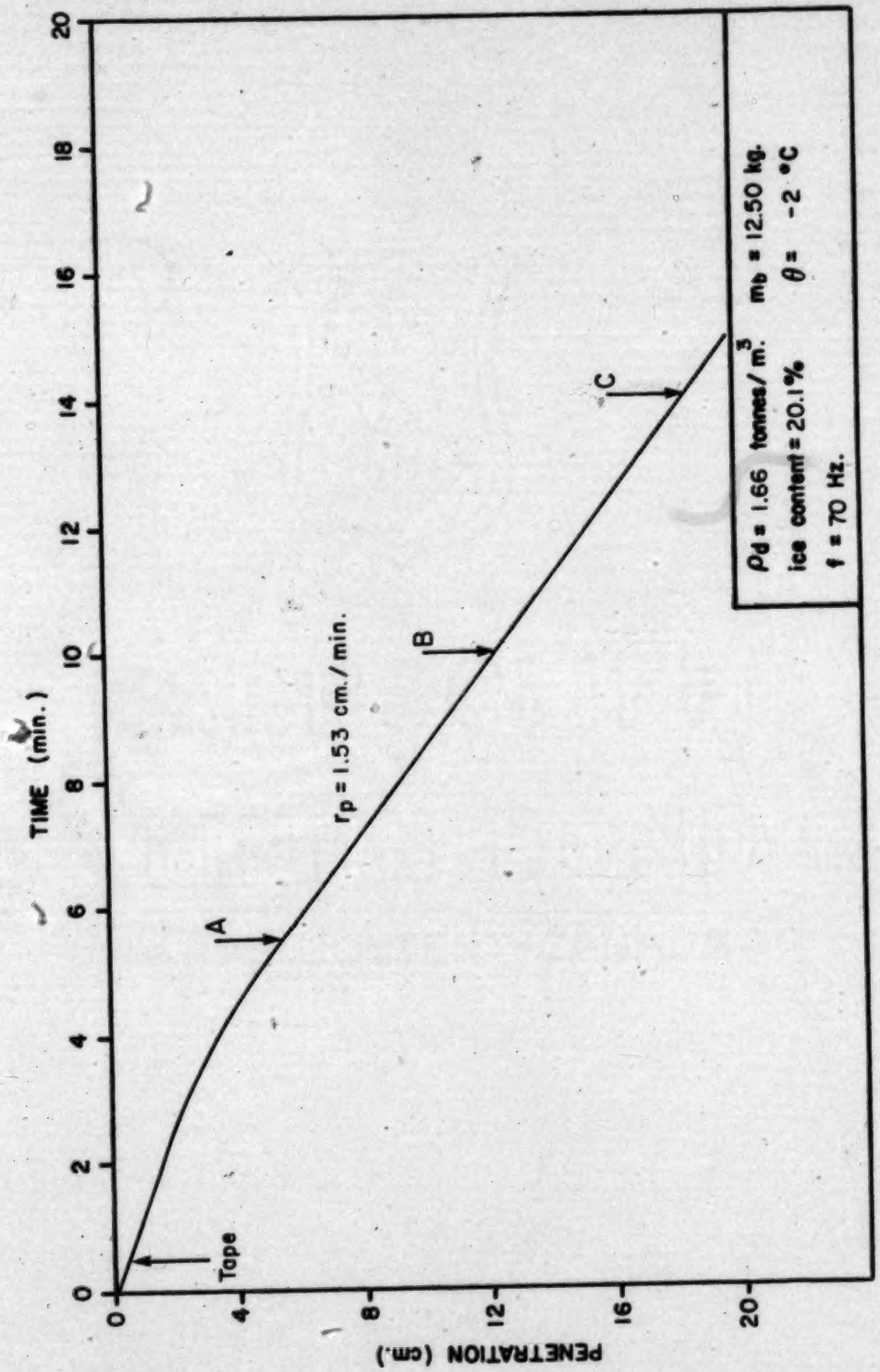

FIGURE C.25 PENETRATION vs. TIME CURVE, TEST NO. LS 3-6

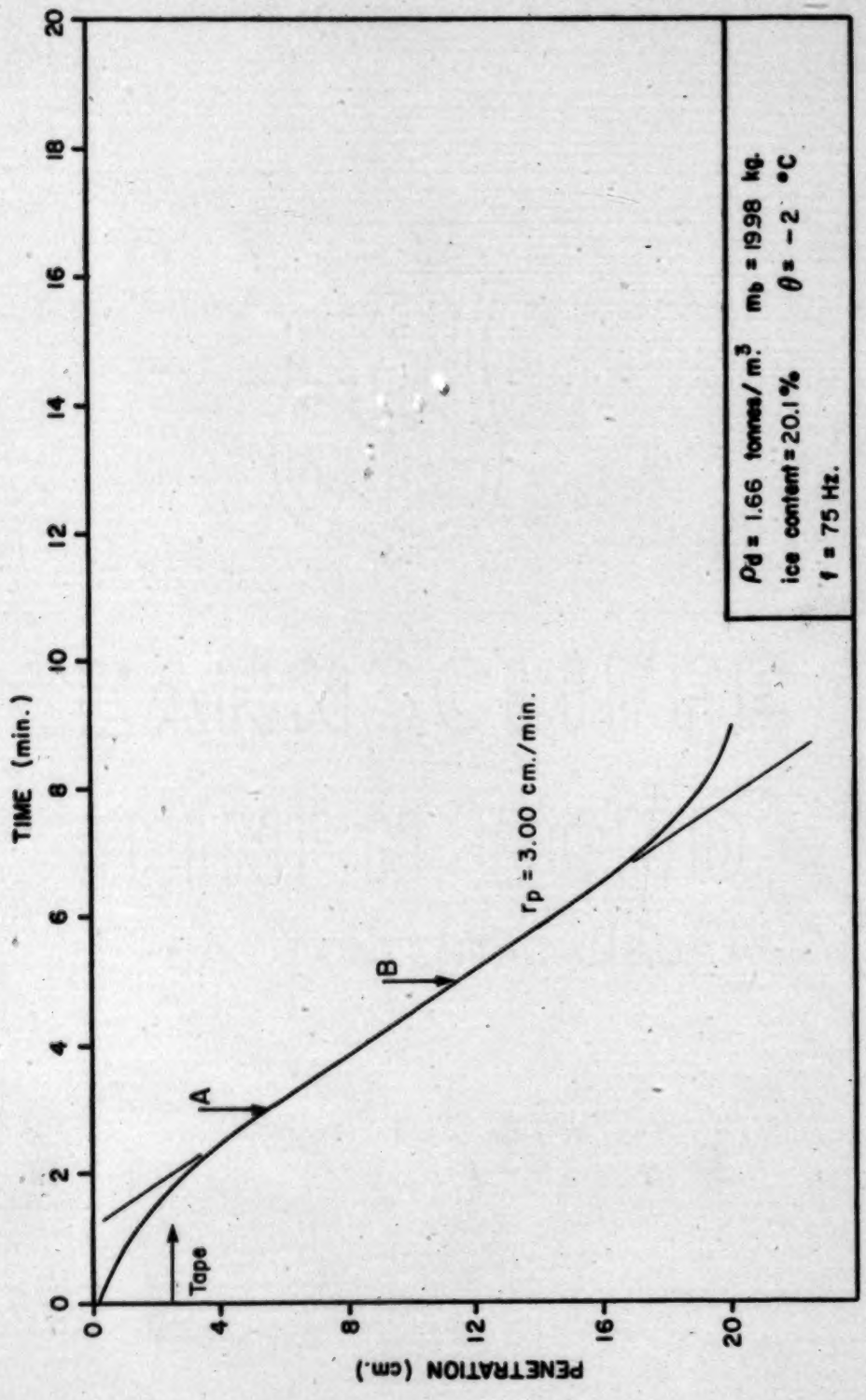

FIGURE C.26 PENETRATION vs. TIME CURVE, TEST NO. LS 3-7

APPENDIX D

INTEGRATION OF IDEALIZED ACCELERATION SIGNAL

Two idealized acceleration signals were shown in Figure 5.5 of the main text: one for normal wave forms and the other for damped vibration wave forms as shown on Plate 5.3. Each will be discussed under separate headings starting with the simplest case, the damped vibration case.

D.1 Double Integration of Idealized Damped Vibration Wave Form

This wave form is very simple in geometry, see Figure 5.5.b. The dimensions measured on the photographs are shown on Figure 5.5.b. They are the period of vibratory motion, the duration of the impact and the peak impact acceleration. With these measurements, one can easily calculate the other dimensions assuming the area preceding the impact peak is equal to the area below the peak curve. Using the measured and calculated dimensions, the acceleration curve can be integrated once to get the velocity curve. The velocity curve can be fitted about the time axis so that the positive and negative areas are balanced. This is to properly model the physical motion in which some negative velocity has to occur. The permanent deformation is neglected to simplify the analysis. It will be seen later that the permanent

deformation is very small when compared to the total pile displacement. The velocity curve is balanced when velocity is zero at peak acceleration. This is to properly model the fact that the pile reverses its motion at that point. Before peak acceleration, velocity is in the opposite direction from acceleration. After that procedure, the velocity curve can be integrated to obtain the displacement curve. It can be shown that the displacement (d) corresponding to peak acceleration (a) is given by:

$$d=a\times t^2/24 \qquad (D.1)$$

where t is the impact duration.

D.2 Double Integration of Idealized Normal Acceleration Wave Form

This wave form is more complex than the preceding wave form. From the measured dimensions shown on Figure 5.5.a, the dimensions of the inter-peak area above the time axis can be calculated since both negative and positive areas have to be equal. It should be noted that the negative area on either side of the impact spike is not necessarily symmetric. The lower slope of the left hand side of the peak is the same as that of the adjacent positive area. The required time to decelerate to the base of the impact peak is calculated from the calculated slope of the positive

area. The impact duration and the duration of negative acceleration are measured from the photographs. The impact duration and calculated time required to decelerate to the base of the impact spike are subtracted from the duration of negative acceleration to give the time to go from the right hand side base of the spike to positive acceleration of the next motion cycle. The latter time is rarely equal to the time interval between the spike and positive acceleration.

Because the spike is not symmetric, no simple equation can be written that will represent a balanced velocity curve. To perform the integrations and to balance the positive and negative areas of the velocity curve, a computer program was written. The program can be found at the end of this Appendix. Working principles of the program will be outlined in the following lines.

The measured dimensions of the acceleration signal are first read in. Then, the program calculates the missing dimensions of the wave form. The velocity curve is then established by numerical integration of the simple linear acceleration curve. The time axis of the velocity curve is arbitrarily set such that zero velocity corresponds to peak positive acceleration. Once the velocity curve is calculated, it is numerically integrated using Simpson's rule which is accurate for second degree curves. The displacement curve is obtained. If the velocity curve is well balanced, the last calculated displacement is zero. When the last displacement differs from zero, given a

certain tolerance, the time axis is moved up or down towards equilibrium of the positive and negative areas. The first translation of the time axis is arbitrarily set at 5% of the peak velocity in the required direction. If not enough, the axis is translated in the same direction by the same amount at the following iteration. The method of bisection is used for quick convergence once translation has exceeded the required amount.

Utilization of the program is described in the program comments.

Computer Program

```
      DIMENSION TEMPS(49),VELO(49),DISP(25)
CCCCCCCCCCCCCCCCCCCCCCCCCCCCCCCCCCCCCCCCCCCCCCCCCCCCCCCCCCCCCCCCCCCCCCC
C
C     PROGRAM TO CALCULATE THE VIBRATORY DISPLACEMENT OF MODEL
C     LABORATORY PILE.
C     THE PROGRAM USES SIMPSON'S RULE TO PERFORM THE INTEGRATION.
C     DATA TO BE INPUT:
C     1ST CARD:   NUMBER OF CURVES TO BE CALCULATED
C     2ND CARD:   TEST NUMBER (NO MORE THAN SIX DIGITS)
C     3RD CARD:   DIMENSIONS T,TIM,D,B,P OF THE ACCELERATION CURVE.
C                 T  =PERIOD OF MOTION
C                 TIM=DURATION OF NEGATIVE ACCELERATION
C                 D  =IMPACT DURATION
C                 B  =ACCELERATION AT BASE OF PEAK
C                 P  =PEAK ACCELERATION
C                 ONE CARD PER CURVE.
C     THE SECOND AND THIRD CARDS ARE REPEATED AS MANY TIMES AS
C     THERE ARE TESTS
C
CCCCCCCCCCCCCCCCCCCCCCCCCCCCCCCCCCCCCCCCCCCCCCCCCCCCCCCCCCCCCCCCCCCCCCC
C
1     FORMAT (I2)
2     FORMAT (3F5.2,2F6.1)
3     FORMAT (2A3)
20    FORMAT (' ***** VELOCITY CURVE DOES NOT CLOSE TO ZERO, CHECK FORMU
     *LAE. *****')
21    FORMAT (/,' TIME',5X,'VELOCITY',3X,'DISPLACEMENT',/,2X,'MS',9X,'M/
     *S',10X,'MM',/)
22    FORMAT (1X,F5.2,6X,F6.3,6X,F5.2)
23    FORMAT (/,' PERIOD==>',F5.2,' MS',/,' SMALL T==>',F5.2,' MS',/,' I
     *MPACT DURATION==>',F5.2,' MS',/,' B==>',F6.1,' M/S2',/,' PEAK==>',
     *F6.1,' M/S2',/)
24    FORMAT (/,' TEST NO ',2A3)
25    FORMAT (' ***** IMPACT SIDE OF SIGNAL DOES NOT LAST LONG ENOUGH **
     ****')
      READ (5,1) NUMBER
      NO=1
C
C     READ DATA AND CALCULATE MISSING DIMENSIONS
C
90    READ (5,3) TIT1,TIT2
      WRITE (6,24) TIT1,TIT2
      READ (5,2) T,TIM,D,B,P
      WRITE (6,23) T,TIM,D,B,P
      TT=T-TIM
      X=(TIM*B+P*D)/TT
      T23=TT*B/(2.0*X)
      T56=TIM-T23-D
      IF (T56.LT.0.0) GO TO 920
C
C     ESTABLISH VELOCITY CURVE
C
      TEMPS(1)=0.0
      VELO(1)=-X*TT/4000.0
      DO 100 I=2,20
         XI=I-1
         TEMPS(I)=TT*XI/20.0
         IF (I-11) 94,96,98
94       VELO(I)=VELO(1)+X*(TEMPS(I)**2.0)/(TT*1000.0)
         GO TO 100
```

```
 96       VELO(I)=0.0
          GO TO 100
 98       DUR=TEMPS(I)-TT/2.0
          VELO(I)=X*DUR/1000.0-X*(DUR**2.0)/(TT*1000.0)
100    CONTINUE
       TEMPS(21)=TT
       VELO(21)=-VELO(1)
       DO 110 J=22,28
          XJ=J-21
          TEMPS(J)=(T23*XJ/8.0)+TT
          VELO(J)=VELO(21)-(X*(TEMPS(J)-TT)**2.0)/(TT*1000.0)
110    CONTINUE
       TEMPS(29)=TT+T23
       VELO(29)=VELO(21)-TT*(B**2.0)/(4000.0*X)
       DO 120 JJ=30,40
          XJJ=JJ-29
          TEMPS(JJ)=TEMPS(29)+D*XJJ/12.0
          IF (JJ-35) 114,116,118
114       DUR=TEMPS(JJ)-TEMPS(29)
          VELO(JJ)=VELO(29)-B*DUR/1000.0-(P-B)*(DUR**2.0)/(D*1000.0)
          GO TO 120
116       VELO(JJ)=VELO(29)-D*(P+B)/4000.0
          GO TO 120
118       DUR=TEMPS(JJ)-TEMPS(35)
          VELO(JJ)=VELO(35)-P*DUR/1000.0+(P-B)*(DUR**2.0)/(D*1000.0)
120    CONTINUE
       TEMPS(41)=T-T56
       VELO(41)=VELO(29)-D*(P+B)/2000.0
       DO 130 JZ=42,49
          XJZ=JZ-41
          DUR=T56*XJZ/8.0
          TEMPS(JZ)=TEMPS(41)+DUR
          VELO(JZ)=VELO(41)-B*DUR/1000.0+B*(DUR**2.0)/(2000.0*T56)
130    CONTINUE
       IF (ABS(VELO(49)-VELO(1)).GT.0.01) GO TO 900
       KOUNT=1
C
C      ESTABLISH DISPLACEMENT CURVE
C
135    DISP(1)=0.0
       AREA=0.0
       DO 140 JY=2,20,2
          JYY=JY-1
          JYJ=JY+1
          AREA=AREA+(TEMPS(JY)-TEMPS(JYY))*(VELO(JYY)+4.0*VELO(JY)+VELO(J
     *YJ))/3.0
          JL=(JY/2)+1
          DISP(JL)=AREA
140    CONTINUE
       DO 150 JA=22,28,2
          JAA=JA-1
          JAJ=JA+1
          AREA=AREA+(TEMPS(JA)-TEMPS(JAA))*(VELO(JAA)+4.0*VELO(JA)+VELO(J
     *AJ))/3.0
          JL=(JA/2)+1
          DISP(JL)=AREA
150    CONTINUE
       DO 160 JB=30,40,2
          JBB=JB-1
          JBJ=JB+1
```

```
          JL=(JB/2)+1
          AREA=AREA+(TEMPS(JB)-TEMPS(JBB))*(VELO(JBB)+4.0*VELO(JB)+VELO(J
     *BJ))/3.0
          DISP(JL)=AREA
160   CONTINUE
      DO 170 JC=42,48,2
          JCC=JC-1
          JCJ=JC+1
          JL=(JC/2)+1
          AREA=AREA+(TEMPS(JC)-TEMPS(JCC))*(VELO(JCC)+4.0*VELO(JC)+VELO(J
     *CJ))/3.0
          DISP(JL)=AREA
170   CONTINUE
C
C     CHECK IF THE DISPLACEMENT CURVE CLOSES AT ZERO.
C     IF NOT, CHANGE THE VELOCITY AXIS AND RECALCULATE DISPLACEMENTS
C        ERR = PREVIOUS AREA
C        AREA= CLOSURE ERROR IN VELOCITY AREA (CURRENT ITERATION)
C
      IF (ABS(AREA).LT.0.05) GO TO 910
      IF (AREA.GT.0.0) GO TO 180
      IF (KOUNT.EQ.1) GO TO 193
      IF (ERR.GT.0.0) DIFF=-DIFF*0.5
      GO TO 194
180   IF (KOUNT.EQ.1) GO TO 192
      IF (ERR.LT.0.0) DIFF=-DIFF*0.5
      GO TO 194
192   DIFF=0.05*VELO(1)
      GO TO 194
193   DIFF=-0.05*VELO(1)
194   ERR=AREA
      KOUNT=KOUNT+1
      DO 200 JD=1,49
          VELO(JD)=VELO(JD)+DIFF
200   CONTINUE
      GO TO 135
900   WRITE (6,20)
      STOP
C
C     PRINTOUT DATA
C
910   WRITE (6,21)
      DO 915 JE=1,25
          JEE=(JE-1)*2+1
          WRITE (6,22) TEMPS(JEE),VELO(JEE),DISP(JE)
915   CONTINUE
916   NO=NO+1
      IF (NO.GT.NUMBER) STOP
      GO TO 90
920   WRITE (6,25)
      GO TO 916
      END
```

Sample Data

```
 2
DS1-1A
12.50 7.18 0.79 120.05332.0
DS1-1A
12.50 5.05 0.79 133.03286.0
```

Typical Output

TEST NO DS1-1A

PERIOD==>12.50 MS
SMALL T==> 7.18 MS
IMPACT DURATION==> 0.79 MS
B==> 120.0 M/S2
PEAK==>5332.0 M/S2

TIME MS	VELOCITY M/S	DISPLACEMENT MM
0.0	-0.761	0.0
0.53	-0.710	-0.40
1.06	-0.558	-0.74
1.60	-0.304	-0.97
2.13	0.051	-1.04
2.66	0.507	-0.90
3.19	0.964	-0.50
3.72	1.319	0.11
4.26	1.573	0.88
4.79	1.725	1.76
5.32	1.776	2.70
5.40	1.775	2.85
5.49	1.771	3.00
5.57	1.765	3.14
5.65	1.756	3.29
5.79	1.626	3.52
5.92	1.267	3.71
6.05	0.679	3.84
6.18	0.091	3.89
6.31	-0.268	3.87
6.44	-0.398	3.83
7.96	-0.557	3.10
9.47	-0.670	2.17
10.99	-0.738	1.09
12.50	-0.761	-0.05

TEST NO DS1-1A

PERIOD==>12.50 MS
SMALL T==> 5.05 MS
IMPACT DURATION==> 0.79 MS
B==> 133.0 M/S2
PEAK==>3286.0 M/S2

TIME MS	VELOCITY M/S	DISPLACEMENT MM
0.0	-0.705	0.0
0.74	-0.672	-0.52
1.49	-0.574	-0.98
2.23	-0.410	-1.36
2.98	-0.182	-1.58
3.72	0.112	-1.61
4.47	0.406	-1.41
5.21	0.635	-1.02
5.96	0.799	-0.48

6.70	0.897	0.15
7.45	0.929	0.84
7.73	0.925	1.10
8.01	0.910	1.36
8.30	0.887	1.61
8.58	0.854	1.86
8.71	0.767	1.97
8.84	0.542	2.05
8.97	0.179	2.10
9.11	-0.185	2.10
9.24	-0.410	2.06
9.37	-0.496	2.00
10.15	-0.587	1.57
10.93	-0.653	1.09
11.72	-0.692	0.56
12.50	-0.705	0.01

APPENDIX E

TEST DATA AND ANALYSIS RESULTS

Table E.1 Test results

TEST No	ACCELERATION m/s^2	MEASURED FORCE kg	PENETRATION RATE cm/min	CALCULATED DISPLACEMENT mm	ENERGY FOR PEN. J/cm
DS1-1A	5332/3286	285	1.33	3.89/2.10	58.8/36.2
1B	3720	292/219	0.60	2.75	40.8
1C	2480	219	1.10	1.34	27.7
DS1-2A	5456	-	3.46	5.03	59.1
2B	4216	-	3.46	2.25	46.1
DS1-3A	4712	-	2.36	4.24	51.3
3B	2480	-	2.36	2.81	27.7
DS1-4A	1739	147	0.028	1.72	19.9
4B	1240	102	0.028	0.43	14.7
DS1-5A	2356	255	1.39	0.63	26.4
5B	2480	-	1.39	0.94	27.7
LS2-1A	4712/4340	263	3.60	4.37/4.00	51.3/47.4
1B	4340	-	3.60	3.87	47.4
LS2-5A	2360	-	2.25	2.00	26.5
5B	1910	220	2.25	1.83	21.7
LS2-6B	2772	-	0.43	2.07	30.8
6D	2135	-	0.077	2.02	24.1
DS2-1A	-	-	3.21	-	-

Table E.1 (foll'd) Test results

TEST No	ACCELERATION m/s^2	MEASURED FORCE kg	PENETRATION RATE cm/min	CALCULATED DISPLACEMENT mm	ENERGY FOR PEN. J/cm
DS2-2A	-	175/117	0.52	-	18.7/13.1
2C	-	131	1.07	-	14.4
DS2-3	-	-	0.025	-	-
DS2-4A	-	-	0.97	-	-
4B	-	-	2.28	-	-
DS2-5	-	-	0.75	-	-
DS2-6A	2247	-	0.92	1.94	25.3
6B	2772	-	0.92	1.78	30.8
6C	2734	-	1.10	1.84	30.4
6D	2037	-	1.10	2.40	23.1
DS2-7A	1873	195	0.41	1.20	21.3
7C	2322	248	0.13	1.51	26.1
7D	2097	232	0.13	1.14	23.7
LS3-1A	2247	216	1.07	1.43	25.3
1B	2022	252	1.07	0.75	22.9
1C	1461	200	2.48	1.93	17.0
1D	1648	195	2.48	1.75	19.0
LS3-2A	2097	228	3.29	0.11	23.7

Table E.1 (foll'd) Test results

TEST No	ACCELERATION m/s^2	MEASURED FORCE kg	PENETRATION RATE cm/min	CALCULATED DISPLACEMENT mm	ENERGY FOR PEN. J/cm
LS3-4	974/712	187/114	3.10	1.21	11.2/9.1
LS3-5A	2022	187	2.86	0.104	22.9
5B	1498	277	2.86	0.174	17.4
LS3-6A	1011	130	1.53	0.90	12.2
6B	1199	114	1.53	1.10	14.2
LS3-7A	3258/1985	216	3.00	1.65	35.9/22.5
7B	1798	183	3.00	0.145	20.5
DS3-1A	2060	224	0.069	1.06	23.3
1B	2022	220	0.069	1.56	22.9
DS3-2A	1835/1011	236/90	0.00	1.17/0.97	
DS3-3A	3431	204	3.86	0.276	37.8
3B	2247	187	3.86	2.11	25.3
DS3-4	1124	-	0.30	2.21	13.4
DS3-5A	2172	187	1.52	2.65	24.5
5B	1573/1873	147/204	1.52	4.21/4.56	18.2/21.3
5C	1573	163	0.75	1.93	18.2
DS3-6A	4270	-	1.65	0.22	46.6
6B	2097	-	1.65	3.07	23.7